



Rijkswaterstaat
Ministerie van Infrastructuur en Milieu

Bowthruster-induced flow on the bottom of a vertical quay wall

A field measurement



MSc Thesis written by
Irene Cantoni

Photo in the cover page taken during field measurements on Tuesday, 18th of June 2019, by Erik-Jan Houwing

Bowthruster-induced flow on the bottom of a vertical quay wall

A field measurement

by

Irene Cantoni

in partial fulfillment of the requirements to obtain the degree of
Master of Science in Civil Engineering
at the Delft University of Technology
to be defended publicly on
Monday February 17, 2020 at 2:00 PM.

Student number: 4743474

Thesis committee: Dr. Ir. B. Hofland, TU Delft
Ir. A. van der Hout, TU Delft and Deltares
Dr. Ir. A. A. Roubos, TU Delft
Ir. M. Ruijter, Rijkswaterstaat

Preface

This research is the result of collaboration within TU Delft, Deltares, Rijkswaterstaat and Ports of Rotterdam. It fits in the bigger research framework on knowledge gaps on propeller jets, and presents an unique dataset of full scale measurements. Being part of it has been a great opportunity, and I take here the time to thank who allowed me to add my small contribution with this master thesis. First and foremost, thanks to my committee for guiding and advising me. To Arne, for the infinite patience and time that he dedicated to me, helping to organise my thoughts and bringing clarity. To Alfred, for introducing me to the project and for always offering a different perspective. Bas, thanks for being such an inspirational asset to the committee: always bringing new energy and ideas to the project. Michel, thank you for all the practical insights and the constant support from Rijkswaterstaat. Without the excellent project management abilities of Erik-Jan Houwing and the ability of Boskalis diver team, field measurements would have not been possible: thank you. A special thanks also to Charlotte van der Vorm, who ensured continuation of the project, and to all the schroefstraal group, who offered an incredible opportunity for learning even more about my thesis topic.

But life of a student is not only consisting of their thesis, even if, from times to times, it might seem so. Unavoidably, academic life is also shaped by what happens outside classrooms. And, sometimes, this two sides become more intertwined than expected.

And how strange, he thought suddenly, that this idea should have come to him when his mind was far away from anything to do with science, when the discussions that so excited him were those of free men, when his words and the words of his friends had been determined only by freedom [...] ¹.

Therefore, thanks also to whom of my thesis heard only excited stories and incomprehensible rambling about bowthrusters. Thanks to my family, for their constant support. My mom, who taught me that everything can be done and nothing, not even engineering, is as difficult as it seems. My dad, because he never asks back for the books I steal from his shelves, so that I can forget about numbers and calculations a little longer. Thanks to my sister for the drama, and to my brother for being the serious sibling, relieving us from this burden. Thanks also to Sergio and Laura for being part of the family. Thanks to my classmates, who always set an example of which kind of student and engineer I want to be, and manage to do so while being true friends. Susana, for all the shared projects, laughs, and for being the yin to my engineering yang. Luis, for the jokes that softened exam and thesis stress. Camila: in joy and sorrow, thanks for helping me navigate through the kaleidoscope of feelings that these two years have been. To Laurie and Tessa, thanks for all the magic Canadian adventures, which keep us together even in these final steps of our masters. I have been blessed with flatmates who took care of me in the most disparate ways: Sofia, thanks for ensuring that I always made it home safe. Benedetta, philosopher by nature and engineer by choice, and Francesco, living paradigm of responsibility and adulthood, thanks for pointing the way. Fernando, thanks for bringing some spice to this house (and for the good tequila). Thanks to DIG for being the refuge from dull reality that every TU Delft student needs: all praise and glory to our Woolly Lady of Improv. And Jan: even though you are a systematic provider of distractions, you've always been ready to feed me at the most improbable hours: thanks for both. If your food allowed me to survive the deadlines, your distractions make life more colourful.

¹Vasily Grossman, *Life and Fate*. Translated by R.Chandler. Penguin Random House, 2006.

Summary

During mooring operations, ships tend to make an extensive use of bowthruster in order to minimize the need for tug assistance. Jet caused by transverse thrusters directly impinges quay walls, and can cause scour on the bed, therefore threatening structural stability of quay walls. Presence of vertical quay walls induces reflection of bowthruster's jet, further complicating the already complex flow field. Despite extensive research has been conducted on free flow, several knowledge gaps are still present regarding propeller induced flow when confined, for instance by a vertical quay wall.

In this research, focus is on flow field on the bottom of a vertical quay wall induced by channel-type bowthrusters, which are commonly used for inland vessels. Field measurements have been conducted at the Antarcticade, Ports of Rotterdam, using inland vessel MTS Vorstenbosch. The vessel is equipped with a 4-channel Veth Jet type bowthruster system. Use of a combination of Acoustic Doppler Velocimeters and Acoustic Doppler Current Profilers allowed measurements of flow velocities on the bottom of the quay. Data from the measurements has been analysed to investigate influence of distance between outlet and quay wall, and keel clearance, on the flow pattern at the bottom. Results have then been contextualized within the literature framework, and their impact on design of bottom protection according to most used guidelines has been assessed.

The results of this field measurement showed mean flow velocities near the quay wall generally in the order of magnitude of 1 m/s, with the exception of one test, where mean flow velocities in the order of magnitude of 2 m/s were recorded. This relatively low mean flow velocities were often correlated with large turbulent fluctuations, leading to values of relative turbulence intensities higher than the ones found in literature, and sometimes even equal to 1. Comparison with the theoretical calculations of velocities according to Dutch and German methods suggested by PIANC, showed both methods to be conservative if compared with data from most tests. Furthermore, it appeared that both formulae's sensitivity to wall and keel clearance was not reflected by the data. Similarly, results from this measurement showed that the flow generated by simultaneous use of two bowthrusters was characterized by velocities on the bed lower than expected according to the guidelines. Recommendation would be to use either linear superposition or to multiply by \sqrt{n} (where n is the number of used propellers) when considering the use of multiple propellers, but this was not reflected by most of the data. However, two of the tests taken into exam represented an exception to these general observations: ADV1, the instrument nearer to the quay wall, recorded velocities higher than the theoretical values for tests 12 (use of bowthruster 2 at high water) and 22 (use of both bowthrusters simultaneously at low water).

Results from this study showed how the use of a 4-channel bowthruster system induced a flow on the bottom of a vertical quay wall which is mainly divided in two zones. Near the quay wall is where the highest velocities have been measured, and where the flow is strictly influenced by use of the bowthrusters. There is a return flow beneath the ship, which is dissipated in the space of few meters. Underneath the suction points of the bowthrusters, it is the inflow to determine the flow characteristics on the bed. In this research, the extent of the bowthruster-induced flow was found to be less than 14 m from the quay wall. The instrument hereby located, in fact, didn't record velocities which were affected by the use of bowthrusters. This research represents a step towards filling the knowledge gaps about use of bowthrusters at a vertical quay wall. The unique dataset collected can be used in the future for validating numerical or on-scale models, working for a better understanding of the phenomenon and a more accurate and optimized design of bed protections.

Contents

Preface	iii
Summary	v
List of symbols	ix
List of Figures	xi
List of Tables	xvii
1 Introduction	1
1.1 Motivation	1
1.2 Problem definition	2
1.3 Thesis Outline	2
2 Background	3
2.1 Channel bowthrusters	3
2.2 Flow field cause by propellers	4
2.3 Reflection on quay wall: previous researches	5
2.4 Calculation methods for the hydraulic load on the bed according to the most common guidelines	7
2.5 Stability formulae for bottom materials.	9
2.6 Equipment used to measure velocities	10
3 Methodology	15
3.1 Scope of the measurements	15
3.2 General information	15
3.3 Reference system	19
3.4 Instruments set-up	20
3.5 Considered ship positions	22
3.6 Summary of measurement location	22
3.7 Set-up limitations	23
3.8 Measurement programme	23
4 Post-processing approach	29
4.1 Correlation checks	30
4.2 Amplitude checks.	34
4.3 Statistical analysis of velocities	35
4.4 Pressure fluctuations compared to velocity increase	38
4.5 Stationarity of the flow	39
4.6 Most representative cell for ADCPs	40
4.7 Dominant direction	41
4.8 Conclusions.	42
5 Test Results	43
5.1 General observations.	43
5.2 Use of different bowthrusters: bowthruuster 1, bowthruuster 2 and simultaneous use of both	46
5.3 Influence of keel clearance.	50
5.4 Spatial distribution of flow velocities	52
5.5 Conclusions.	57

6	Comparison with theory and guidelines	59
6.1	Maximum velocities at the bottom	59
6.2	Use of multiple propellers	61
6.3	Influence of keel clearance.	64
6.4	Relative turbulence intensity	65
6.5	Impact of measurements results on bottom protection design	67
6.6	Conclusions.	69
7	Discussion	71
7.1	Assessment of the adopted measurement set-up and protocol	71
7.2	Contextualisation in the theoretical framework	77
7.3	Impact on bed protection design.	80
7.4	Conclusions.	81
8	Conclusions and recommendations	83
8.1	Conclusions.	83
8.2	Recommendations	85
A	Measurement of the free flow	87
A.1	Measurement set-up	87
A.2	Considered ship positions	88
A.3	Measurement programme	88
B	Test Results	89
C	Tables of test results	101
D	Calculation parameter for comparison with theory	105
E	Surveys	107
	Bibliography	111

List of symbols

A list of the main symbols utilized in this report is hereby reported. For brevity, symbols for instantaneous values are presented. Time averaged values are reported using the same symbol as the instantaneous value, but with an overbar: ex. \bar{V} [m/s] indicates the average horizontal velocity magnitude.

ADCP: Acoustic Doppler Current Profiler

ADV: Acoustic Doppler Velocimeter

BT1: bowthruster 1

BT2: bowthruster 2

D_t [m]: bowthruster diameter

h_t [m]: height of thruster in the water column

KC [m]: keel clearance

L [m]: wall clearance

t [date] : time

v_2 [m/s]: instantaneous velocity along Beam 2 of ADCPs

v_4 [m/s]: instantaneous velocity along Beam 4 of ADCPs

v_x [m/s]: instantaneous velocity along x axis

v_y [m/s]: instantaneous velocity along y axis

\bar{V} [m/s]: instantaneous horizontal velocity magnitude

C_2 [%]: instantaneous correlation along beam 2 of ADCPs

C_4 [%]: instantaneous correlation along beam 4 of ADCPs

C_x [%]: instantaneous correlation along x

C_y [%]: instantaneous correlation along y

C_z [%]: instantaneous correlation along z

A_2 [db]: instantaneous amplitude along beam 2 of ADCPs

A_4 [db]: instantaneous amplitude along beam 4 of ADCPs

θ [degrees]: horizontal velocity dominant direction

σ_{θ} [degrees]: standard deviation for θ

σ_x [m/s]: standard deviation for \bar{v}_x

σ_y [m/s]: standard deviation for \bar{v}_y

σ [m/s]: standard deviation for \bar{V}

r [-]: relative turbulence intensity

k [-]: turbulence factor

p [dbar]: instantaneous pressure

Δp [dbar] : pressure velocity fluctuation

V_p [m/s]: instantaneous velocity magnitude corresponding to pressure fluctuations

V^* [m/s]: full 3D velocity magnitude, calculated as $\sqrt{v_x^2 + v_y^2 + v_z^{*2}}$,

v_z^* [m/s]: instantaneous vertical velocity component, assumed to have a value equal to the maximum between the measured v_x and v_y

List of Figures

2.1	Veth Jet bowthruster. From Veth Propulsion website [16].	3
2.2	Velocity distribution induced by a transverse thruster. From PIANC [15].	4
2.3	Differences in flow velocities between propeller jet and free jet. From [15].	5
2.4	Zones of a flow field from a transverse thruster against a quay wall. From [1].	6
2.5	Factor a_L as a function of the wall and bottom distance. From PIANC [15].	8
2.6	Picture of a Nortek Signature 1000 ADCP (left) and of a Nortek Vector ADV (right).	10
2.7	Illustration of the shift in frequency of the acoustic echo reflected from moving particles. From Nortek’s comprehensive manual [12].	11
2.8	Vector transmit and receive beams. The bisector of the angle between them indicates the velocity to which the receivers are sensitive. The blue arrow in the lower image indicates a positive velocity. From Nortek Comprehensive Manual Velocimeters [14].	12
2.9	Vector measuring volume, identified by the interception of the three beams. From Nortek Comprehensive Manual Velocimeters [14].	12
2.10	Definition of velocity profile. The centre of each cell is located at a distance from the transducer equal to centre of cell $n = \text{blanking distance} + n \cdot \text{cell size}$. From Nortek Signature Operation Principles [13].	13
3.1	Location of measurements on the Maasvlakte. From Deltares report on field measurements conducted in 2018 [22].	16
3.2	Location of measurements on the Maasvlakte. From Deltares report on field measurements conducted in 2018 [22].	16
3.3	Bowthrusters system in the Vorstenbosch. In figure, bowthruster 1 and 2 are indicated, as well as their channel lengths, distance between the outlet and the quay wall (assuming that the ship is moored perfectly against it), and distance between the two channel axis. The suction points of each bowthruster are highlighted in orange. From technical drawings of the vessel, modified by the autor.	17
3.4	MTS Vorstenbosch moored at the Antarcticakade during the measurements, on June 18th, 2019. Photocredits E.J. Houwing.	18
3.5	Illustration of the ADCP’s beam reference system compared to the general reference system and of the transformation from beam velocities to x and y velocities. An outline of cell 2 is also indicated. Source: author.	20
3.6	Schematic representation of the instrument mounted on the scaffolding. The green squares symbolizes the ADCPs, while the purple triangles the ADVs. The number associated with each instrument is also illustrated. Source: author.	20
3.7	Picture of ADCP and ADV mounted on their wooden frame and then on the scaffolding. Picture taken during the measurement preparation day, on Monday 17th of June, 2019. Photocredits: author.	21
3.8	Picture of ADCP1 (left) and ADV1 (right), when submerged and measuring. Photocredits: Boskalis diving team.	21
3.11	Ship position 1. Horizontal line indicates position of the instruments. Source: author.	22
3.12	Ship position 2. Horizontal line indicates position of the instruments. (5 m behind position 1). Source: author.	22
3.13	Ship position 3. Horizontal line indicates position of the instruments. (5 m ahead of ship position 1). Source: author.	22
3.9	Plan view of instrument set-up for the reflected flow. The grid of the chosen reference system is illustrated, as well as the quay wall and the reference point of bollard 31. Source: author.	25

3.10	Cross view of instrument set-up for the reflected flow. The grid of the chosen reference system is illustrated, as well as the quay wall and the schematized ship outline. Outlets and inflow points of the bowthrusters are indicated. Source: author.	26
3.14	Illustration of the reference system. Position of the instrument is depicted: ADVs are illustrated as triangles and cell 2 of ADCPs as circles. Inflow and outflow coordinates of both bowthrusters can be seen, as well as a simplified outline of the ship. Reference point Bollard 31 is illustrated as well. Source: author.	27
4.1	Instantaneous correlation during Test 1 for ADCP1. Correlation values for beam 2 (C_2) and beam 4 (C_4) are represented. Subtest corresponding to 25%, 50%, 75% and 100% of applied power are indicated, while minimum suggested value of 50% of correlation is highlighted in red. Values from cell 2 of the ADCP are presented.	30
4.2	Instantaneous correlation during Test 1 for ADCP2. Correlation values for beam 2 (C_2) and beam 4 (C_4) are represented. Subtest corresponding to 25%, 50%, 75% and 100% of applied power are indicated, while minimum suggested value of 50% of correlation is highlighted in red. Values from cell 2 of the ADCP are presented.	31
4.3	Instantaneous correlation during Test 1 for ADV1. Correlation values for x (C_x), y (C_y) and z (C_z) are represented. Subtest corresponding to 25%, 50%, 75% and 100% of applied power are indicated, while minimum suggested value of 50% of correlation is highlighted in red.	31
4.4	Instantaneous correlation during Test 1 for ADV1. Correlation values for x (C_x), y (C_y) and z (C_z) are represented. Subtest corresponding to 25%, 50%, 75% and 100% of applied power are indicated, while minimum suggested value of 50% of correlation is highlighted in red.	32
4.5	Mean correlation profile for each subtest of Test 1, along cells of beam 2 (\bar{C}_2) and 4 (\bar{C}_4) of ADCP1.	33
4.6	Mean correlation profile for each subtest of Test 1, along cells of beam 2 (\bar{C}_2) and 4 (\bar{C}_4) of ADCP2.	33
4.7	Mean amplitude profile for each subtest of Test 1, along cells of beam 2 (\bar{C}_2) and 4 (\bar{C}_4) of ADCP1.	34
4.8	Mean amplitude profile for each subtest of Test 1, along cells of beam 2 (\bar{C}_2) and 4 (\bar{C}_4) of ADCP2.	35
4.9	Histograms of all measured instantaneous velocities, and only velocities with a >50% correlation for ADCPs in Test 1, at 25% of applied power.	36
4.10	Histograms of all measured instantaneous velocities, and only velocities with a >50% correlation for ADVs in Test 1, at 25% of applied power.	36
4.11	Histograms of all measured instantaneous velocities, and only velocities with a >50% correlation for ADCPs in Test 1, at 100% of applied power.	37
4.12	Histograms of all measured instantaneous velocities, and only velocities with a >50% correlation for ADVs in Test 1, at 100% of applied power.	37
4.13	Time series of measured instantaneous horizontal velocity magnitude in cell 1 of ADCP1, and velocity correspondent to pressure fluctuations in Test 1.	38
4.14	Time series of measured instantaneous horizontal velocity magnitude in cell 1 of ADCP2, and velocity correspondent to pressure fluctuations in Test 1.	39
4.15	Comparison between mean horizontal velocity (\bar{V}) and its standard deviation for each whole subtest and for the final minute of each subtest in Test 1.	40
4.16	Mean x velocity (\bar{V}_x) and standard deviation (σ_x) profile along the first 5 cells of ADCP1 in Test 1.	41
4.17	Histograms of instantaneous direction calculated for Test 1 at 25% of rpm. All instruments are represented.	42

5.1	Results of test 1. Mean of horizontal velocity magnitude and standard deviation represented for each instrument, for each subtest. Non reliable data is presented in grey.	44
5.2	Results of test 12. Mean of horizontal velocity magnitude and standard deviation represented for each instrument, for each subtest. Non reliable data is presented in grey.	45
5.3	Results of test 22. Mean of horizontal velocity magnitude and standard deviation represented for each instrument, for each subtest. Non reliable data is presented in grey.	46
5.4	Comparison of horizontal flow velocity magnitude and standard deviation for each applied step of power for Test 1 and Test 2.	47
5.5	Comparison of mean velocity and dominant direction measured by ADV2 for 100% of applied power in Test 1 and Test 2. The suction points of both bowthrusters are depicted, on scale.	48
5.6	Comparison of x and y velocities measured by ADV2 for Test 1 and 2.	48
5.7	Comparison of velocity magnitude and standard deviation for Test 1, 2 and 3 where bowthruster 1, 2 and both bowthrusters are respectively used.	49
5.8	Comparison of velocity magnitude and standard deviation for Test 11, 12 and 13 where bowthruster 1, 2 and both bowthrusters are respectively used.	50
5.9	Comparison of velocity magnitude and standard deviation for Test 1 and 11, where bowthruster 1 is used respectively with a keel clearance of 1.03 m and 2.57 m.	51
5.10	Comparison of velocity magnitude and standard deviation for Test 2 and 12, where bowthruster 2 is used respectively with a keel clearance of 1.03 m and 2.79 m.	51
5.11	Mean horizontal velocity magnitude and dominant direction for tests 1, 5 and 7, at 50% of applied power. Range in dominant direction, corresponding to $\pm\sigma_{theta}$, is indicated by dotted lines.	52
5.12	Mean horizontal velocity magnitude and dominant direction for tests 1, 5 and 7, at every step of applied power.	53
5.13	Mean horizontal velocity magnitude and dominant direction for tests 1, 5, 7, and 2, 4, 8 at 50% of applied power.	54
5.14	Mean horizontal velocity magnitude and dominant direction for tests 1, 5, 7; 2, 4, 8, and 3, 6, 9 at 25% of applied power.	55
5.15	Mean horizontal velocity magnitude and dominant direction for tests 1, 5, 7, and 11, 14, 17 at 50% of applied power.	56
5.16	Mean horizontal velocity magnitude and dominant direction for tests 2, 4, 8, and 12, 15, 18 at 50% of applied power.	57
6.1	Comparison between maximum bottom velocities calculated by Dutch and German method, and measured maximum velocities from ADV1 and ADCP1 data in Test 1 and Test 2. Unreliable data is depicted in grey.	60
6.2	Comparison between maximum bottom velocities calculated by Dutch and German method, and measured maximum velocities from ADV1 and ADCP1 data in Test 11 and Test 12. Unreliable data is depicted in grey.	60
6.3	Comparison of theory of linear superposition and velocities being proportional to the square root of number of propellers used, with data from test 13. Dutch method used to calculate theoretical maximum velocities. Unreliable data are depicted in grey.	61
6.4	Comparison of theory of linear superposition and velocities being proportional to the square root of number of propellers used, with data from tests 3 and 22. Dutch method used to calculate theoretical maximum velocities. Unreliable data are depicted in grey.	62

6.5	Comparison of theory of linear superposition and velocities being proportional to the square root of number of propellers used, with data from tests 11, 12 and 13 where respectively bowthruster 1, 2 and both bowthruster simultaneously are used. Unreliable data are depicted in grey.	63
6.6	Comparison of theory of linear superposition and velocities being proportional to the square root of number of propellers used, with data from tests 1, 2 and 22 where respectively bowthruster 1, 2 and both bowthruster simultaneously are used. Unreliable data are depicted in grey.	63
6.7	Dependence on thruster height in the water column for bowthruster 1, comparison between data and Dutch method.	64
6.8	Dependence on thruster height in the water column for bowthruster 2, comparison between data and Dutch method.	65
6.9	Relative turbulence intensity in function of the distance from the quay wall, associated with the use of bowthruster 1 (test 1) and bowthruster 2 (test 2). Unreliable data are depicted in grey.	66
6.10	Relative turbulence intensity measured by each instrument for each step of applied power. Comparison between bowthruster 1 (Test 1) and bowthruster 2 (Test 2) is illustrated. Unreliable data are depicted in grey. Reference lines of turbulence intensity values expected from literature is illustrated.	66
7.1	Beam velocity profile for ADCP1 test1. Average for each subtest is taken.	72
7.2	Beam velocity profile for ADCP1 test2. Average for each subtest is taken.	72
7.3	Illustration of ADCP1 with respect to the vessel. Beam 2 and 4 of the instruments are depicted by dashed lines, and distances where a sudden increase of in-line velocities along the beams is observed in test 1 and 2 are indicated. Source: author.	73
7.4	Comparison of velocity correspondent to pressure fluctuations according to Bernoulli's theorem, measured horizontal velocity magnitude and 3D velocity magnitude, calculated assuming vertical component equal to maximum between x and y measured components. Data presented for ADCP1.	74
7.5	Velocity profile in the direction perpendicular to the quay wall, obtained combining measured velocities and velocities correspondent to pressure fluctuations for Test 1, for all steps of applied power.	75
7.6	Velocity profile in the direction perpendicular to the quay wall for Test 1 as obtained from pressure fluctuations (upper graph) and measured velocities (lower graph). All steps of applied power are represented.	76
7.7	Test 23 results: mean horizontal velocity magnitude timeseries. All instruments are represented, except for ADV2.	77
7.8	Re-elaboration of Schmidt identified zones for a reflected jet on a vertical quay wall. Created by the author based on [19].	79
7.9	Cross-section of the proposed redesign of bottom protection at the Antarticakade, based on the observed bowthruster-induced flow. 10-60 kg rocks, penetrated with concrete for the first 5m from the quay wall, for a total width of 15 m.	80
A.1	Top view of measurement set-up for the free flow. Dimensions are indicated in millimeters.	87
A.2	Ship position 4.	88
A.3	Ship position 5.	88
B.1	Results of test 1. Mean of horizontal velocity magnitude and standard deviation represented for each instrument, for each subtest.	89
B.2	Results of test 2. Mean of horizontal velocity magnitude and standard deviation represented for each instrument, for each subtest.	90
B.3	Results of test 3. Mean of horizontal velocity magnitude and standard deviation represented for each instrument, for each subtest.	90

B.4	Results of test 4. Mean of horizontal velocity magnitude and standard deviation represented for each instrument, for each subtest.	91
B.5	Results of test 5. Mean of horizontal velocity magnitude and standard deviation represented for each instrument, for each subtest.	91
B.6	Results of test 6. Mean of horizontal velocity magnitude and standard deviation represented for each instrument, for each subtest.	92
B.7	Results of test 7. Mean of horizontal velocity magnitude and standard deviation represented for each instrument, for each subtest.	92
B.8	Results of test 8. Mean of horizontal velocity magnitude and standard deviation represented for each instrument, for each subtest.	93
B.9	Results of test 9. Mean of horizontal velocity magnitude and standard deviation represented for each instrument, for each subtest.	93
B.10	Results of test 11. Mean of horizontal velocity magnitude and standard deviation represented for each instrument, for each subtest.	94
B.11	Results of test 12. Mean of horizontal velocity magnitude and standard deviation represented for each instrument, for each subtest.	94
B.12	Results of test 13. Mean of horizontal velocity magnitude and standard deviation represented for each instrument, for each subtest.	95
B.13	Results of test 14. Mean of horizontal velocity magnitude and standard deviation represented for each instrument, for each subtest.	95
B.14	Results of test 15. Mean of horizontal velocity magnitude and standard deviation represented for each instrument, for each subtest.	96
B.15	Results of test 16. Mean of horizontal velocity magnitude and standard deviation represented for each instrument, for each subtest.	96
B.16	Results of test 17. Mean of horizontal velocity magnitude and standard deviation represented for each instrument, for each subtest.	97
B.17	Results of test 18. Mean of horizontal velocity magnitude and standard deviation represented for each instrument, for each subtest.	97
B.18	Results of test 19. Mean of horizontal velocity magnitude and standard deviation represented for each instrument, for each subtest.	98
B.19	Results of test 20. Mean of horizontal velocity magnitude and standard deviation represented for each instrument, for each subtest.	98
B.20	Results of test 21. Mean of horizontal velocity magnitude and standard deviation represented for each instrument, for each subtest.	99
B.21	Results of test 22. Mean of horizontal velocity magnitude and standard deviation represented for each instrument, for each subtest.	99
E.1	Survey of the Yangtzekanaal near to the Antarcticakade, Ports of Rotterdam, taken in the morning of 18 June 2019, before the measurements.	108
E.2	Survey of the Yangtzekanaal near to the Antarcticakade, Ports of Rotterdam, taken in the afternoon of 19 June 2019, after the measurements.	109

List of Tables

3.1	MTS Vorstenbosch characteristic dimensions.	17
3.2	Veth jeth bowthruster characteristics.	17
3.3	Table illustrating the measurement protocol for tests 1-23 (Reflected Flow). For each test are stated the power steps applied, the duration of each subtest, the number of subtests, total duration of the test, which bow thruster is used, the position of the ship, the set-up of the instruments and the average water depth at the quay.	24
6.1	Cases identified for calculation of rock size needed for the bottom protection. Both collected data and theoretical values according to Dutch method are presented.	67
6.2	General input used to calculate rock D_{50} stable under conditions described by case 1, 2 and 3 according to Pilarczyk and Izbash formulas.	68
6.3	D_{50} and corresponding rock class calculated using Izbash approach. A comparison between values obtained from data, considering both mean velocity and maximum velocity $V_{max} = \bar{V} + 3\sigma$, and from theoretical values calculated following the Dutch method is presented.	68
6.4	D_{50} and corresponding rock class calculated using Pilarczyk formula. A comparison between values obtained from data, considering both mean velocity and maximum velocity $V_{max} = \bar{V} + 3\sigma$, and from theoretical values calculated following the Dutch method is presented.	68
A.1	Table illustrating the measurement protocol for tests 24-30 (Free Flow). For each test are stated the power steps applied, the duration of each subtest, the number of subtests, total duration of the test, which bow thruster is used, the position of the ship, the set-up of the instruments and the average water depth at the quay.	88
C.1	ADV2 results form test 1-9. Mean flow velocity \bar{V} , standard deviation σ , relative turbulence intensity $r = \frac{\sigma}{\bar{V}}$, maximum velocity $V_{max} = \bar{V} + 3\sigma$, dominant direction θ_{dom} and standard deviation of direction σ_{theta} are reported for each step of applied power.	101
C.2	ADV1 results form test 1-9 and 11-22. Mean flow velocity \bar{V} , standard deviation σ , relative turbulence intensity $r = \frac{\sigma}{\bar{V}}$, maximum velocity $V_{max} = \bar{V} + 3\sigma$, dominant direction θ_{dom} and standard deviation of direction σ_{theta} are reported for each step of applied power.	102
C.3	ADCP1 results form test 1-9 and 11-22. Mean flow velocity \bar{V} , standard deviation σ , relative turbulence intensity $r = \frac{\sigma}{\bar{V}}$, maximum velocity $V_{max} = \bar{V} + 3\sigma$, dominant direction θ_{dom} and standard deviation of direction σ_{theta} are reported for each step of applied power.	103
C.4	ADCP2 results form test 1-9 and 11-22. Mean flow velocity \bar{V} , standard deviation σ , relative turbulence intensity $r = \frac{\sigma}{\bar{V}}$, maximum velocity $V_{max} = \bar{V} + 3\sigma$, dominant direction θ_{dom} and standard deviation of direction σ_{theta} are reported for each step of applied power.	104
D.1	Efflux velocity calculated for each step of applied power.	105
D.2	Parameters used to calculate maximum expected velocities at the bottom according to German and Dutch method, for each test taken into account.	105

D.3 Data recorded by ADCP1 and ADV1 during the tests 1, 2, 11, 12. Mean flow velocity magnitude, standard deviation, and maximum velocity calculated as $V_{max} = \bar{V} + 3\sigma$ are presented.	106
--	-----

Introduction

1.1. Motivation

Manoeuvring of ships next to berthing facilities (quay walls) causes the hydraulic load on the bottom to be dominated by propeller's jet. Jet induced by propellers is characterised by the phenomena of diffusion and turbulence, and has been studied by comparison to free jets [2] [24]. Flow field generated by the action of propellers jet is complex, due to the influence of blades of the propellers in jet creation, and then due to the intricate geometry of ship's hull [9]. Ships are often equipped with transverse thrusters to perform mooring operations without the need for tug assistance. Transverse thrusters induced jet has an immediate interaction with quay wall, further complicating the flow field. Moreover, while unconfined jet has received attention from several studies, fewer research has been focussed on flow field induced by propellers when confinement elements such as vertical quay walls or proximity to the sea bed are present [27]. Hence, several knowledge gaps are still present regarding confined propeller jet [8], especially when taking into account the variability among different types of propellers, which vary in number and shape of blades; may be equipped with rudders or nozzles, or, in case of transverse thrusters, can draw water from different locations, such as the side or the bottom of ship's hull [5]. Propeller's induced flow can cause scour on the bed if unprotected, representing a threat for structural stability of mooring facilities. Therefore, an accurate understanding of propeller's induced flow field is fundamental to engineers, in order to quantify scour and proceed to design an adequate bed protection when deemed necessary [9]. In the design phase, the magnitude of the load can affect not only dimensions but also the choice of bed protection typology. Most of the state of the art knowledge is summarized in the PIANC 2015 guidelines, that provide a design strategy consisting in the calculation of the hydraulic load on the bed first, and then of the bottom protection dimension according to stability formulae. The guidelines recommend two alternative methods ("German" and "Dutch") to estimate velocities and design dimensions of the bed protection [15], that are based on the theories of propeller's jet flow (see, for instance [21], [7], [2]). The main design formulas are based on empirical relations, that require constant updating and validation if the input parameters (e.g. typology of propellers, propellers power, material used for the bed protection) change. Specifically, they're mainly based on traditional propellers type. In this research, a ship with a 4-channel systems is utilized, giving also the possibility of investigating the influence of the influx on the bottom that, even though neglected in the calculation of the hydraulic load suggested by the guidelines, has already been identified as relevant for the flow velocities at the bottom [8]. While the design formulae are mainly developed based upon flow velocities, the mechanisms that lead to failure are often due to the loads or forces acting on the bed protection and vary depending on the different types of protection. Traditionally, bottom protections are designed using rock as a material; but rarely stability formulae for rock have been validated under the load of propeller's jet. Furthermore, the formulae traditionally used to calculate the hydraulic load are based on research which considered a limited combination of wall and keel clearance, which doesn't necessary reflects

the most common situations. Guidelines don't provide a clear indication on the width of the bed protection either, which often is designed based on vessel dimensions instead that on the extent of the flow velocities [15]. Therefore, the recommendation proposed in the guidelines might not lead to the most optimized design.

This MSc thesis falls within the bigger framework of a joint research among different companies with the objective of deepening the knowledge surrounding propeller's action near the berthing structures. Following some field measurements at the end of 2018, a consultation took place in early 2019 among Deltares, Rijkswaterstaat, TU Delft, Port of Rotterdam Authority and Rotterdam Public Works Department, leading to the launch of more research on the following subjects:

- Reflection of the propeller jet on the quay wall
- 4-channel bow-thrusters
- Velocity profile of bow-thruster

The data acquired from full scale measurements at the Port of Rotterdam is used to gain better insights in the flow field caused by 4-channel transverse thruster.

1.2. Problem definition

In order to gain a better insight on the complex flow pattern caused by the quay wall reflection of the bowthruster, and to focus the analysis of the data from field measurements, a main research question and four research subquestions are formulated.

Research main question

How does the flow generated by a 4-channel bowthruster develop and evolve on the bottom of a vertical quay wall?

Research sub-questions

- How does the proposed measurement set-up perform and which recommendations can be proposed for future measurements?
- How is the flow field on the bottom influenced by parameters such as: relative distance between outlet and quay wall, height of the outlet in the water column?
- In a 4-channel bowthruster system, what's the difference in the flow field if one or two bowthrusters are used? Does the different configuration of the two bowthruster result in a difference in the flow velocities?
- How can the results of the measurements impact the stability of the bottom material and, consequently, the design of the bottom protection, according to the commonly used guidelines?

1.3. Thesis Outline

In Chapter 1, motivation for the research is presented and research questions are formulated. In Chapter 2, theoretical background concerning propeller's jet is given. Chapter 3 describes fieldwork set-up and measurement programme. In Chapter 4, in-depth checks for a base case and post-processing steps are outlined. Test results are presented in Chapter 5. Comparison with main theoretical formulas is presented in Chapter 6, and Chapter 7 discusses the main findings and discrepancies of the results. In Chapter 9, conclusions of the present research and some recommendations for further studies are proposed. In Appendix A, measurement set-up and protocol for tests not analysed in this report are presented. Appendix B and C presents results for all the analysed tests, Appendix D provides further details on the calculations carried out in Chapter 6. Lastly, in Appendix E surveys of measurement location conducted by Ports of Rotterdam before and after the experiments are depicted.

2

Background

In this chapter, a review of background information and literature relevant to the research is provided. Firstly, a description of channel bowthrusters' characteristics is provided; and a review of the classical formulation of the bowthruuster induced flow field is given. Then, the interaction between bowthrusters and quay wall is investigated, as well as its influence on the bottom material mobility. Then, an overview of the most commonly used guidelines to calculate the propeller-induced hydraulic load on bottom protection is presented. Lastly, instruments utilized during the field measuring campaign and their functioning principles are described.

2.1. Channel bowthrusters

This research focusses on the analysis of data collected during a field experiment where Veth Jet bow-thrusters are used. Veth Jet channel bowthrusters's principle of operation is fairly simple: water is drawn from under the vessel through a horizontal propeller, then, by the means of a rotating drum, it's guided through a channel that ends in the bowthruuster outlet, providing thrust to the vessel. 2 or 4 channel bowthrusters are commonly used in inland transportation vessel, since they provide high maneuverability [5]. An illustration of the bowthruuster is depicted in figure 2.1.

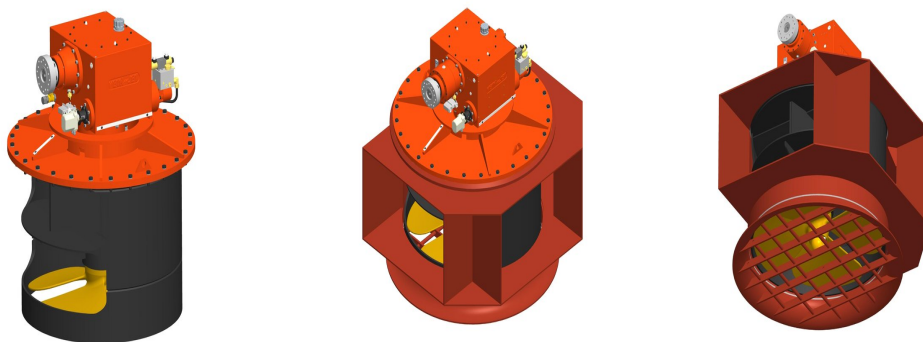


Figure 2.1: Veth Jet bowthruuster. From Veth Propulsion website [16].

2.2. Flow field cause by propellers

Velocity distribution

Albertson et al. suggested that velocity field caused by a propeller can be investigated through the resemblance with a plain water jet, and that the investigation can be conducted using the axial momentum theory [2]. General features of jets are: diffusion, mixing layers and a great amount of turbulence that derives by the decelerating flow [26]. The flow field generated by a free, unrestricted jet can be divided in two regions: a core where the flow velocity is equal to the efflux velocity, and the diffused jet. Other terms that can be used to describe these two different zones are zone of flow establishment and zone of establishment flow. Velocity distribution induced by a transverse thruster can be observed in figure 2.2.

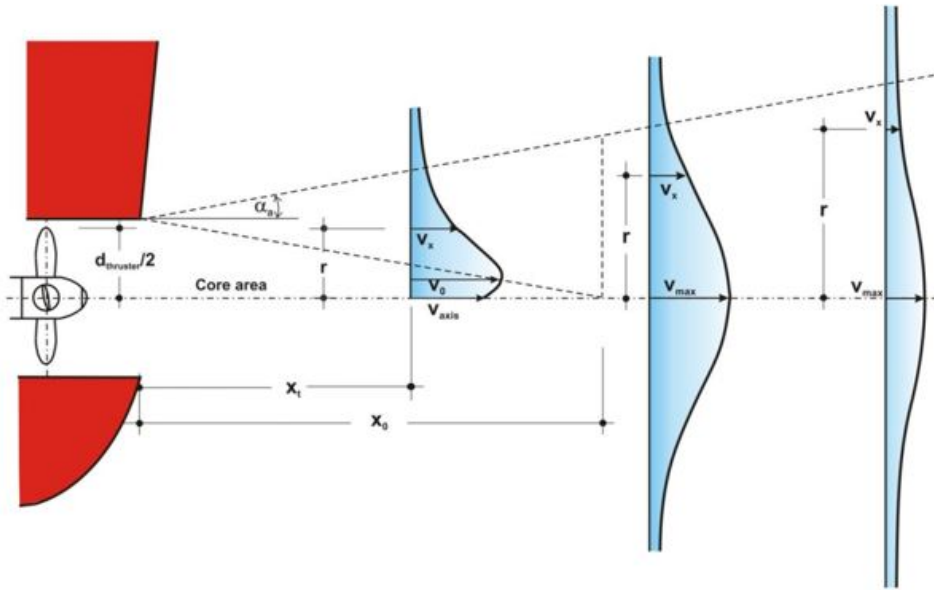


Figure 2.2: Velocity distribution induced by a transverse thruster. From PIANC [15].

To model the free jet, Albertson et al. presented the following equations for the zone of the established flow:

$$V_{axis} = \frac{1}{2C} V_0 \frac{D_0}{x} \quad (2.1)$$

and

$$\frac{V_{x,r}}{V_{axis}} = \exp\left[-\frac{1}{2C^2} \frac{r^2}{x^2}\right] \quad (2.2)$$

where:

V_{axis} : flow velocity in the axis of the jet [m/s]

V_0 : efflux velocity [m/s]

D_0 : jet diameter at the beginning of the jet [m]

x : horizontal distance from the outflow of the jet [m]

r : radial distance from the jet axis [m]

C : coefficient [-]

The equations are valid for a free jet, meaning that the jet is not restricted by any boundary, nor affected by any other feature such as rudders, ducts, etc. A Gaussian distribution of the flow around the axis is assumed. In reality, the propeller's jet is limited by the bed and the berthing structures, and, depending on the type of propellers, the effect of rudders, ducts, etc. has to be taken into account. This introduces some discrepancies between the velocity field of a free jet and the one. Furthermore, the rotational flow velocity and the swirl at the

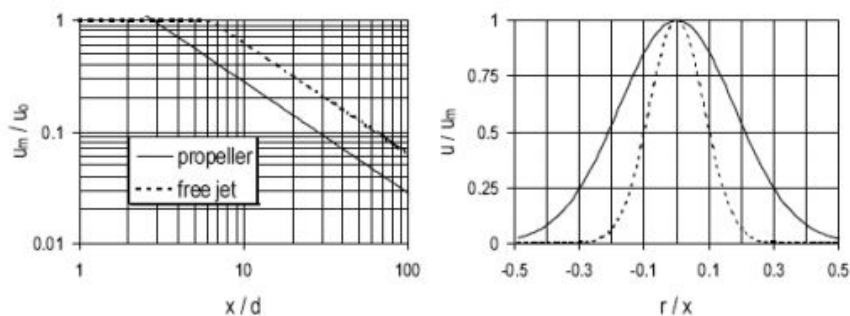


Figure 2.3: Differences in flow velocities between propeller jet and free jet. From [15].

tip of the propeller blades induce a higher turbulence level, a shorter length of the flow establishment zone and a wider radial spread, as illustrated by Hamill and Johnston [17]. Verheij [25] [26] compared the velocities and turbulence of a free jet with the ones resulting from a propeller's jet. As it can be seen in figure 2.3, the maximum value of turbulence intensities for propeller jets are higher than for a free jet, while the mean flow velocity decreases quickly with the increasing distance from the propeller. This lead Verhagen to the conclusion that the propeller jet is diverging more with respect to a free jet [24].

2.3. Reflection on quay wall: previous researches

Blokland (1997)

In collaboration with Ports of Rotterdam, Blokland conducted measurements on flow velocities and erosion at the bottom of a vertical quay wall in the Beneluxhaven. Measurements were conducted using a tug equipped with two bowthrusters. The angle of the propeller's blades could be adjusted between -20 degrees and +23 degrees ('pitch'). Angle and distance between propeller axis and quay wall, and pitch were varied during the measurements. Measurements were made using both acoustic and electro-magnetic instruments (UCM and EMS). Blokland found velocities higher with a factor between 1.3 and 1.45 than the ones calculated with German and Dutch methods, based on free jet theory. He also found high turbulence intensities, with maximum flow velocities ca 1.8 times time-averaged velocities.

Schmidt (1998)

If the propeller jet is caused by a bow thruster, it reflects on the quay wall. Schmidt [19] identified different zones of the reflected flow, as depicted in figure 2.4. Zone 1 is the zone of flow establishment, where the velocity is equal to the efflux velocity. Zone 2 is the zone of established flow, where the axial and radial velocities can be calculated according to formulas 2.2 and 2.1. In zone 3, the velocity is converted into pressure, while in zone 4 the pressure becomes again kinetic energy, and the flow is reflected along the quay wall. In zone 5, a return flow along the bottom is present.

Schmidt theory has been derived from scale-model measurements, conducted varying keel clearance and quay clearance of the model, and it is one of the theory behind the German method recommended by PIANC.

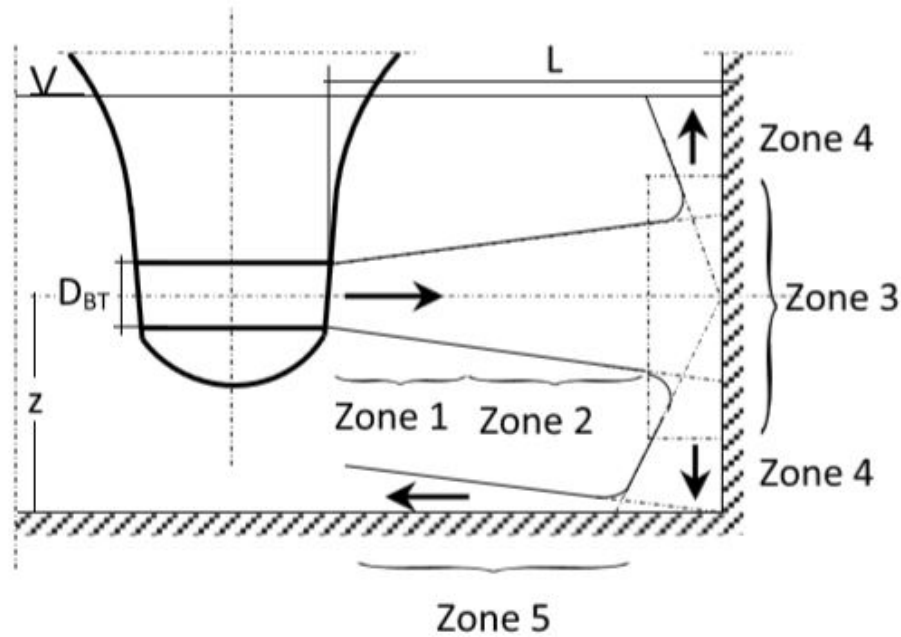


Figure 2.4: Zones of a flow field from a transverse thruster against a quay wall. From [1].

TU Delft Master Thesis (2000s)

In the first years of 2000s, several master thesis at TU Delft undertook bowthruster's jet as a topic. Van der Laan [23] used a physical model to validate a numerical (CFD) model, not finding a good correspondence between them, probably due to a limited number of measuring points and a possible overestimation of flow rate of the bowthruster in the physical model [20]. Van Blaaderen [20] adopted a similar approach, highlighting the importance of modelling turbulence correctly in the CFD model in order to obtain similar turbulence intensity levels as in the physical model. He also pointed out influence of bowthruster characteristics on the flow velocities. Both these master thesis questioned the assumption that a bowthruster jet can be modelled as a free flow, upon which the classic formulas by Römisch and Fuherer [7], and Blaauw and van de Kaa [21] have been developed.

Deltares Knowledge Gap (2015)

Within the framework of research on knowledge gaps about propeller jets issued by SBR-CURnet, model tests have been performed in Deltares to investigate flow patterns induced by a propeller's jet reflecting on a vertical quay wall. Discrepancies with the guidelines have been highlighted: while the guidelines have been found conservative for most of the tests, some tests with a large wall clearance induced velocities higher than expected. Furthermore, maximum velocities didn't occur always in the expected location [8]. This study was conducted with a schematic model of a ship's hull: therefore, the effect of the shape of the ship was not studied. However, in some tests were recorded velocities directed towards the quay wall, identifying thus influence of the inflow.

Wei and Chiew (2019)

Wei and Chiew [27] conducted experiments in a recirculating flume using particle image velocimetry. Velocities induced by a rudder-less propeller impinging a vertical wall were measured, testing the effect of four different wall clearances. Both streamwise central plane and transverse impingement plane at the wall have been measured. Results shown how two mechanisms control development of the jet: jet diffusion and wall obstructions. Wall clearance determines relative importance of the two: with increasing wall clearance, wall obstruction dominance decreases. Velocities at the bottom were though not measured, leaving

unknown how different wall clearances translate into bottom flow patterns.

2.4. Calculation methods for the hydraulic load on the bed according to the most common guidelines

Several guidelines are available to calculate the hydraulic load on the bed. Bed velocities are needed in order to estimate the scour hole depth and length, and the bed protection dimensions, according to the adopted approach. BAW and PIANC guidelines are examples of policies adopted in Europe. PIANC 2015 guidelines suggest two methods ("German" and "Dutch", from the nationalities of the researchers whose theories are the formulas based on) to calculate bottom velocities and, then, estimate protection dimension accordingly. It has to be noted that both the methods are developed with the final objective of the design and not of the accurate physical representation of the propeller jet; therefore, the two methods should not be mixed [15]. In this section, the formulas suggested by the guidelines are illustrated. The first step is to calculate the efflux velocity of the propeller. The main factors affecting the efflux velocity are the diameter of the propeller, the maximum number of revolutions and the thrust coefficient (dimensionless relationship between propulsive force, number of revolutions (n) and diameter of the propeller (D)). A proposed relation is derived from the Bernoulli equation and the thrust force:

$$V_0 = \alpha n D \sqrt{K_T} \quad (2.3)$$

In many situations, though, it is difficult to obtain exact information about the number of revolutions and/or the thrust coefficient; therefore, empirical relations are used. One of the most used empirical formula for the efflux velocity is equation 8-10 from PIANC Report 180 [15]:

$$V_{0,thruster} = 1.15 \left(\frac{P_{thruster}}{\rho_w D_{thruster}^2} \right)^{0.33} \quad (2.4)$$

where:

$V_{0,thruster}$: efflux velocity [m/s].

$P_{thruster}$: propeller's power [W].

ρ_w : water density [kg/m³].

$D_{thruster}$: propeller diameter [m].

To calculate the velocity in the axis of the jet and at the generic location x,r (where x is the distance along the jet plan and r is the radial distance from the jet axis), both Dutch and German method start from the formulas elaborated by Albertson et al. [2]:

$$V_{axis} = \frac{1}{2C} V_0 \frac{D}{x} \quad (2.5)$$

and

$$V_{x,r} = V_{axis} \exp \left[-\frac{1}{2C^2} \frac{r^2}{x^2} \right] \quad (2.6)$$

where:

V_{axis} : flow velocity in the axis of the jet [m/s]

V_0 : efflux velocity [m/s].

D: diameter at the beginning of the jet [m].

x: horizontal distance from the outflow of the jet [m].

r: radial distance from the jet axis [m]. C: coefficient [-] that varies according to the formula used.

German method

German method, presented in EAU and BAW regulation, is based on research by Fuehrer, Römisch and Engelke [7], who, after the derivation of values for each coefficient in Albertson et al. equations, obtained the following formulae for a free jet:

$$V_{axis} = V_0 \quad \text{in the zone of flow establishment (for } x_p < 2.6) \quad (2.7)$$

$$V_{axis} = 2.6V_0 \left(\frac{x}{D_p} \right)^{-1} \quad \text{in the zone of free jet propagation (for } x_p > 2.6) \quad (2.8)$$

$$V_{x,r} = V_{axis} \exp \left[-\frac{22.2r^2}{x^2} \right] \quad (2.9)$$

It has to be noted that these formulae are derived for conventional propellers and should be modified in case ducted propellers are adopted [3].

Maximum velocity at the bottom is expected in the corner between bottom and quay wall, and can be computed according to:

$$V_{bottom} = a_L 1.9V_0 \left(\frac{L}{D_p} \right) \quad (2.10)$$

where: a_L : empirical coefficient V_0 : efflux velocity [m/s] L : distance between quay wall and outlet [m] D_p : diameter of the propeller [m] Value of a_L follows from figure 2.5.

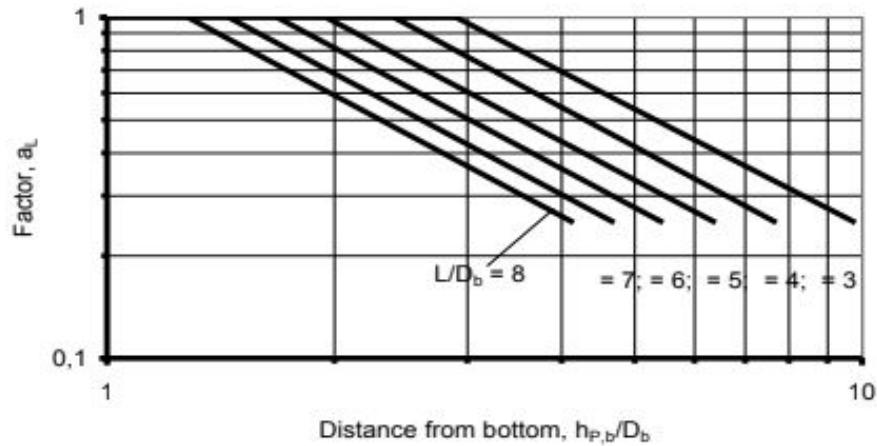


Figure 2.5: Factor a_L as a function of the wall and bottom distance. From PIANC [15].

Dutch method

Similarly to the German method, also the Dutch method derives coefficients for the equations 2.5 and 2.6, resulting in:

$$V_{axis} = 2.8V_0 \left(\frac{D_p}{x} \right) \quad (2.11)$$

and

$$V_{x,r} = V_{axis} \exp \left[-\frac{15.4r^2}{x^2} \right] \quad (2.12)$$

The length of the establishment zone, where $V_{axis} = V_0$, is here assumed as 2.8 times the propeller's diameter. The coefficients are derived for ducted propellers.

On the quay side, the maximum velocity at the bottom is calculated as

$$V_{b,max} = 1.0V_0 \frac{D_{thruster}}{h_{thruster}} \quad \text{for } L/h_{thruster} < 1.8 \quad (2.13)$$

$$V_{b,max} = 2.8V_0 \frac{D_{thruster}}{L + h_{thruster}} \quad \text{for } L/h_{thruster} > 1.8 \quad (2.14)$$

with L representing the distance between outflow opening and quay wall.

2.5. Stability formulae for bottom materials.

Bowthrustrer induced flow field, especially when the flow is reflected on a vertical quay wall, can affect the stability of the bottom material, cause scour and, therefore, give the need for a bottom protection. In this research the focus is on flow velocity; nevertheless, a review of the main stability theories is presented, with the objective of having an insight on the impact that that the studied hydraulic load can have on practical applications.

Izbash

Izbash approach is based on the balance of forces acting on a single grain. Active forces caused by main flow velocity and turbulence (drag force, lift force and shear forces) are contrasted by passive forces (gravity and friction between the grains). If the load, represented by the active forces, is higher than the strength, the grains move. The resulting balance of forces leads to the design equation 2.15:

$$d_{n50} \leq \beta_{Iz,cr} \frac{V_{b,max}^2}{2g\Delta} \quad (2.15)$$

where:

d_{n50} : median stone diameter [mm].

$\beta_{Iz,cr}$: Izbash stability parameter [-].

$V_{b,max}$: maximum velocity at the bottom [m/s].

Δ : dimensionless relative buoyancy of rock in water [-].

Izbash relation is based on experiments conducted for big rocks in shallow water, but the location where the bottom velocity is defined is not always clear. Therefore, for design purposes, the maximum velocity at the bottom is assumed. Blokland [4] recommends values of $\beta_{Iz,cr}$ between 2.5 and 3 for flow induced by propellers jet.

Shields

Shields approach is based on the average velocity on an area of the bed, instead that for the single grain. The load on the bed is represented by the shear stress. The classical formulation of Shields stability relation is in equation 2.16.

$$\Psi_c = \frac{\tau_c d^2}{(\rho_s - \rho_w)gd^3} = \frac{u_{*c}^2}{\Delta g d} \quad (2.16)$$

where:

Ψ_c : Shields stability parameter [-].

τ_c : critical shear stress [N/m^2].

u_{*c}^2 : critical shear velocity [m/s].

Δ : dimensionless relative buoyancy of rock in water [-].

Shields critical stability parameter is dependant on the diameter, making the formula not straightforward for the design. Shields used the depth averaged velocity, assuming therefore uniform flow with a logarithmic vertical velocity profile and a fully developed boundary layer. This has been taken into account, especially when the load is induced by propeller's jet.

Pilarczyk

Pilarczyk developed another empirical relation of stability for design purposes:

$$d_{n50} = \frac{\Phi_{sc}}{\Delta} \frac{0.035}{\Psi_{cr}} k_h k_{sl}^{-1} k_t^2 \frac{V^2}{2g} \quad (2.17)$$

where:

Φ_{sc} : stability correction factor. It incorporates the edge effect caused by the transitions in the bottom protection layer, and it depends on the application and placement.

Ψ_{cr} : mobility parameter of the protection element, related to the Shields parameter and material-dependent.

k_h : velocity profile factor. This parameter is used to pass from a depth-average velocity to the velocity near to the one near bottom.

k_t : turbulence factor. It is recommended that this factor is derived from the turbulence intensity $k_t = \frac{1+3r}{1.3}$ [6]. For the flow under propeller jets, several values are recommended by the guidelines, following from the research by Blaaw and van der Kaa [21]; Blokland [4]; Römisch [7] [15].

k_{sl} : slope side factor, taking into account the relation between the internal angle of friction of the material, and the slope of the bottom.

Δ : dimensionless relative buoyancy of rock in water [-].

2.6. Equipment used to measure velocities

In this section, an overview of the Acoustic Doppler Current Profiler (ADCP) and Acoustic Doppler Velocimeter (ADV) characteristics is given. ADCPs measure over a distance from the instrument (range) that can be set. They measure the mean velocity over a measuring volume that increases with the distance from the instrument. Measuring the averaged velocities over an area, and therefore assuming an horizontal homogeneity of the flow, ADCPs are particularly suitable to measure oceanic currents, while ADVs, which measure on a small measurement volume near the instrument, are commonly used to measure turbulence and velocities in boundary layers. A picture of an ADCP (Nortek Signature 1000) and an ADV (Nortek Vector) are presented in figure 2.6.



Figure 2.6: Picture of a Nortek Signature 1000 ADCP (left) and of a Nortek Vector ADV (right).

Principle of operation

Acoustic Doppler Current Profiler (ADCP) and Acoustic Doppler Velocimeter (ADV) use the physical principle of the Doppler effect to measure velocities. The Doppler effect consists in a change of frequency of a wave when the wave source moves with respect to an external observer, or when the observer itself moves with respect to the wave source [12]. The instruments function by transmitting high-frequent sound waves into the water column, measuring the Doppler shift of the returning signal and converting it into velocities using the speed of sound. An illustration of the principle is shown in figure 2.7.

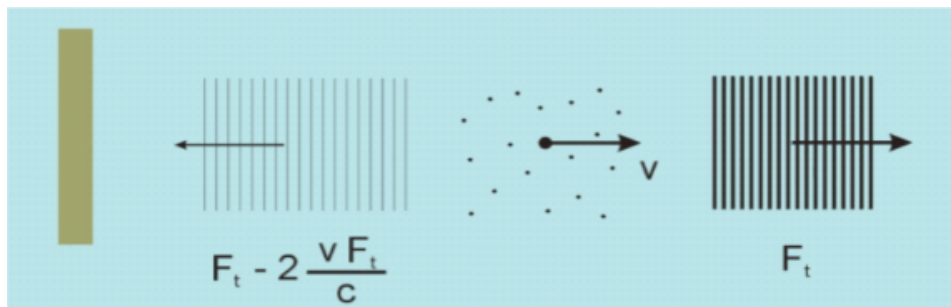


Figure 2.7: Illustration of the shift in frequency of the acoustic echo reflected from moving particles. From Nortek's comprehensive manual [12].

The relative current velocity can be calculated with the equation:

$$V = \frac{F_{Doppler}}{F_{source}} * \frac{C}{2} \quad (2.18)$$

Where:

V : current velocity.

$F_{Doppler}$: change in received frequency.

F_{source} : frequency of the transmitted sound wave.

C : speed of sound in water.

It is important to note that the signal is not reflecting by the water itself, but from particles suspended into the water. These can be sediment, zooplankton or air bubbles. Key assumption of the use of these instruments is therefore that the particles move at the same velocity as the water. In case there is not sufficient scattering material in the water, it is necessary to provide it. This is usually the case during laboratory experiments, while for measurement in the field the natural presence of sediment and air bubbles in the water provide sufficient seeding.

Measuring with ADVs

The two types of instrument, despite using the same physical principle to measure velocities, present substantial differences. Vector, Nortek's Acoustic Doppler Velocimeter, or ADV, presents a configuration composed by a head and a case. In the head, the three beams host the three velocities receivers, that, measures the echo of the initial pulse emitted from the transmitter, located in the centre. Knowing the relative orientation of the axes, the 3D water velocity in the sampling volume can be calculated. Being the three beams slanted 30 degrees with the vertical axes, their angular bisector is 15 degrees away from the transmit beam, ensuring a lower measurement uncertainty to the vertical component of the velocity. The sampling volume is defined by the intersection of the beams, that happen at 157 mm from the transmitter, and by the range gating. Figure 2.8 depicts the vector system of transmit and receive beams while an illustration of the measuring volume is illustrated in figure 2.8 and 2.9.

In the Nortek Vector, all the sensors are stored in case that can be connected to the head via cable, or via fixed stem. The correct orientation of the case is fundamental to ensure the usage of compass and other sensors data [14].

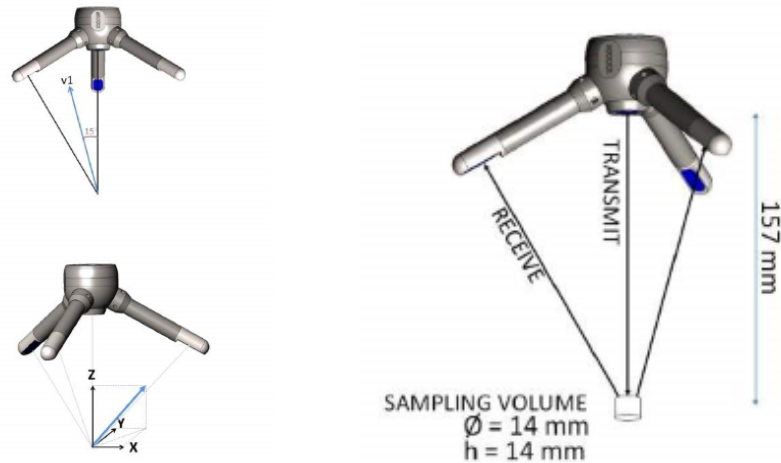


Figure 2.8: Vector transmit and receive beams. Figure 2.9: Vector measuring volume, identified by the interception of the three beams. The bisector of the angle between them indicates the velocity to which the receivers are sensitive. From Nortek Comprehensive Manual Velocimeters [14]. The blue arrow in the lower image indicates a positive velocity. From Nortek Comprehensive Manual Velocimeters [14].

Measuring with ADCPs

Acoustic Doppler Current Profilers, as well as the ADVs, use the Doppler shift to measure water velocities. Differently than the ADV, though, velocities measured by the beams are averaged on the area that the beams cover. Horizontal homogeneity is therefore assumed in this area. Nortek Signature 1000 is equipped with 4 beams, slanted of 25 degrees with respect to the vertical, and a central 5th beam (altimeter), that ensures a well resolved vertical motion [13]. Each pair of beams measure one vertical and one horizontal velocity component: the redundancy in the measurement allows for a check on the assumption of horizontal homogeneity of the velocity. The measurement area is defined by the beams, and covers a distance (range) that depends on the available scattering in the water. The range is divided in cells, which depth can be chosen by the user. Minimum cell size is 20 cm. The transducers work both as transmitters and as receivers: this yields to the necessity of a blanking distance between the instrument and the first cells. An illustration of the velocity profile is illustrated in figure 2.10.

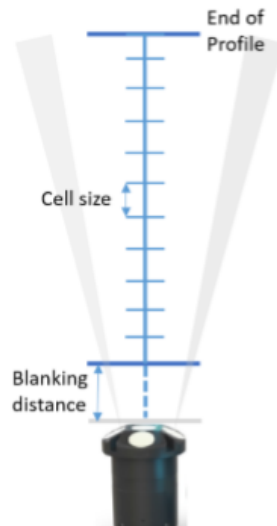


Figure 2.10: Definition of velocity profile. The centre of each cell is located at a distance from the transducer equal to centre of cell $n = \text{blanking distance} + n \cdot \text{cell size}$. From Nortek Signature Operation Principles [13].

It has to be noted how the volume of the cell increases with the distance from the instrument, depending on the angle between the beams. Under the assumption of horizontal homogeneity, this doesn't represent a reduction in accuracy of measured velocity. However, if the ADCP is used to measure a turbulent flow, this has to be taken into account while evaluating the representativity of the averaged velocity on the general flow pattern.

3

Methodology

In this chapter, a description of the measurements is presented, starting from the scope of it. Equipment used, measurement set-up and protocol, and reference system are presented. An overview of the conducted tests characteristics is presented.

3.1. Scope of the measurements

The following measurements scope and programme are the outcome of the compromise between the interest of several parties involved, among which there are Rijkswaterstaat, Ports of Rotterdam, Deltares, Gemeente Rotterdam, Boskalis, TU Delft. Main objectives of the measurements are:

- Investigate the reflection of the 4-channel system bow-thruster flow at the quay
- Investigate the free flow by the 4-channel system bow-thruster. In this report, however, only the reflected flow of the bowthruster are examined. Therefore, in this chapter, only the measurement programme and set-up for the reflected flow can be found. A summary of measurement set-up and programme for free flow measurements can be found in appendix A.

Focus is primarily on the bottom velocities, with the objective of comparing the data with the proposed design methods for the bottom protection. Flow pattern resulting from the interaction of the bow-thruster jet with the quay, the bottom and the ship's hull might give the hydraulic load dominant for the bottom stability. At the same time, investigation of the spatial distribution of the flow along the quay wall will give further insights in understanding the phenomenon, with possible applications in numerical modelling calibration and design of bottom protection.

3.2. General information

Location of the measurements - Antarcticakade, Port of Rotterdam

The Antarcticakade is located next to the Yangtzekanaal in the Maasvlakte. Depth of the quay varies between 7 m and 9 m along the quay. The bottom of the quay is protected with loose rock of 10-60 kg, partially penetrated with colloidal concrete. Width of the bottom protection varies between 20 and 25 m, with a thickness of around 0.85 m. Location of the quaywall on the Maasvlakte can be seen in figure 3.1.

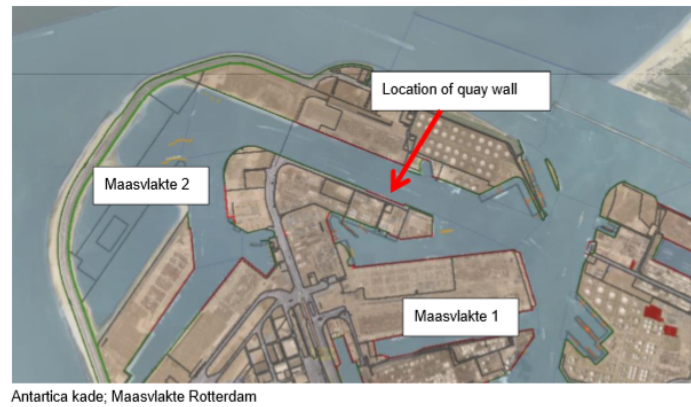


Figure 3.1: Location of measurements on the Maasvlakte. From Deltares report on field measurements conducted in 2018 [22].

A cross-section of the quay is provided in figure 3.2.

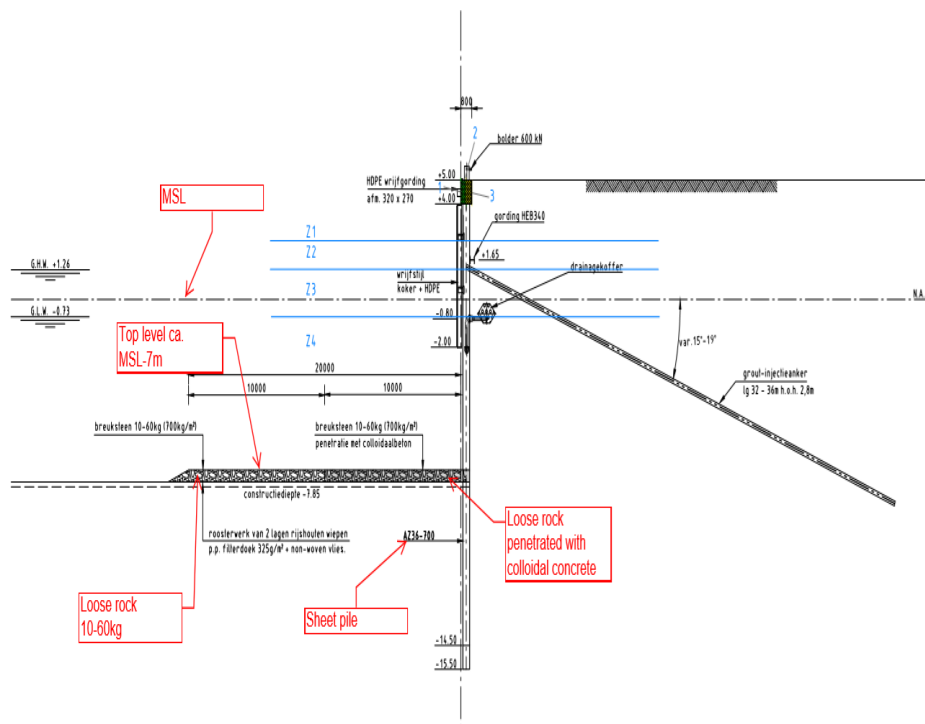


Figure 3.2: Location of measurements on the Maasvlakte. From Deltares report on field measurements conducted in 2018 [22].

Vessel used for the measurements - MTS Vorstenbosch

The vessel found for the measurements is the MTS Vorstenbosch, an inland vessel with the main dimensions listed in table 3.1.

Table 3.1: MTS Vorstenbosch characteristic dimensions.

Characteristic dimension	Value
Length	147.5 m
Breadth	22.8 m
Max. Draught	5.4 m

MTS Vorstenbosch is equipped with two Veth Propulsion 4-channel bowthrusters, type Veth Jet 4-K-1400A. A summary of their characteristics is listed in table 3.2.

Table 3.2: Veth jeth bowthruster characteristics.

Characteristic	Value
Max power	618 kW
Nom. revolution rates/min	1800
Reduction	4, 909:1
Propeller diameter	1420 mm
Thrust	11 kg/kW

The two channels have a different length; therefore the position of the two outlets with respect to the quay varies. From now on, the bow-thruster positioned more towards the stern is named bow-thruster 1, while the bow-thruster positioned more towards the bow is called bow-thruster 2. A technical drawing of the bow-thrusters is shown in figure 3.3.

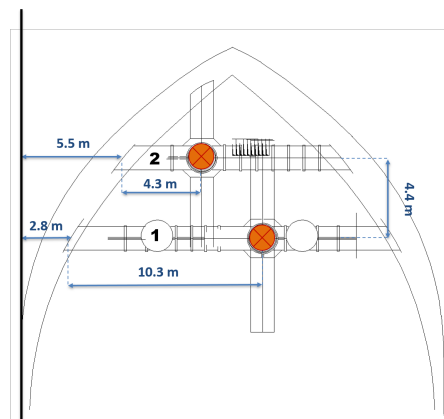


Figure 3.3: Bowthrusters system in the Vorstenbosch. In figure, bowthruster 1 and 2 are indicated, as well as their channel lengths, distance between the outlet and the quay wall (assuming that the ship is moored perfectly against it), and distance between the two channel axis. The suction points of each bowthruster are highlighted in orange. From technical drawings of the vessel, modified by the autor.

Figure 3.4 shows the ship moored at the quay during the measurements.



Figure 3.4: MTS Vorstenbosch moored at the Antarcticakade during the measurements, on June 18th, 2019. Photocredits E.J. Houwing.

3.3. Reference system

A general inertial reference system is adopted for the measurements of the reflected flow. As a fixed reference, the quay wall is taken: direction perpendicular to the quay wall identifies the x axis, direction along the quay wall identifies the y axis. Z axis is in the vertical direction. The x, y, z axis are a positive oriented triplet of axis. Intersection between x and y axis is located at the intersection between the edge of the quay wall and Bollard 31, which is used as a reference point to place the instruments, while origin of the z axis is assumed to be at the bottom of the sea. To obtain coordinates of the bowthrusters with respect to the general reference system, the port side of the ship is assumed to maintain a constant distance from the quay of 0.5 m, and position of the bowthrusters is therefore derived by the technical drawings of the vessel.

This general reference system is not always corresponding to the instrument's one; therefore, transformation are sometimes required in order to obtain velocities according to the reference system. Namely, during tests from 1 to 23, ADCPs are oriented horizontally; as a consequence, beam velocities are retrieved, and not coordinates one. Assuming a correct positioning and no movements of the instruments during the tests, the ADVs' reference system always corresponds to the general one. Furthermore, three ships position are considered for these measurements. It is assumed that moving the ship is equivalent to have more measurement points; therefore, a vessel reference system centered on the first ship position has been assumed. Pictures of the reference system are illustrated in the next section, and a general summary of instrument locations with respect to the vessel is provided in figure 3.14.

From beam velocities to xy velocities

Due to the horizontal orientation, ADCPs are set to measure velocities according to their beam reference system. It is therefore necessary to apply a transformation to change from beam velocities to x and y velocities, in order to have velocities that are consistent with the general reference system and to allow comparison with the ADVs, which measure x, y and z velocities consistently with the general reference system. Only beam 2 and beam 4 are used, and therefore only the horizontal velocity can be calculated. It has to be noted that usually it is the instrument that does the transformation from beam to xyz velocities, automatically correcting for pitch and roll and calculating 2 vertical velocities due to the redundancy of the data, allowing for a check of the accuracy of the calculated velocities. This checks are neglected in the following transformation: it is therefore assumed that the cells of beam 2 and the cells of beam 4 are not slanted. The transformation applied follows from the transformation matrix of the instrument:

$$v_x = 0.5v_2\cos\alpha + 0.5v_4\cos\alpha \quad (3.1)$$

$$v_y = -0.5v_2\sin\alpha + 0.5v_4\sin\alpha \quad (3.2)$$

where:

v_x : instantaneous velocity component along x in the general reference system.

v_y : instantaneous velocity component along y in the general reference system.

v_2 : instantaneous velocity measured in beam 2.

v_4 : instantaneous velocity measured in beam 4.

$\alpha = 25^\circ$: angle of which the beams are slanted with respect to the central axis.

It has to be noted how the in-line velocity recorded on beams 2 and 4 is averaged as representative to the entire cell.

In figure 3.5 , an illustration of the vectors representing the velocities can be seen.

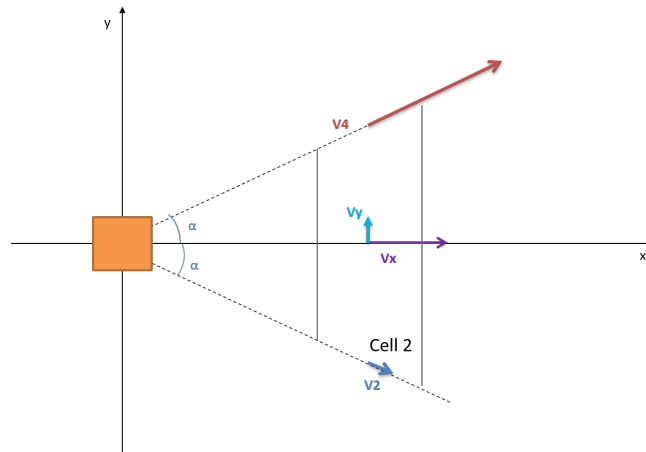


Figure 3.5: Illustration of the ADCP's beam reference system compared to the general reference system and of the transformation from beam velocities to x and y velocities. An outline of cell 2 is also indicated. Source: author.

3.4. Instruments set-up

The instruments (2 ADVs and 2 ADCPs) are mounted on singular frames made of wood and then fixed on a scaffolding. This is then laid on the sea bottom by the team of divers from Boskalis. For the reflected flow, the scaffolding is positioned next to the quay wall, in correspondence of bollard 31. The ADCPs are mounted horizontally: beam 2 and beam 4 define the horizontal plane. A schematic representation of the instruments mounted on the scaffolding and their relative distance is depicted in figure 3.6.

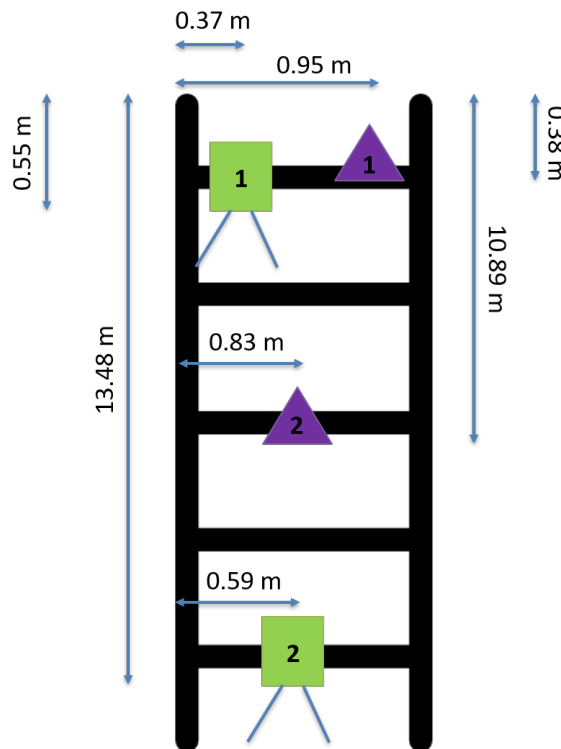


Figure 3.6: Schematic representation of the instrument mounted on the scaffolding. The green squares symbolizes the ADCPs, while the purple triangles the ADVs. The number associated with each instrument is also illustrated. Source: author.

Position of the instrument with respect to the adopted reference system is illustrated in figure 3.9 and 3.10. A picture of the instruments mounted on the wooden frame is presented in figure 3.7.

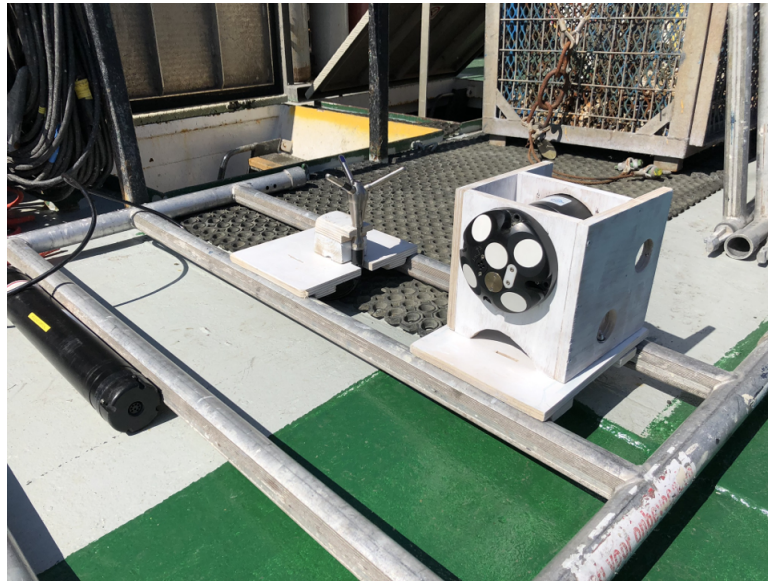


Figure 3.7: Picture of ADCP and ADV mounted on their wooden frame and then on the scaffolding. Picture taken during the measurement preparation day, on Monday 17th of June, 2019. Photocredits: author.

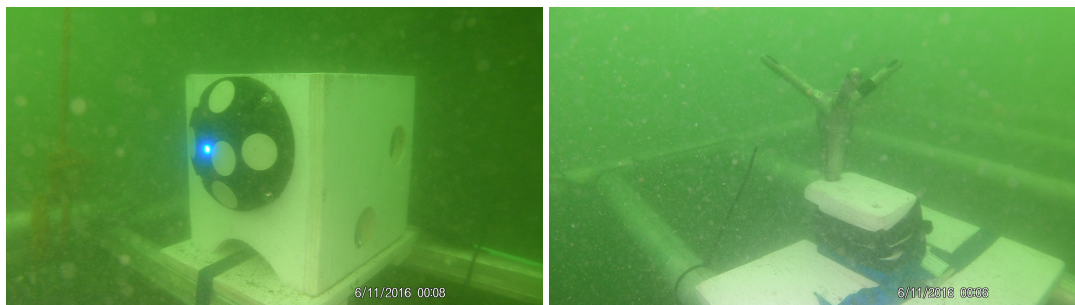


Figure 3.8: Picture of ADCP1 (left) and ADV1 (right), when submerged and measuring. Photocredits: Boskalis diving team.

3.5. Considered ship positions

For the measurements of reflected flow, the three considered ship positions are illustrated in figure 3.11, 3.12 and 3.13. The reference line in correspondence of bollard 31 indicates the position of the instruments. Ship is moored against the quay wall and assumed to be 0.5 m distant from it.

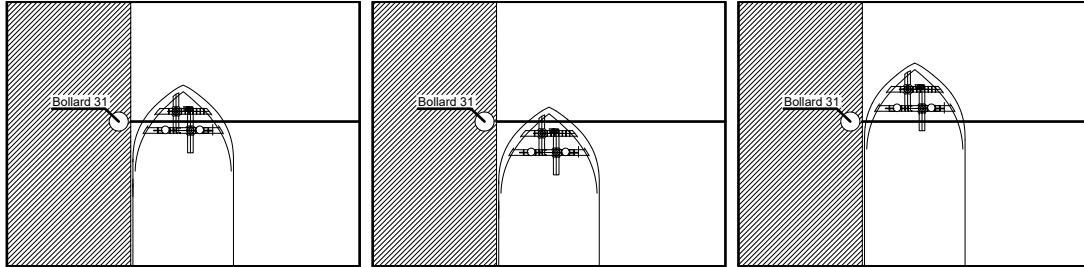


Figure 3.11: Ship position 1. Horizontal line indicates position of the instruments. Source: author.

Figure 3.12: Ship position 2. Horizontal line indicates position of the instruments. (5 m behind position 1). Source: author.

Figure 3.13: Ship position 3. Horizontal line indicates position of the instruments. (5 m ahead of ship position 1). Source: author.

3.6. Summary of measurement location

As a summary of the density of measurement points on the bottom of the quay wall, the location of the instruments with respect to the bow-thrusters for each ship position can be seen in figure 3.14. In the analysis of the data it is assumed that moving the ship is equivalent to have an instrument located in the correspondent relative distance with the bowthrusters. For the ADCPs, central location of cell 2 is indicated. A schematic outline of the ship is also presented, including inlets and outlets of the bowthrusters.

3.7. Set-up limitations

It has to be noted that this instrument set-up presents some limitations. Firstly, the horizontal orientation of the ADCPs has as a consequence that only 2 beams can be used to retrieve velocity. Indeed, beam 3, directed upwards, hits the ship; while beam 4, directed downwards, hits the bottom protection. Therefore, only the velocities in the horizontal plane can be retrieved for the ADCPs, and without any redundancy. Furthermore, utilizing the ADCPs to measure a turbulent flow present intrinsic limitations: since the measurement volume increases considerably with the distance from the ADCPs, in presence of a turbulent and highly variable in space flow, only the first smaller cells can be trusted to have data which is representative of the flow. Regarding the ADVs, a limitation deriving from this measurement set-up lies in the fact that the case of the instrument is not located in correspondence of the measurement head. Therefore, information that are collected by sensors in the case (such as pressure) can't be appropriately correlated with velocity measurements. Moreover, ADV1's case is supposed to be mounted vertically, which can't be done in the current measurement set-up.

3.8. Measurement programme

After the first day of preparation, the following final measurement plan is defined. 30 tests are performed, divided in two main categories: in the first one, the bow-thrusters on the port side of the vessel are activated against the quay wall, generating a reflected flow; in the second one, the ship is rotated and the same bow-thrusters are activated on the free side of the ship. The duration of each test is around 8 minutes: each test is divided in subtests, each of them representing a step in percentage of power applied. This way, the relation between applied power, mean flow velocity and turbulence intensity can be investigated. The general measurement protocol for the test against the quay wall is:

- Each bow-thruster is activated for 2 minutes for 4 applied power steps (25%, 50%, 75% and 100%), then both bow-thrusters are activated. The three tests are repeated for three different ship positions: ship positioned such that the instruments are in the middle between the two bow-thrusters axis (position 1); 5 m behind with respect to position 1 (position 2) and 5 m ahead with respect to position 1 (position 3).

Two tests represents exceptions to this general protocol, namely Test 10, where the two bow-thrusters are left on at 50% of power during rising tide, and Test 23, where a de-berthing manoeuvre is performed using both bow-thrusters.

A summary of the tests characteristics is presented in table 3.3.

Table 3.3: Table illustrating the measurement protocol for tests 1-23 (Reflected Flow). For each test are stated the power steps applied, the duration of each subtest, the number of subtests, total duration of the test, which bow thruster is used, the position of the ship, the set-up of the instruments and the average water depth at the quay.

Test	Subtest			Bow thruster	Ship Position	Set-up	Average water depth at the quay [m]
	Steps of applied power	Duration of each subtest [min]	Total duration of the test [min]				
1	25%, 50%, 75%, 100%	2	8	1	1	(Reflected Flow)	6.43
2	25%, 50%, 75%, 100%	2	8	2			6.43
3	25%, 50%	2	4	Both			6.44
4	25%, 50%, 75%, 100%	2	8	2	2		6.46
5	25%, 50%, 75%, 100%	2	8	1			6.5
6	25%, 50%, 75%, 100%	2	8	Both			6.52
7	25%, 50%, 75%, 100%	2	8	1	3		6.7
8	25%, 50%, 75%, 100%	2	8	2			6.78
9	25%, 50%, 75%, 100%	2	8	Both			6.9
10	50%	30	30	Both	1		7.47
11	25%, 50%, 75%, 100%	2	8	1			7.97
12	25%, 50%, 75%, 100%	2	8	2			8.19
13	25%, 50%, 75%, 100%	2	8	Both	2		8.28
14	25%, 50%, 75%, 100%	2	8	1			8.22
15	25%, 50%, 75%, 100%	2	8	2			8.16
16	25%, 50%, 75%, 100%	2	8	Both	3		8.09
17	25%, 50%, 75%, 100%	2	8	1			7.98
18	25%, 50%, 75%, 100%	2	8	2			7.94
19	25%, 50%, 75%, 100%	2	8	Both	1		7.91
20	25%, 50%, 75%, 100%	2	8	1			6.73
21	25%, 50%, 75%, 100%	2	8	2			6.7
22	25%, 50%, 75%, 100%	2	8	Both	Moving		6.66
23	100%	7	7	Both			6.61

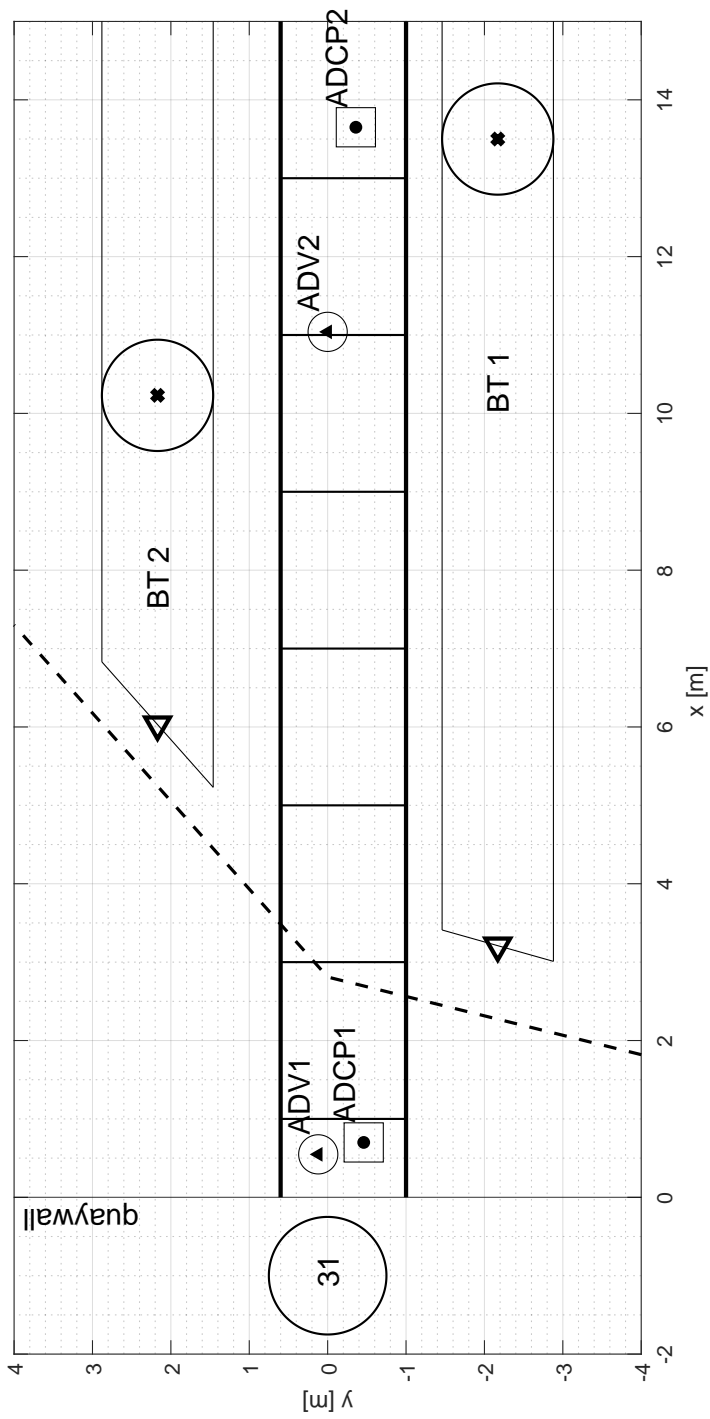


Figure 3.9: Plan view of instrument set-up for the reflected flow. The grid of the chosen reference system is illustrated, as well as the quay wall and the reference point of bollard 31. Source: author.

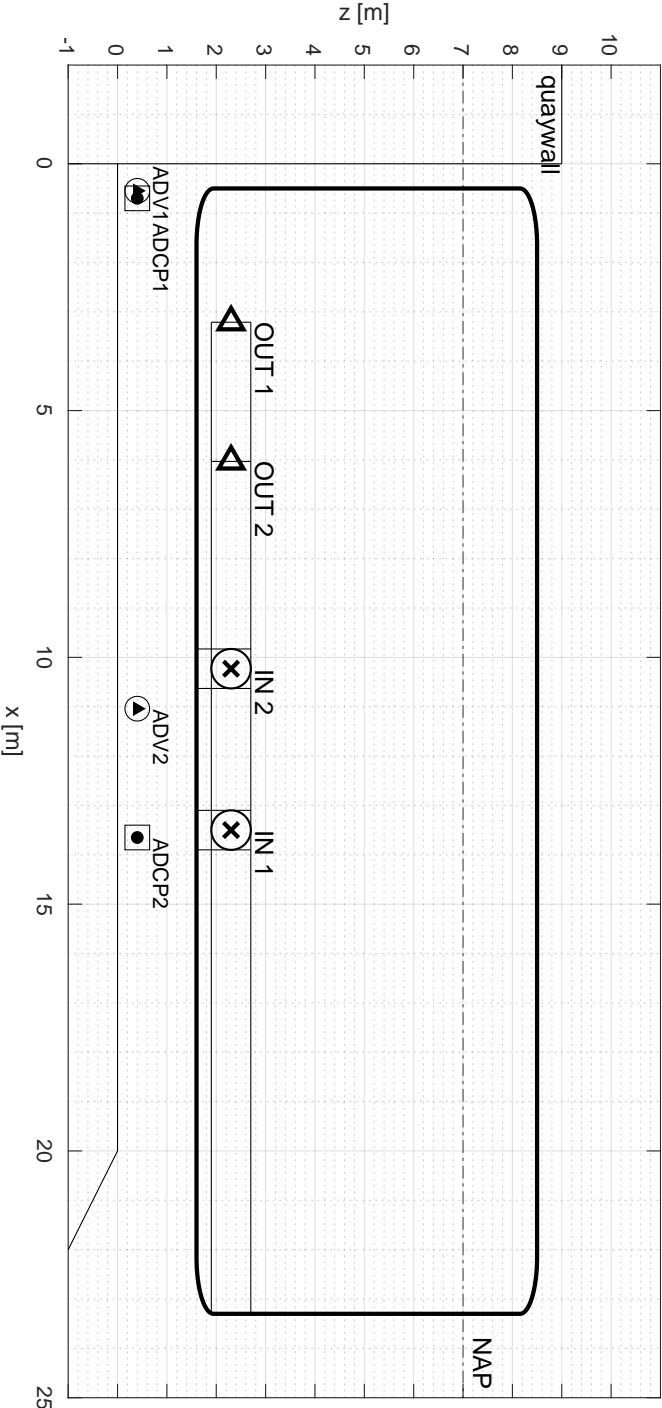


Figure 3. 10: Cross view of instrument set-up for the reflected flow. The grid of the chosen reference system is illustrated, as well as the quay wall and the schematized ship outline. Outlets and inflow points of the bowthrusters are indicated. Source: author.

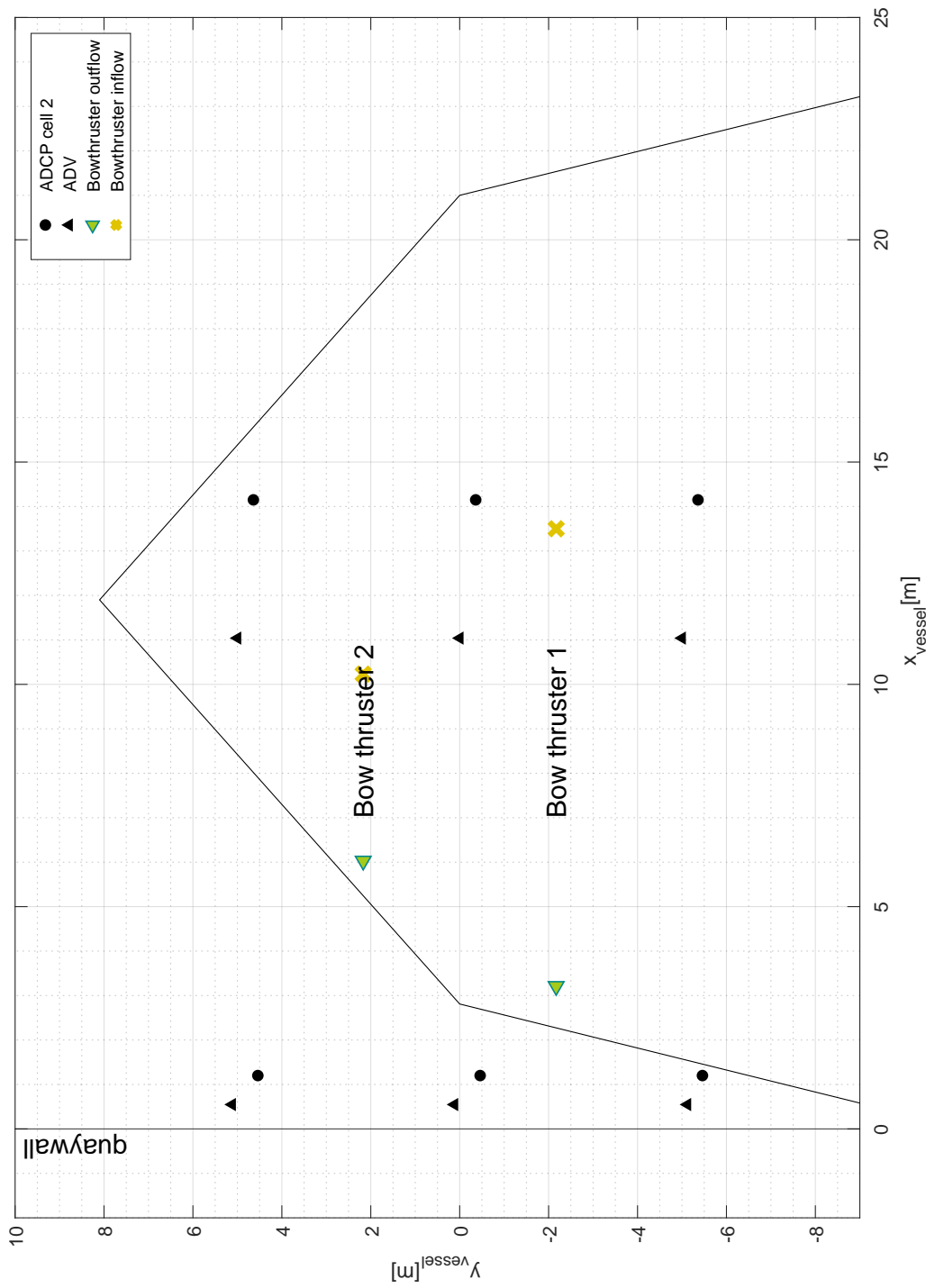
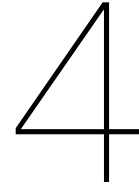


Figure 3.14: Illustration of the reference system. Position of the instrument is depicted: ADVs are illustrated as triangles and cell 2 of ADCPs as circles. Inflow and outflow coordinates of both bowthrusters can be seen, as well as a simplified outline of the ship. Reference point Bollard 31 is illustrated as well. Source: author.



Post-processing approach

After the data collection, post-processing of the data is undertaken. In order to elaborate a solid post-processing strategy and to gain a clear picture on the level of confidence of the measurements, several checks are conducted on the technical functioning of the instruments and on the assumptions behind the measurement programme. The checks are presented in this chapter for Test 1, considered representative for all tests, but the issues highlighted are considered for every test, and the consequent post-processing steps are applied uniformly. Post-processing is made following the reasoning: firstly, a correct functioning of the instrument is ensured checking the raw data, such as amplitude and correlation of the signal. Secondly, Nortek indication of excluding all the velocities measured with a correlation lower than 50% is applied; to check how this measure affects the data, histograms of both raw velocities and velocities that respect the correlation threshold are analyzed. As a third step, a transformation is applied to raw velocities in order to obtain velocity components in the main reference system, and the horizontal velocity magnitude. Then, the assumptions lying underneath the choice of measuring programme are tested.

To assess the correct functioning of the instruments, the following checks are made:

- **Correlation.** Correlation between the emitted ping and the received signal gives a good indication of the proper functioning of instruments based on Doppler effect.
- **Amplitude.** Amplitude of the signal can be checked to investigate how the surroundings affect the signal.
- **Velocity distributions.** In order to check if the instruments are set correctly, a statistical analysis of the velocities is conducted.
- **Pressures corresponding to velocities.** In order to check if the data recorded by the instrument is consistent, a comparison between pressure fluctuations and velocity magnitude is done using Bernoulli's theorem.

Then, values of mean horizontal flow velocity and standard deviation calculated for the whole duration of the subtest are compared with the ones obtained taking only the last minute into consideration. This check gives insight on the validity of the assumption according to which a duration of two minutes is sufficient to smooth out any possible transitional effect arising from the increase in power steps. Finally, a discussion on the reliability of the dominant direction parameter is presented.

4.1. Correlation checks

According to Nortek Manual [12], the instrument is functioning properly when the correlation is higher than 50%; therefore, data with a lower correlation should be discarded. Checks on the correlation are meant to investigate when the correlation is lost (i.e. distance from the instrument in case of the ADCPs, or higher applied power steps).

Correlation is therefore checked both in time (for all the instruments) and in space (for the ADCPs). To check correlation in time for the ADCPs, a timeseries of the correlation is produced for the second cell of both beams. As explained in the following paragraphs, cell 2 is chosen as the most representative cell for the flow pattern and the best compromise between vicinity to the instrument (desired due to a reduced cell volume, and therefore a higher representativity of the flow) and interference of the instrument itself on the the flow.

In figure 4.1 and 4.2, the time series of correlation are depicted, together with the suggested minimum threshold of 50% . It can be observed how correlation stays above the limit for the whole test duration, leading to think that there isn't a correlation between increase in applied power and correlation loss.

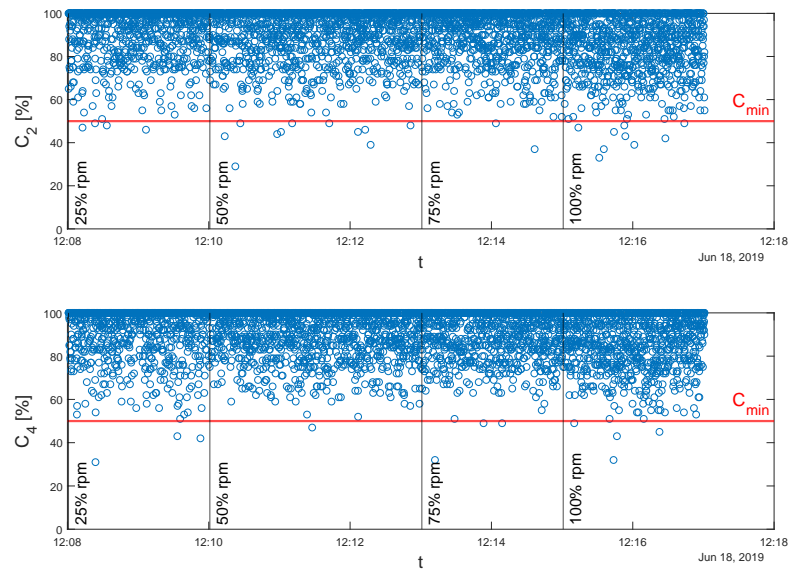


Figure 4.1: Instantaneous correlation during Test 1 for ADCP1. Correlation values for beam 2 (C_2) and beam 4 (C_4) are represented. Subtest corresponding to 25%, 50%, 75% and 100% of applied power are indicated, while minimum suggested value of 50% of correlation is highlighted in red. Values from cell 2 of the ADCP are presented.

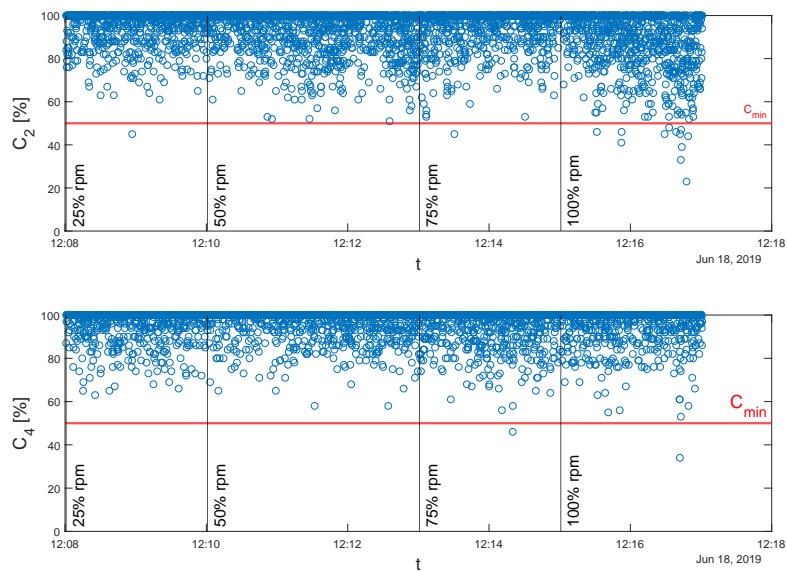


Figure 4.2: Instantaneous correlation during Test 1 for ADCP2. Correlation values for beam 2 (C_2) and beam 4 (C_4) are represented. Subtest corresponding to 25%, 50%, 75% and 100% of applied power are indicated, while minimum suggested value of 50% of correlation is highlighted in red. Values from cell 2 of the ADCP are presented.

For the ADVs, which record on a single spot, a simple time series of the correlation is shown in figures 4.3 and 4.4.

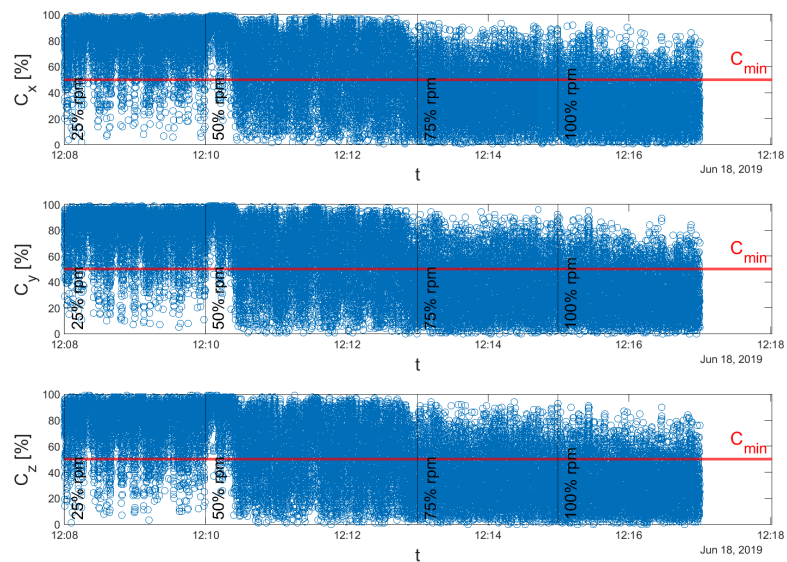


Figure 4.3: Instantaneous correlation during Test 1 for ADV1. Correlation values for x (C_x), y (C_y) and z (C_z) are represented. Subtest corresponding to 25%, 50%, 75% and 100% of applied power are indicated, while minimum suggested value of 50% of correlation is highlighted in red.

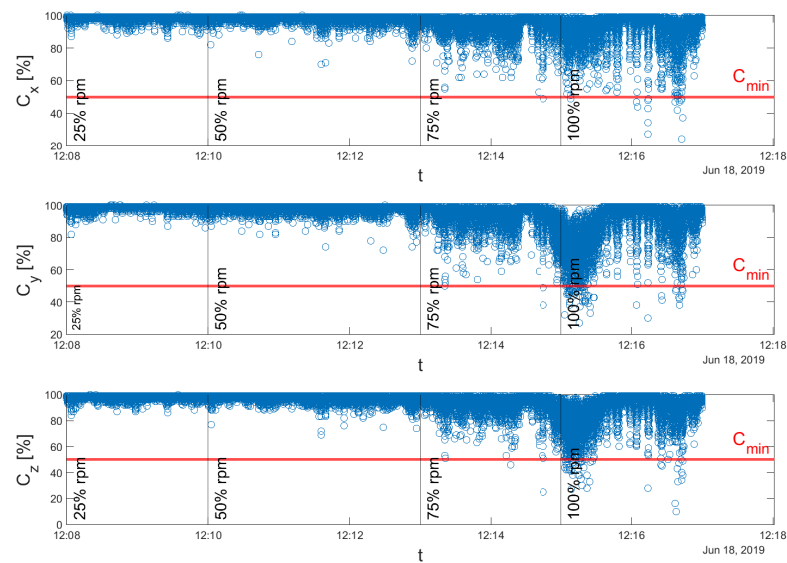


Figure 4.4: Instantaneous correlation during Test 1 for ADV1. Correlation values for x (C_x), y (C_y) and z (C_z) are represented. Subtest corresponding to 25%, 50%, 75% and 100% of applied power are indicated, while minimum suggested value of 50% of correlation is highlighted in red.

It can be observed that over time (and therefore, at the progressive increase of applied power), the correlation decreases. For ADV1, a large amount of data is affected by the loss of correlation, leading to think that the reliability of the instrument for test 1, especially above 50% of applied power, is low. However, due to the high sampling frequency, the number of measured velocities is still large even after discarding the ones that have a correlation lower than 50%. Therefore, the instrument is not discarded from the analysis. A statistical analysis of the velocities is nevertheless conducted in order to understand if the loss of correlation leads to a capping of the velocities or to other statistical distortions (see paragraph 4.3 as an illustrative example).

To check correlation in space for the ADCPs, the mean correlation over each subtest is calculated, and a spatial profile along the two beams is created. As it can be observed in figures 4.5 and 4.6, correlation progressively decreases with the increasing distance from the instrument. It's possible to observe how correlation progressively decrease with an increase in distance from the instrument. Also, it can be noted that the profiles vary depending on the subtest: there is a consistent trend that shows how to higher applied power corresponds a faster decay of mean correlation over time.

From this check it can be concluded that correlation in s is sufficient until around 1 m (5 cells) from the instrument, where in both ADCPs the first correlation drop happens. As part of the post-processing all the velocities measured with a correlation lower than 50% are excluded from the analysis.

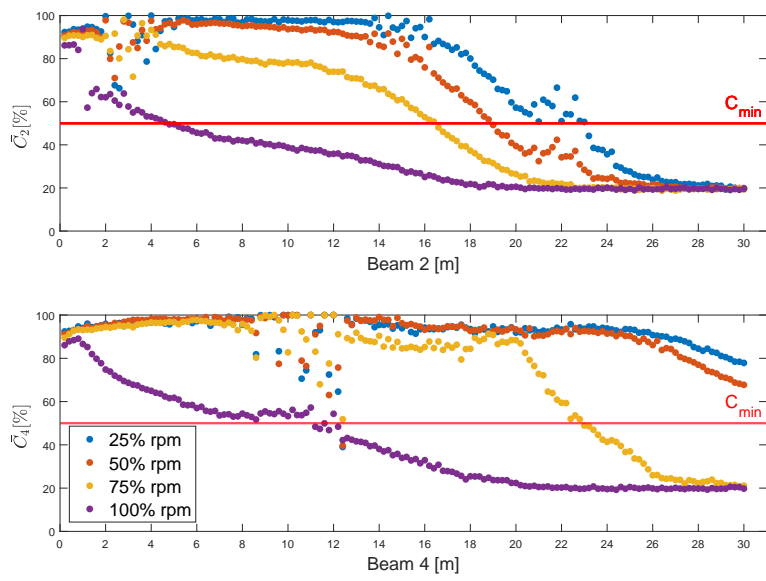


Figure 4.5: Mean correlation profile for each subtest of Test 1, along cells of beam 2 (\bar{C}_2) and 4(\bar{C}_4) of ADCP1.

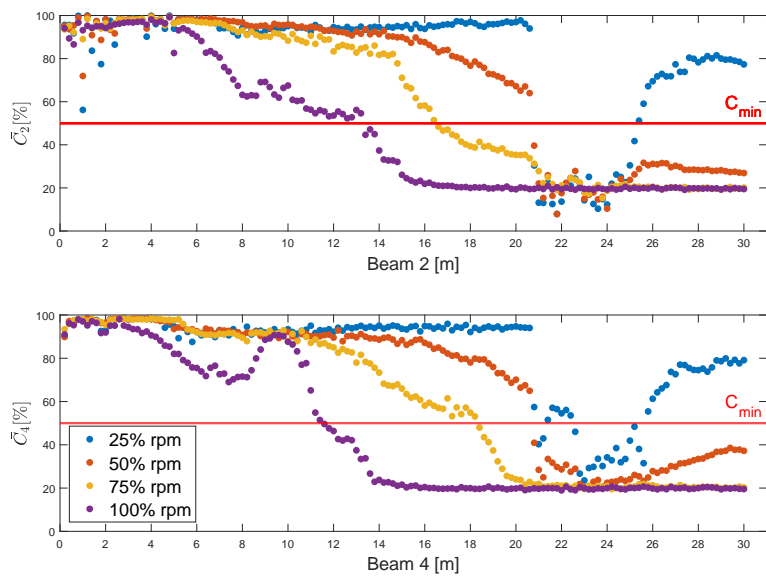


Figure 4.6: Mean correlation profile for each subtest of Test 1, along cells of beam 2 (\bar{C}_2) and 4(\bar{C}_4) of ADCP2.

4.2. Amplitude checks

This check is made for ADCPs only. The amplitude of the signal along the two beams used for the derivation of x and y velocity is checked to assess until which distance from the instrument the data can be trusted. Amplitude of the signal normally decreases with the increasing distance from the instrument. If the amplitude has a sudden increase, it can mean that the beam of the instrument hit an obstacle, such as the bottom, the surface, or a generic solid object that could not pass through. In figure 4.7, the amplitude along cells of beams 2 and 4 of ADCP1, averaged for each subtest, is represented. It can be observed how there is a sudden peak along beam 4, around 8 m from the instrument. The peak is present in subtest A, B, and C, but not in subtest D. This is probably indicating reflection against an obstacle, perhaps a loose rock from the bottom protection. The disappearance of the peak in subtest D might indicate that the obstacle moved due to the flow. Similarly, mean amplitude for each subtest along cells of beam 2 and 4 for ADCP2 is shown in figure 4.8. It can be concluded that the reflection problems that occur for ADCP1 affect the data after 8 m (40 cells) from the instrument, while for ADCP2 problems occur after 10 m (50 cells) from the instrument. This is anyway not going to affect the analysis, since the data reliability at this distance is already affected by other aspects such as the increase of measuring volume and the loss of correlation.

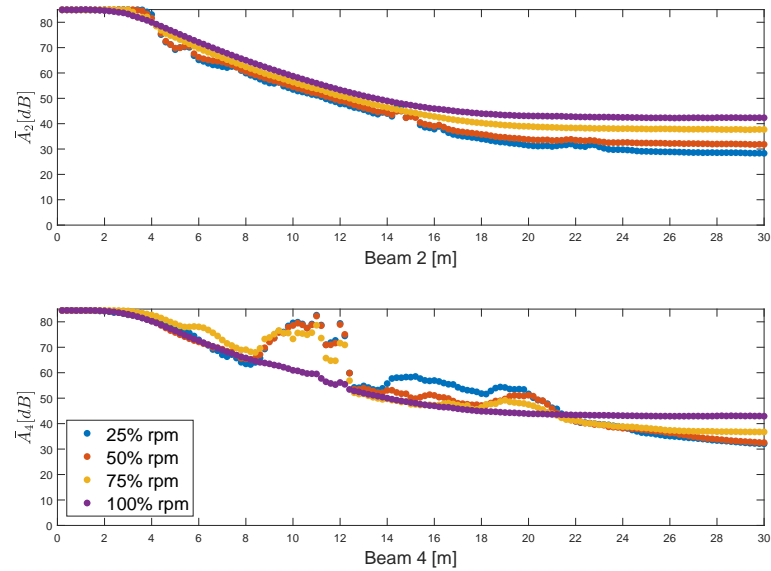


Figure 4.7: Mean amplitude profile for each subtest of Test 1, along cells of beam 2 (\bar{C}_2) and 4 (\bar{C}_4) of ADCP1.

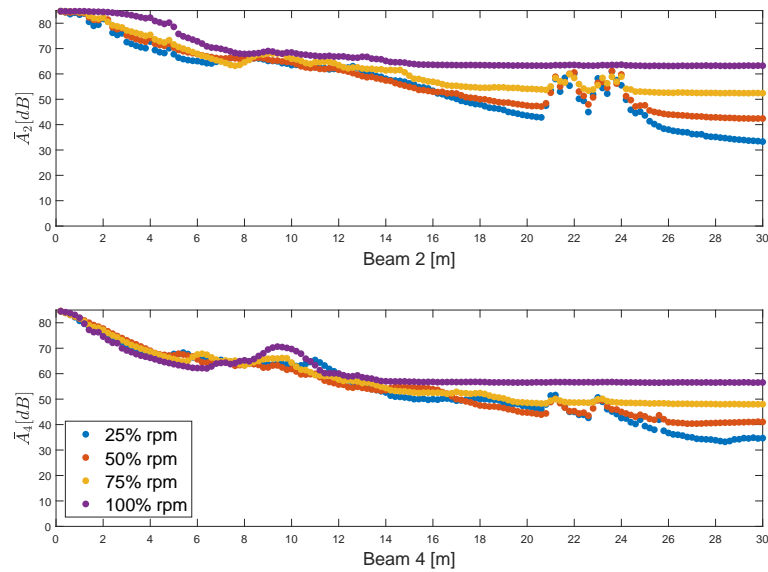


Figure 4.8: Mean amplitude profile for each subtest of Test 1, along cells of beam 2 (\bar{c}_2) and 4 (\bar{c}_4) of ADCP2.

4.3. Statistical analysis of velocities

In order to assess the validity of the statistical parameters derived for each subtest, the histograms of velocities for each subtest are produced. The histograms have a uniform bin width of 0.05 m/s; furthermore, they've been normalized, meaning that the height of each bar is equal to the probability of selecting an observation within that bin interval, and the height of all bars sums to 1. To investigate how discarding of velocities with a low correlation affects the statistical distribution, both raw velocities and processed velocities are shown, where processed velocities consist in velocities without the values that are measured with a beam correlation lower than 50%. As an example, subtest 1A is shown in figures 4.9 and 4.10.

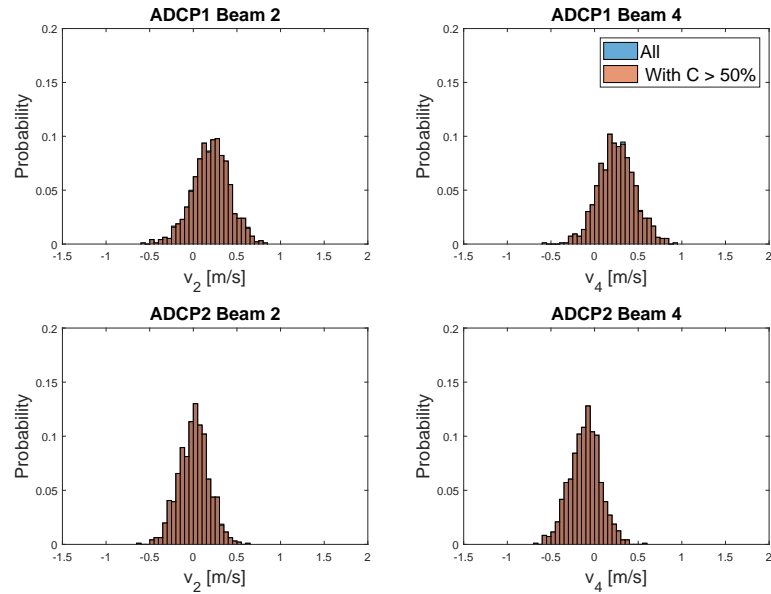


Figure 4.9: Histograms of all measured instantaneous velocities, and only velocities with a >50% correlation for ADCPs in Test 1, at 25% of applied power.

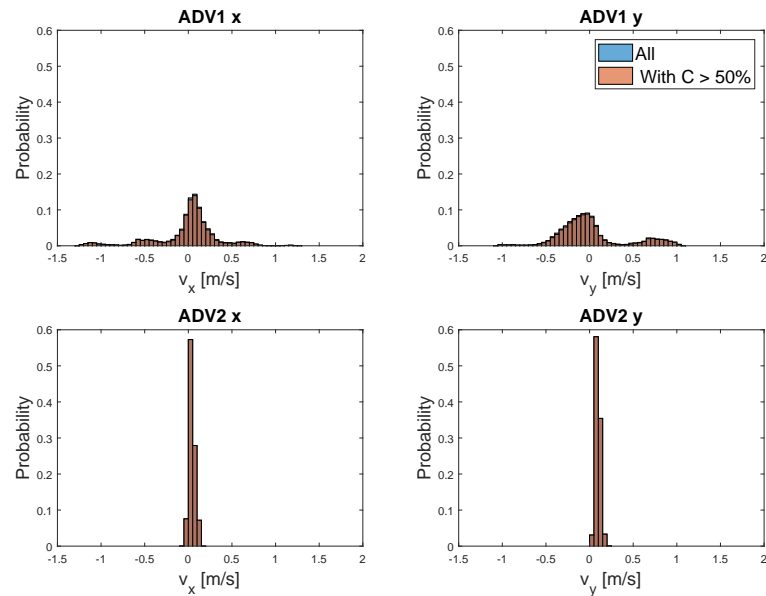


Figure 4.10: Histograms of all measured instantaneous velocities, and only velocities with a >50% correlation for ADVs in Test 1, at 25% of applied power.

It can be observed how the distribution is different for the instruments: while ADCPs show a more clearly distributed velocities, ADV 1 presents some noise and a double peak in y velocities, while ADV2 shows a clear peak in velocity distribution. It looks like there is no clear cut in the distribution; therefore, the instrument settings didn't affect the measured velocities, for instance capping them in case the velocity range is put incorrectly. In the first subtest, it appears that there is no significant correlation loss. From the correlation time

series, it appears that the correlation loss is increasing in time, and this is represented in the histograms as well. As it can be seen from figures 4.11 and 4.12, while for ADCPs the correlation loss doesn't affect the statistics even in the last subtest, ADV1 is strongly affected by the correlation loss and, therefore, discarded from the analysis of subtests 1C and 1D.

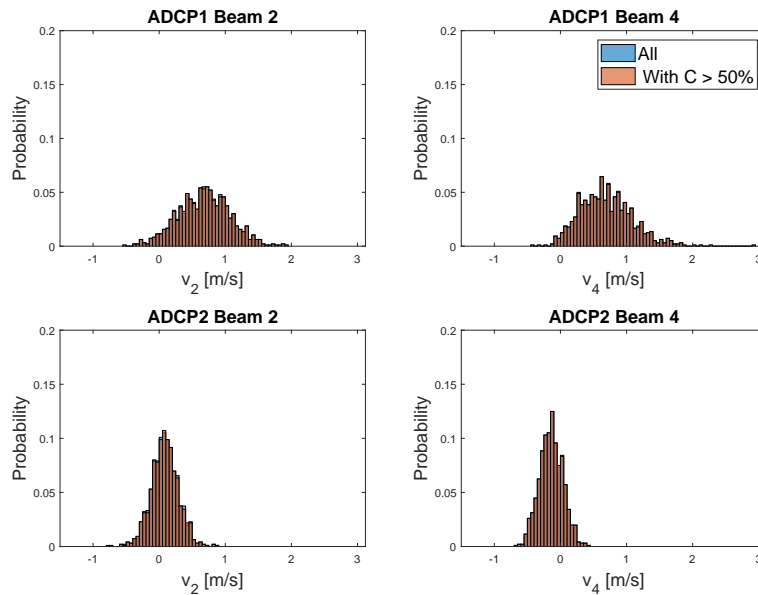


Figure 4.11: Histograms of all measured instantaneous velocities, and only velocities with a >50% correlation for ADCPs in Test 1, at 100% of applied power.

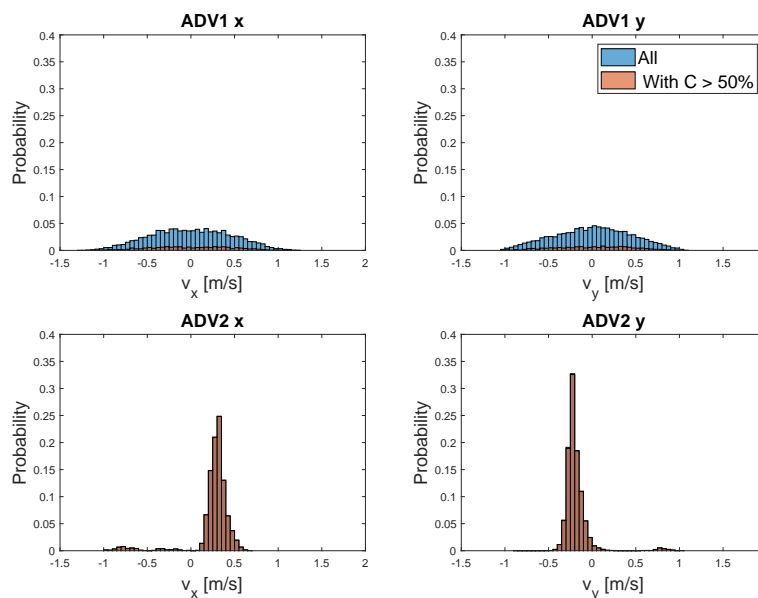


Figure 4.12: Histograms of all measured instantaneous velocities, and only velocities with a >50% correlation for ADVs in Test 1, at 100% of applied power.

4.4. Pressure fluctuations compared to velocity increase

In order to check if the pressure and velocities recording are consistent, a comparison between the measured velocities and velocities correspondent to pressure fluctuations according to Bernoulli is made. Since the pressure sensor of ADVs is located at a different position than the head where velocities are recorded, this check is conducted only for ADCPs. Velocities measured in cell 1 are the one used to compare, since they're the closest to the instrument and, therefore, to the pressure sensor. The pressure oscillations are calculated with respect to the average pressure in the ten minutes before the start of the test. Since test 1 is performed around slack water, the water level is considered to be constant and, therefore, no correction for the tide is deemed necessary.

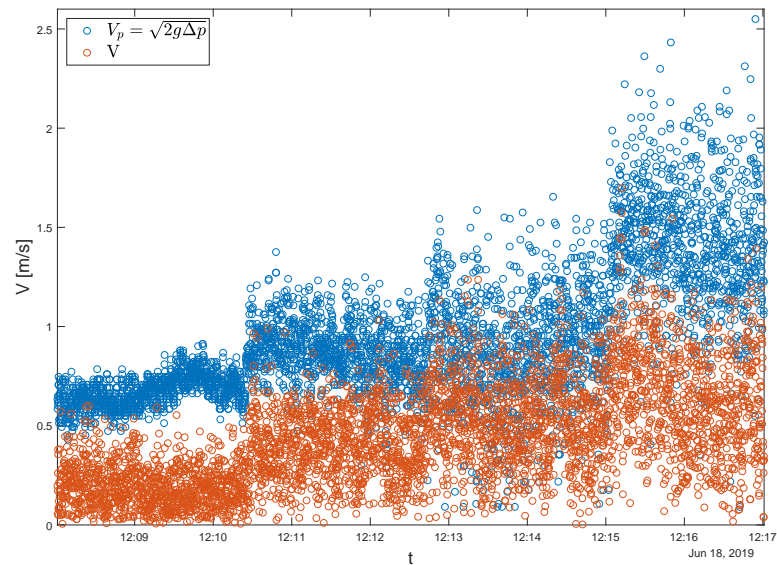


Figure 4.13: Time series of measured instantaneous horizontal velocity magnitude in cell 1 of ADCP1, and velocity correspondent to pressure fluctuations in Test 1.

From figures 4.13 and 4.14 it can be observed that there is a noticeable mismatch between pressures fluctuations and recorded horizontal velocity magnitude in cell 1.

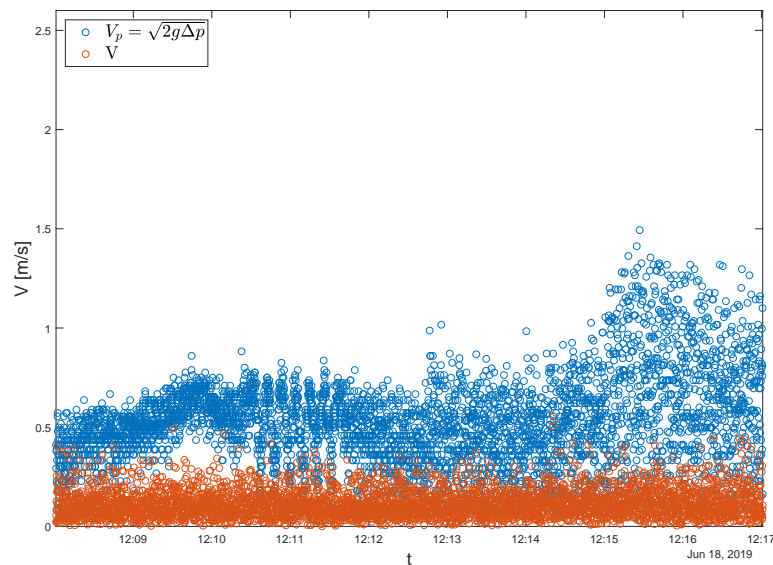


Figure 4.14: Time series of measured instantaneous horizontal velocity magnitude in cell 1 of ADCP2, and velocity correspondent to pressure fluctuations in Test 1.

4.5. Stationarity of the flow

When deciding the measurement protocol, a two-minutes interval in between each power test is considered enough for the flow to be established. In order to check whether this assumption is true, the flow mean magnitude and standard deviation are calculated both for the whole duration of the subtest and for the last minute of the subtest. It has also to be noted that, due to human error, not all the subtests have a perfect duration of 2 minutes. This check contributes also in assessing the impact of this on the total uncertainties. The results of this check can be observed in figure 4.15.

The variation within different subtests appears to be more pronounced than the variation between the values calculated for the whole test and the values calculated for the final minute of the test. Therefore, it seems that the flow reached stability. On the other hand, though, it can be observed in figure 4.15 how the mean values calculated for the second half of each subtest are systematically lower than the ones calculated for the full subtest. This is against the expectations, and such a systematic behaviour is not due to natural statistical variability. To investigate this aspect in more depth, more checks on different tests are recommended, but the flow is assumed to be established enough to use the whole two-minutes subtests in the analysis.

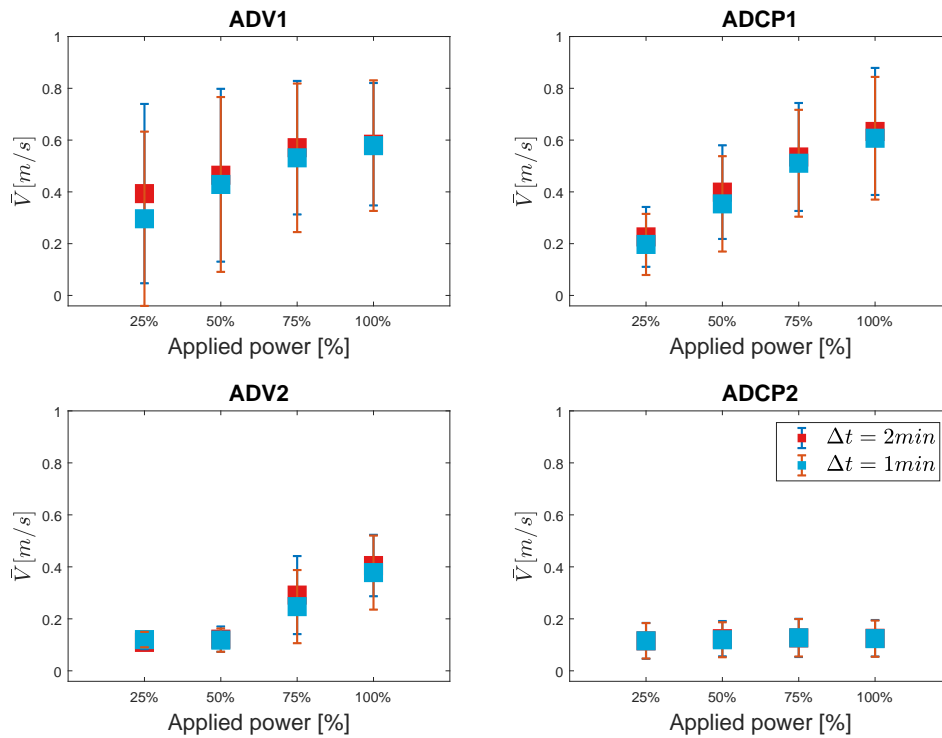


Figure 4.15: Comparison between mean horizontal velocity (\bar{V}) and its standard deviation for each whole subtest and for the final minute of each subtest in Test 1.

4.6. Most representative cell for ADCPs

In order to better compare different tests, it is chosen to show ADCPs data from the most representative cell. The most representative cell should be not too far away from the instrument, since the increase in measuring volume of the instrument leads to less accurate velocities. Furthermore, the correlation checks show a progressive loss of correlation with the increase of distance from the instrument. As a last reason, choosing a close cell for ADCP1 allows a better comparison of results with the near ADV1. From the previous correlation and amplitude cell, together with considerations about the cell volume, the first 5 cells are here compared for x velocities with the objective of choosing the most representative one. In figure 4.16, a plot of the mean velocity along x and the standard deviation for the first 5 cells of ADCP1 is shown.

It can be observed that the expected decrease of mean flow velocity happens only for the maximum applied power, while for the other subtests it stays constant. This suggests a non-linear behaviour of the relation within influence of the reflected flow with distance from the quay wall, and increase in applied bow-thruster power. As for the cell choice, cell 1 is considered to be too close to the instrument and, therefore, here the flow might be influenced by the presence of the instrument itself. This can be deduced for instance by seeing how the standard deviation of the x velocity drops suddenly between cell 1 and cell 2. Cell 2 seems to be the most representative cell, since is the one that measures the highest velocities for the highest applied power. To compare within different instruments and tests, cell 2 is therefore used for ADCPs.

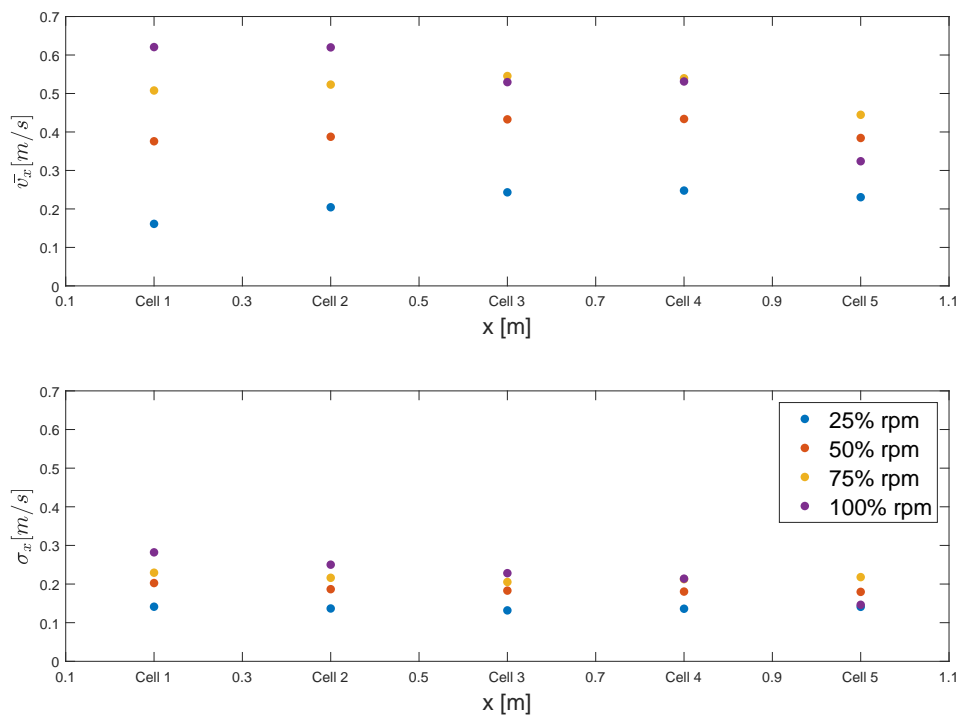


Figure 4.16: Mean x velocity (\bar{v}_x) and standard deviation (σ_x) profile along the first 5 cells of ADCP1 in Test 1.

4.7. Dominant direction

In order to gain an understanding of spatial flow pattern, dominant direction registered from each instrument for each subtest is calculated. The method used to calculate the dominant direction is illustrated by the following steps:

- Instantaneous direction for the whole duration of the test is calculated from x and y velocity components.
- Instantaneous direction time series is divided in subtests corresponding to each step of applied power.
- For each subtest, instantaneous directions are divided in bins with a 5 degrees width.
- The bin containing the highest number of direction recording is identified as the one corresponding to the dominant direction.

5 degrees wide bin are chosen to allow a high accuracy of the direction. Several checks are made to ensure that the method is not bin-width dependent. To gain a better insight on the directional variation of the flow, histograms of the direction calculated for every subtests are observed. As it can be observed from figure 4.17, not always the dominant direction results from a clear peak in the direction distribution.

Generally, it can be observed that ADCP1 and ADV2 show a clear peak in the direction distribution, while ADV1 and ADCP2 present a more spread out histogram.

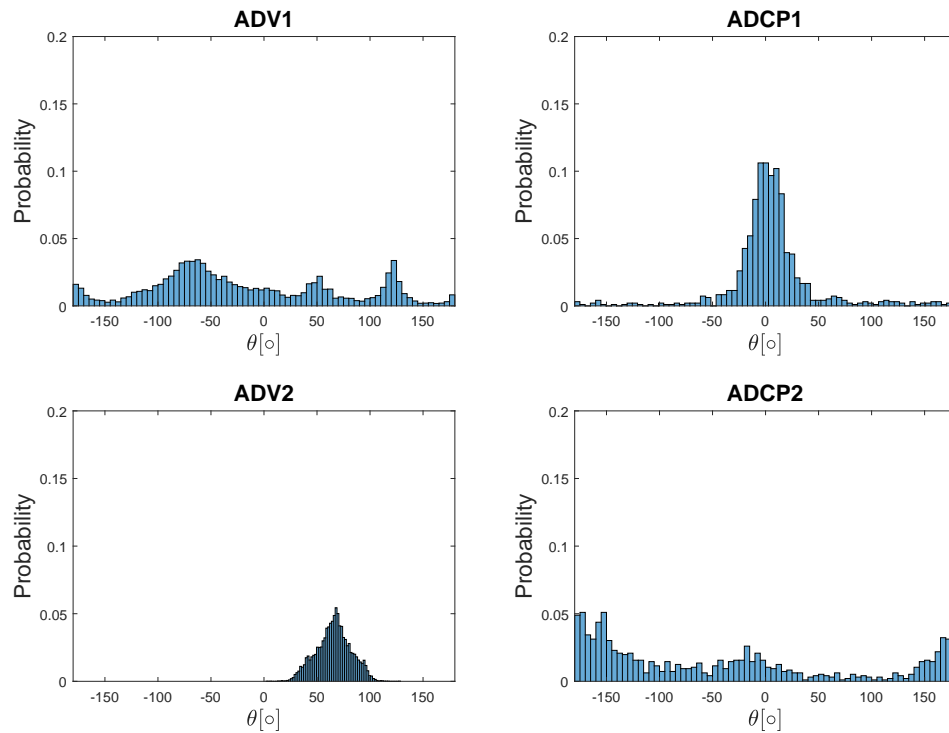


Figure 4.17: Histograms of instantaneous direction calculated for Test 1 at 25% of rpm. All instruments are represented.

4.8. Conclusions

In depth-checks are conducted on Test 1, considered representative of all tests. Correlation in time and space is checked, as well as amplitude, to ensure a correct technical functioning of instrument. Data with a correlation lower than 50% are discarded; in case this affects too much the velocity distribution, data is considered not reliable. Velocities don't appear to be capped. A mismatch between pressure fluctuations and recorded horizontal velocity magnitude is noticed. Duration of two minutes for each step of applied power is considered to be enough to avoid data to be affected by transitional effects, therefore, analysis is conducted on the whole subtest. ADCPs most representative cell is considered to be the second one, and cells after 5th are not trusted. In analysing test results, data affected by high loss of correlation is still retained, but considered unreliable to draw definitive conclusions. Furthermore, when analysing the dominant direction of the flow, its variability is taken into account by looking at the histogram spread.

5

Test Results

In this chapter, results of the tests are presented. The chapter is organised as it follows: at first, results of a single test are analysed, and general observations about the results are made. Test 1 results are presented as in continuity with in depth checks conducted in chapter 4, and eventual differences with other tests are highlighted. Then, a comparison of different tests is made to investigate the impact of use of different bowthrusters, relative position of outlet and instrument, keel clearance. In order to get a spatial picture of the flow pattern, main direction and magnitude of tests conducted in different ship position are compared.

5.1. General observations

Some general observations can be made about each test: regarding the relation between increase in applied power and increase in mean flow velocity, increase of turbulence intensity with increase in applied power, order of magnitude of velocities recorded, differences within the four instruments. Test 1, considered representative for all tests, is taken as a reference, in continuity with the approach adopted in chapter 4. Differences between the base case and other tests are highlighted. In figure 5.1, results from Test 1 are presented. Mean magnitude of the horizontal velocity for each power step and its variability are shown. Errorbars represent the standard deviation of the velocity magnitude for each subtest; each errorbar is 2 standard deviations long. Test 1 consists in the activation of bowthruster 1 of the vessel (the one located more towards the stern) for 2 minutes for each power step, namely 25%, 50%, 75% and 100% of power. The vessel is located in the initial position, with the instruments located symmetrically with respect to the bowthruster axis, and a keel clearance of 1 m.

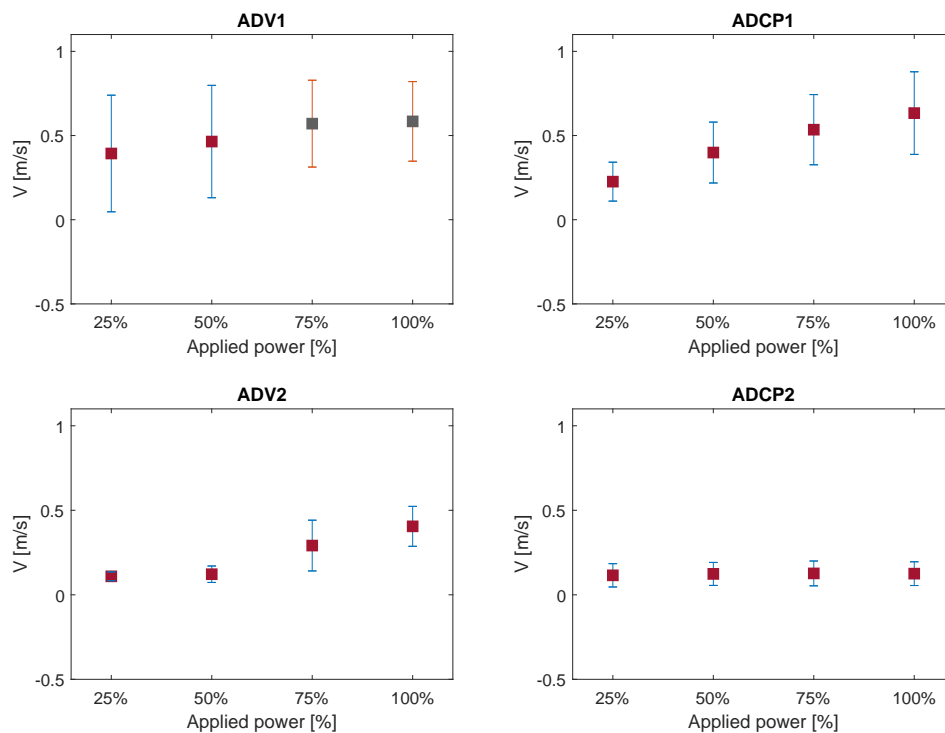


Figure 5.1: Results of test 1. Mean of horizontal velocity magnitude and standard deviation represented for each instrument, for each subtest. Non reliable data is presented in grey.

It is possible to observe that:

- ADCP1 and ADV1 show a correlation between an increase in applied power and increase in horizontal velocity magnitude.
- The two instrument closer to the quay wall (ADCP1 and ADV1), show the largest flow velocities, while velocities measured by ADCP2 don't seem to be related to the use of the bowthrusters.
- ADCP1 and ADV1, which are placed in close vicinity, show a similar trend and comparable velocity magnitude. Nevertheless, ADV1 records much larger standard deviations, and data from last two subtests is not reliable due to correlation loss.
- ADV2, which is located near the suction point of the bowthrusters, registers an increase in velocity magnitude with the increase of applied power. However, the trend is different than for ADCP1 and ADV2: this might suggest that ADV2 measurements are more affected by the influx than by the reflected flow from the quay wall.
- All the instruments record mean horizontal velocity magnitudes lower than 1 m/s.

These observations are valid for most of the tests: generally, the recorded mean velocities are in the order of magnitude of 1 m/s, or lower. The two instruments near the quay wall present a clear relation between the increase in applied power and increase in flow velocities; ADV2 measurements are more influenced by the suction beneath the ship than from the reflected jet, and ADCP2 seems to measure flow velocities not related to the use of the bowthrusters. Despite being so close, not always ADV1 and ADCP1 present the same measured velocities. Often ADV1 registers higher mean velocities than ADCP1; furthermore, the flow presents a larger variability, with larger standard deviations. An example is presented in figure 5.2,

where results from test 12 are presented. Test 12 has been conducted using bowthruster 2 in ship position 1, with a keel clearance of 2.79 m.

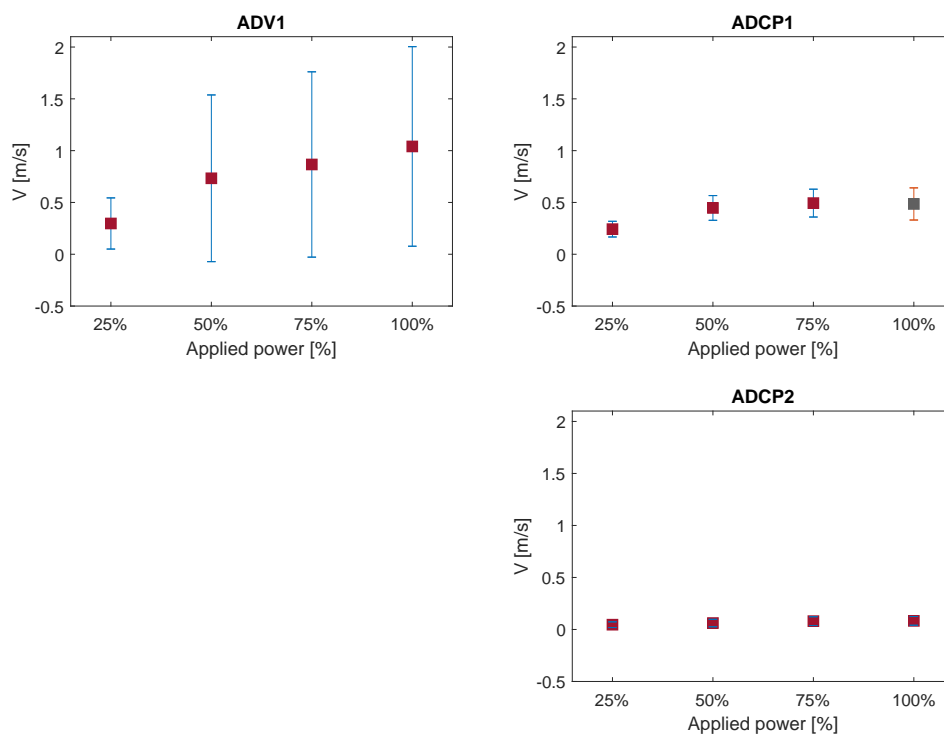


Figure 5.2: Results of test 12. Mean of horizontal velocity magnitude and standard deviation represented for each instrument, for each subtest. Non reliable data is presented in grey.

Discrepancies in measurements from ADV1 and ADCP1 have been observed especially in tests where the flow has more space to develop: for instance, with a larger keel clearance and a wider distance between outlet of bowthruster and quay wall (use of bowthruster 2). Test 22 presents a further exception to this general trend: ADV1 measures velocities in the order of magnitude of 2 m/s, and differences between ADV1 and ADCP1 data are more pronounced. As it can be observed from figure 5.3, in Test 22 ADV1 measures mean horizontal flow velocities up to 2.29 m/s, with a standard deviation of 1.24 m/s. Test 22 has been conducted using both bowthruster simultaneously, with ship in position 1 and a keel clearance of 1.26 m. Results from all tests can be found in appendix B and C.

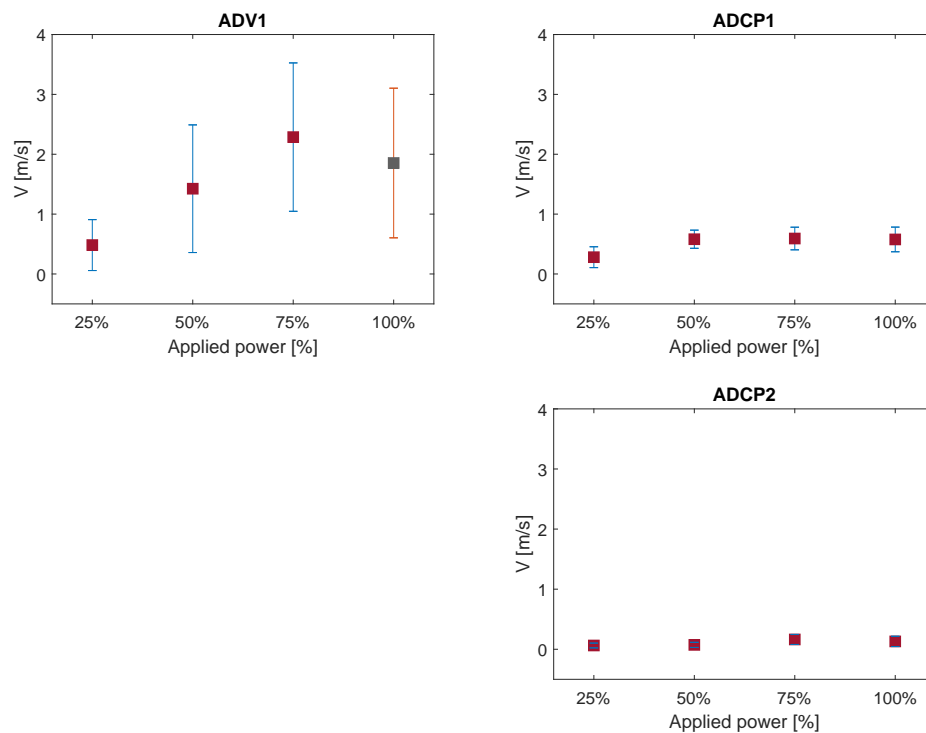


Figure 5.3: Results of test 22. Mean of horizontal velocity magnitude and standard deviation represented for each instrument, for each subtest. Non reliable data is presented in grey.

5.2. Use of different bowthrusters: bowthruuster 1, bowthruuster 2 and simultaneous use of both

To investigate the differences in use of one or the other bowthruuster, Test 1 results are compared with Test 2. Both tests are conducted in similar water depth conditions (keel clearance of circa 1 m) and with the vessel in the same position (ship position 1, see chapter 3, figure 3.11). While for Test 1 bowthruuster 1 is activated, for Test 2 bowthruuster 2 is used. Bowthruuster 1 and bowthruuster 2 differ in length of the channel and, consequently, location of influx and outlet with respect to the quaywall. For more details on bowthruusters geometry, see chapter 3, figure 3.3. In figure 5.4, a comparison of the horizontal flow velocity magnitude and standard deviation for Test 1 and Test 2 is presented.

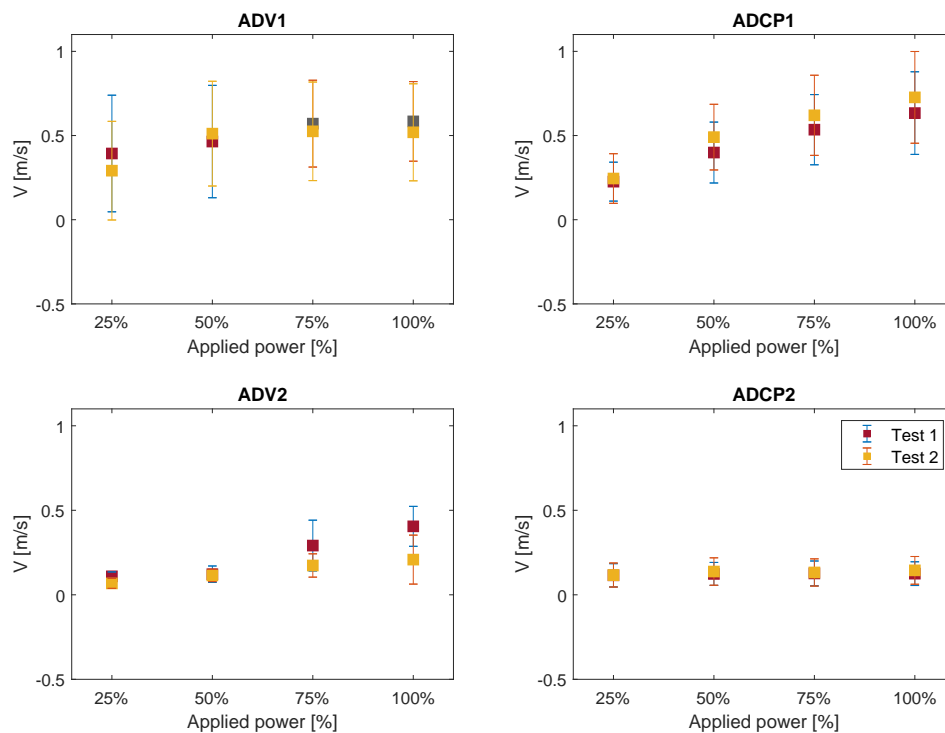


Figure 5.4: Comparison of horizontal flow velocity magnitude and standard deviation for each applied step of power for Test 1 and Test 2.

Flow velocity magnitude and standard deviations are comparable in order of magnitude and general trend, disregarding the fact that one or the other bowthruster is used. Test 2 presents slightly higher horizontal velocities magnitudes measured by ADCP1. Once again, only the instruments near to the quay wall record velocities that show a clear increase with the increase in applied power. The most pronounced difference between mean flow velocities in Test 1 and in Test 2 is recorded by ADV2, which is located in between the suction points of the two bowthrusters and, therefore, might hold information not only from the reflected flow, but also from the inflow beneath the ship. Consequently, the relative influence of the influx with respect to the reflected flow is investigated: mean flow velocity and dominant direction for Test 1 and Test 2 are shown in figure 5.5, while the velocity components along x and y for each tests are presented in figure 5.6. The dominant flow pattern at ADV2 location is well shown by figure 5.5: when each bowthruster is activated, flow is directed towards the respective suction points, as confirmed also by the symmetric flow pattern observable in figure 5.6. It can thus be concluded that, at 11 m from the quay wall, flow on the bottom is dominated by the suction beneath the ship, and not anymore by the jet reflected on the quay wall.

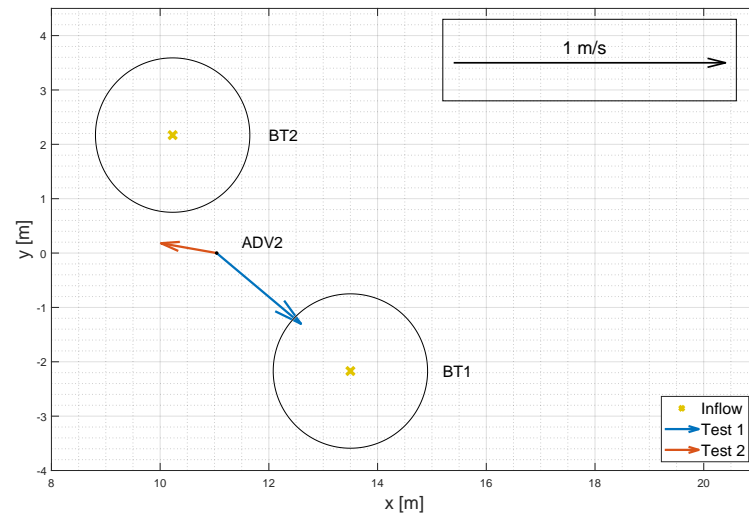


Figure 5.5: Comparison of mean velocity and dominant direction measured by ADV2 for 100% of applied power in Test 1 and Test 2. The suction points of both bowthrusters are depicted, on scale.

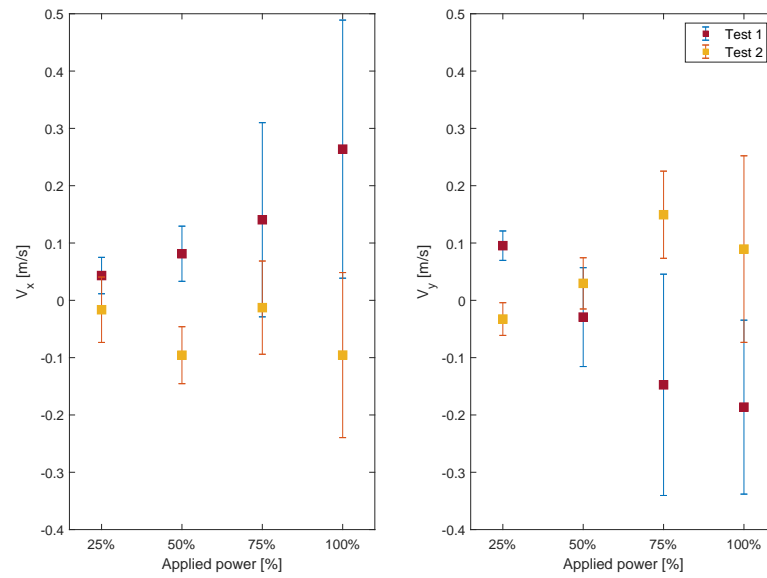


Figure 5.6: Comparison of x and y velocities measured by ADV2 for Test 1 and 2.

Once comparison of Test 1 and Test 2 has given an indication on the equivalence of using one or the other bowthruster, simultaneous use is investigated. In figure 5.7, the results of tests 1, 2 and 3 are compared. In these tests, bowthruster 1, bowthruster 2 and both bowthrusters have been used, respectively. From the comparison of Tests 1, 2 and 3, conducted in similar water depth conditions and same ship position, doesn't seem that the use of both bowthrusters simultaneously yields to significantly higher flow velocities. It has though to be noted that Test 3 has been conducted only for the first two steps of applied power. This comparison is possible also for Tests 11, 12 and 13, where respectively bowthruster 1, 2 and both bowthrusters simultaneously are used. While Tests 1, 2 and 3, presented above, are conducted at low water and with a fairly constant water depth, Tests 11, 12 and 13 are carried out at high water and with a less constant water level. There is, in fact, a difference of circa 30 cm between water depth in Test 11 and in Test 13. As it can be observed in figure 5.8, differences between use of bowthruster 1 and bowthruster 2 are more significant than the ones between use of one or two bowthrusters at the same time. It is also worth noting discrepancies in velocities recorded by ADV1 and ADCP1, and the fact that velocities recorded by ADV1 during Test 13 do not increase constantly with the increase in applied power, differently than in the other tests.

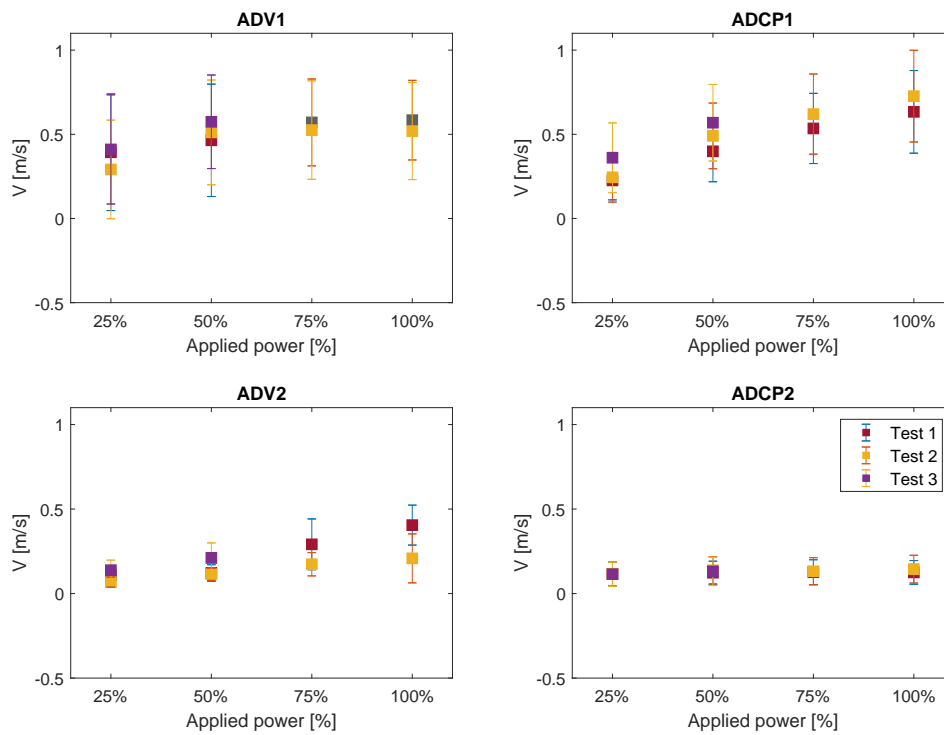


Figure 5.7: Comparison of velocity magnitude and standard deviation for Test 1, 2 and 3 where bowthruster 1, 2 and both bowthrusters are respectively used.

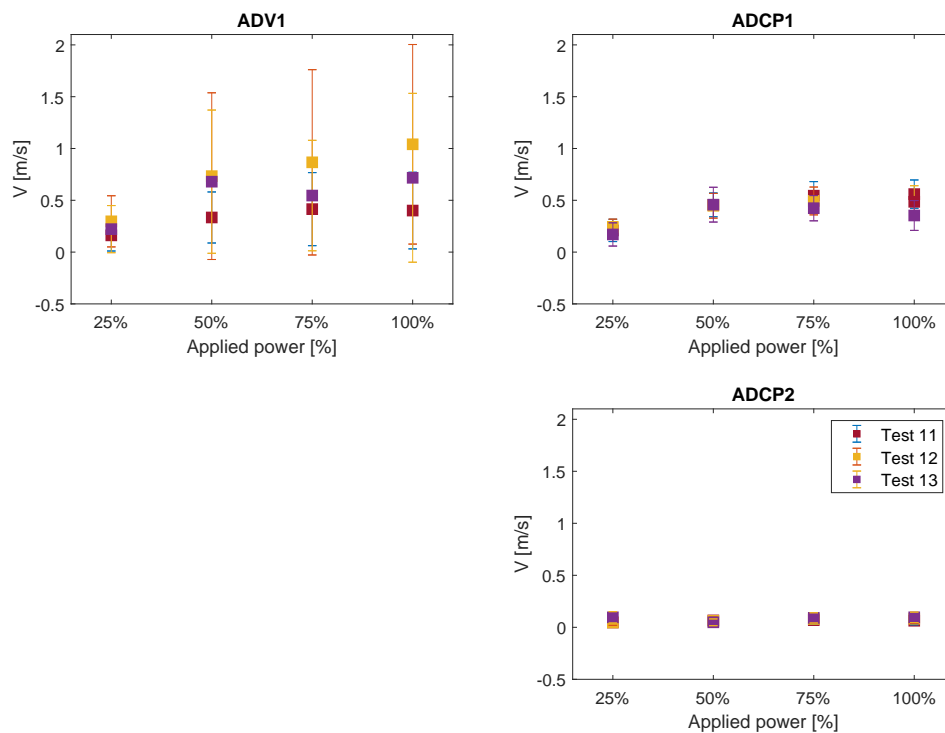


Figure 5.8: Comparison of velocity magnitude and standard deviation for Test 11, 12 and 13 where bowthruster 1, 2 and both bowthrusters are respectively used.

5.3. Influence of keel clearance

Comparing tests conducted at low or high tide, it is possible to observe the influence of keel clearance on bottom velocities. The results, as it can be observed in figure 5.9 and 5.10, vary depending on which bowthruster is used. If at low tide the use of one or the other bowthruster seems to be indifferent, keel clearance seems to have a different impact depending on which bowthruster is used. Observing the data collected by ADV1, the use of bowthruster 1 seems to be connected with values of mean horizontal flow velocities lower with a larger keel clearance, while the opposite holds for what measured during the use of bowthruster 2. ADV1 in fact records higher values of mean horizontal flow velocity for a larger keel clearance, and turbulence intensity increases as well. This is though not reflected by measurements from ADCP1, which records similar velocities for both cases. It is also worth noting how, for bowthruster 2, the difference in mean horizontal flow velocity between low and large keel clearance recorded by ADV1 increases with the increase in applied power, as it can be observed in figure 5.10. Conversely, for bowthruster 1, as seen in figure 5.9, the difference remains fairly constant.

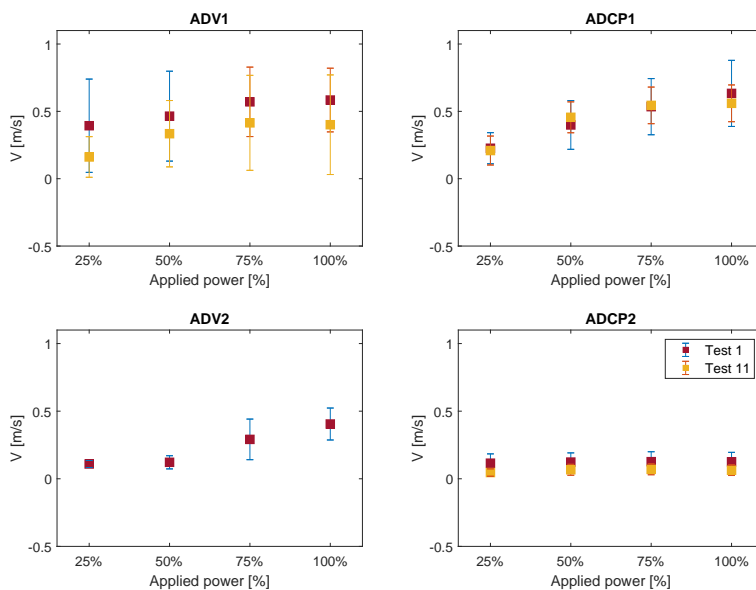


Figure 5.9: Comparison of velocity magnitude and standard deviation for Test 1 and 11, where bowthruster 1 is used respectively with a keel clearance of 1.03 m and 2.57 m.

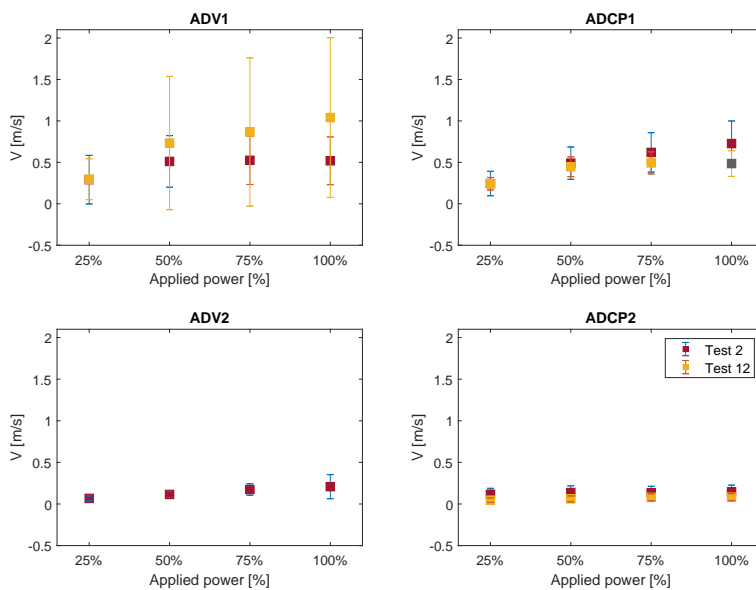


Figure 5.10: Comparison of velocity magnitude and standard deviation for Test 2 and 12, where bowthruster 2 is used respectively with a keel clearance of 1.03 m and 2.79 m.

5.4. Spatial distribution of flow velocities

During the measurement, three different ship positions are adopted: to investigate the spatial distribution of the flow induced by the bowthrusters, data from tests corresponding to different ship positions are combined. Mean velocity magnitude and dominant direction have been calculated for each subtest of every tests. Then, tests have been grouped according to use of the same bowthruuster, similar tide conditions, but different ship positions. The underlying assumption is that moving the ship along the quay wall is the same as having another instrument placed at the same relative distance.

Firstly, three sets of tests where bowthruuster 1 was used during low tide are combined. To have a clearer picture, values at 50% of applied power are depicted, and, to give an indication of the variability in direction, a range in dominant direction equal to plus or minus a standard deviation of the direction ($\pm\sigma_{theta}$) is indicated by dotted lines. In figure 5.11, the spatial picture for tests 1, 5 and 7 is presented, for 50% of applied power.

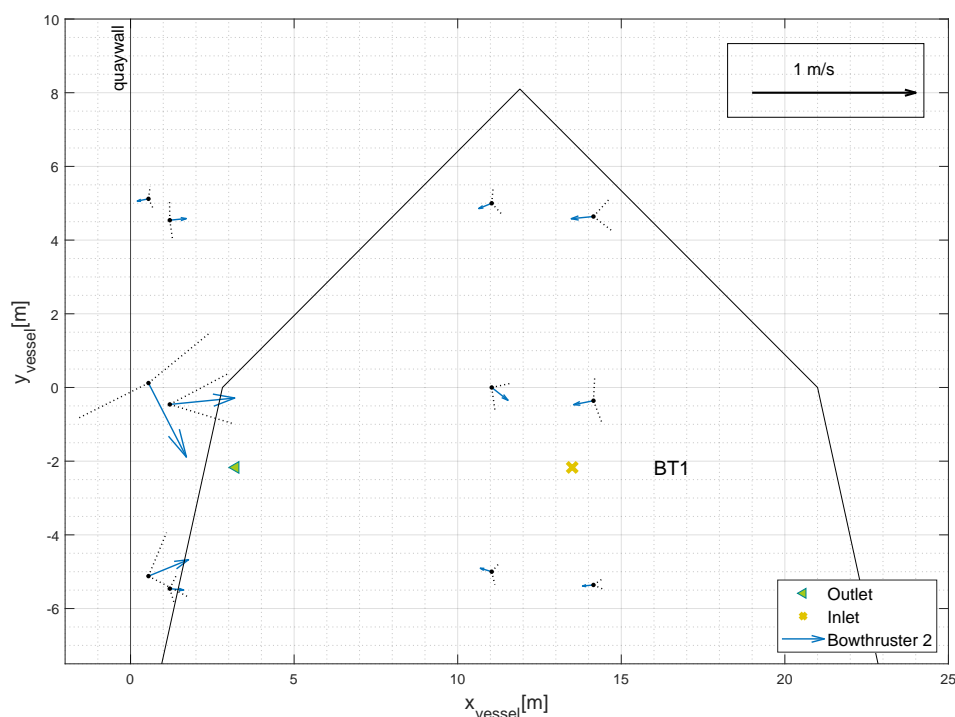


Figure 5.11: Mean horizontal velocity magnitude and dominant direction for tests 1, 5 and 7, at 50% of applied power. Range in dominant direction, corresponding to $\pm\sigma_{theta}$, is indicated by dotted lines.

Firstly, it can be noted that a large variability in direction is present; therefore, the dominant direction parameter could be less representative than wished. Higher velocities are recorded near to the outflow, where it is possible to observe a return flow between the quay wall and the ship. ADCP1 and ADV1, despite being so close, record different dominant directions of the flow: but they both show a reflection from the quay wall in the two position closer to the outlet, when the instruments are located either almost in correspondance of the bowthruuster axis. ADV1 shows more variability in direction than ADCP1. In the position further away from the outflow of bowthruuster 1 (y_{vessel} circa 4.5 m), flow velocities magnitude at the bottom are significantly lower and ADV1 and ADCP1 show opposite dominant direction and large variability, indicating the absence of a clear return flow. The effect of bowthruuster jet reflection seems to exhaust its effect few meters from the quay wall: ADV2, as noted before, is recording influx effect when in the position closest to the suction point, while when is farther

away records feeble velocities in direction of the quay wall, like ADCP2. The flow seems to be highly variable in space, making the spatial resolution of the instruments low.

In figure 5.11, only one subtest is depicted for clarity; to investigate the influence on the spatial distribution of flow caused by the progressive increase of applied power to bowthrusters, all power steps are illustrated in figure 5.12.

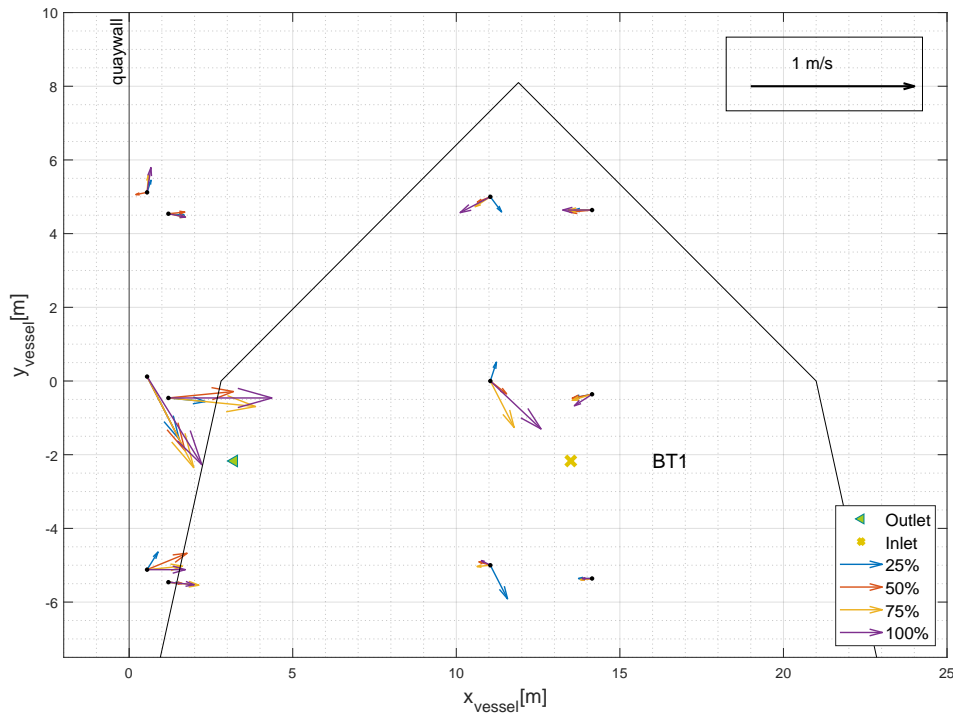


Figure 5.12: Mean horizontal velocity magnitude and dominant direction for tests 1, 5 and 7, at every step of applied power.

From the figure appears clear how the progressive increase of applied power results mainly in an increase in velocity magnitude, having a small effect on dominant direction direction, especially for ADCPs. ADV2 records an influx progressively more directed towards the centre of the influx point: at 25% of power, flow in the vicinity of the inlet seems not yet influenced by the suction, while the direction gets clearer and magnitude stronger at the increasing of applied power. Generally, ADVs present a larger dominant direction variability, while ADCPs record a clear preference of the flow to move along x direction (perpendicular to the quay). Even though in this figure representation of direction variability has been omitted for clarity, it is important to remember what noted above.

In the following figures, the most reliable subtests is chosen to be illustrated, in order to present clearer pictures with a high confidence level in the data. Reliability is assessed based on correlation loss regarding the magnitude, and variability regarding the direction. Indeed, especially for ADV1 and ADCP2, often the distribution of direction is quite flat, indicating that the shown dominant direction might not be representative of a highly turbulent flow.

Use of different bowthrusters

In figure 5.13, a comparison of the flow pattern on the bottom caused by bowthruuster 1 and bowthruuster 2 at low water and 50% of applied power is shown.

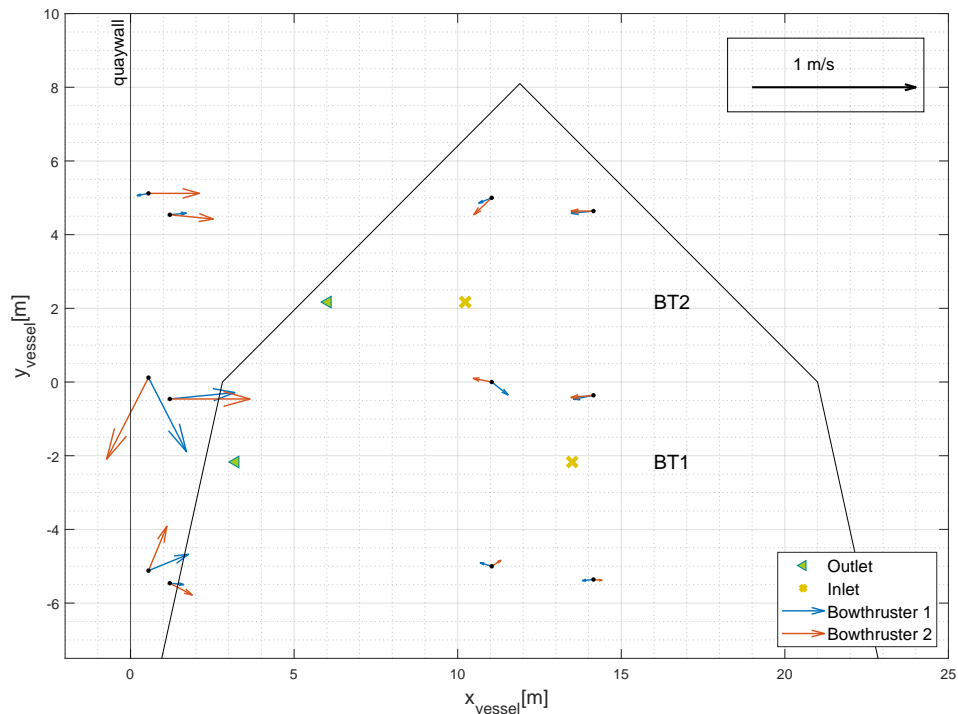


Figure 5.13: Mean horizontal velocity magnitude and dominant direction for tests 1, 5, 7, and 2, 4, 8 at 50% of applied power.

Differences in flow pattern caused by different bowthrusters can be observed especially near to the quay wall: bowthruuster 2 induces higher velocities than bowthruuster 1. Even in the location farther away from the outlet, velocities recorded by ADV1 are of magnitude comparable to the ones recorded near to the bow. Highest velocities are recorded once again near to quay wall at $y = 0$, despite the distance from the outlet is comparable to the instruments located near the bow. This might indicate that having more space to develop, the flow tends to have higher mean velocities. Discordance in direction between ADV1 and ADCP1 is even more pronounced for bowthruuster 1, with the exception of the instruments located near the bow. ADV2, once again, captures the effect of the inflow; for bowthruuster 2, also when located more towards the bow, showing that the extent of the influx might be in a range of about 5 m: 3.5 times the propeller's diameter. This is though not true for influx influence of bowthruuster 1. ADCP2 seems to be recording flow velocities not related to the use of bowthrusters. In figure 5.14, a comparison of the flow pattern on the bottom caused by bowthruuster 1, bowthruuster 2, and both bowthruuster simultaneously at low water and 25% of applied power is shown.

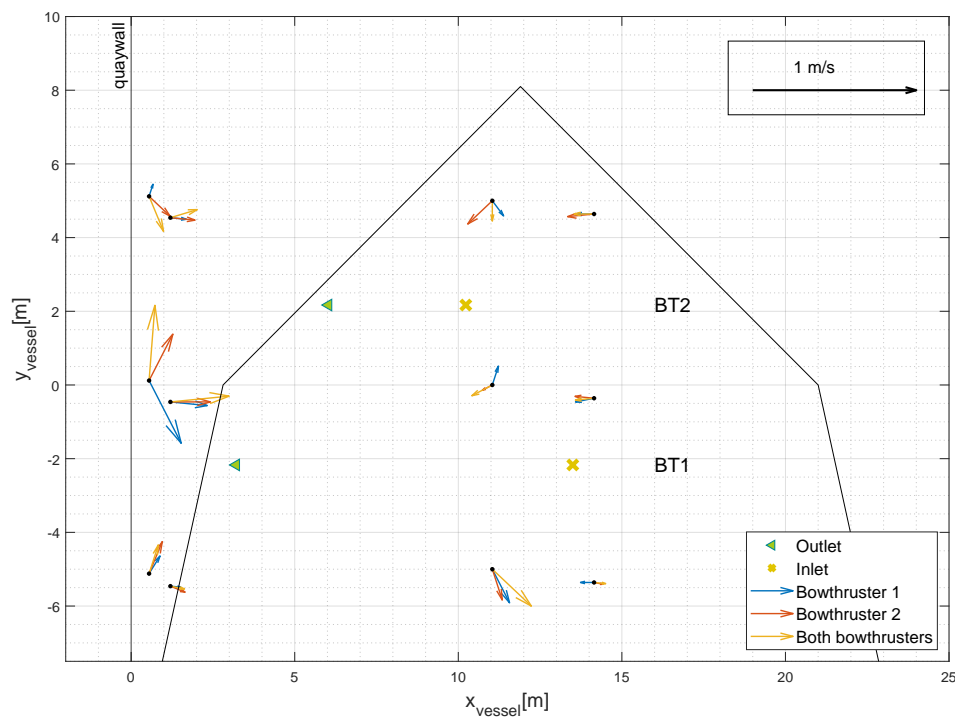


Figure 5.14: Mean horizontal velocity magnitude and dominant direction for tests 1, 5, 7; 2, 4, 8, and 3, 6, 9 at 25% of applied power.

As observed before, the use of both bowthrusters induce slightly higher flow velocities magnitude, but still of a comparable magnitude. Flow pattern induced by both bowthrusters seems to be slightly more similar to the one induced by bowthruuster 2. It has though to be noted that 25% of applied power could be too low to draw definitive conclusions regarding the inflow, as observed before for figure 5.12.

Influence of keel clearance

In figure 5.15, a comparison of flow pattern on the bottom caused by bowthruster 1 at different keel clearances (circa 1 m and circa 2.5 m) is depicted.

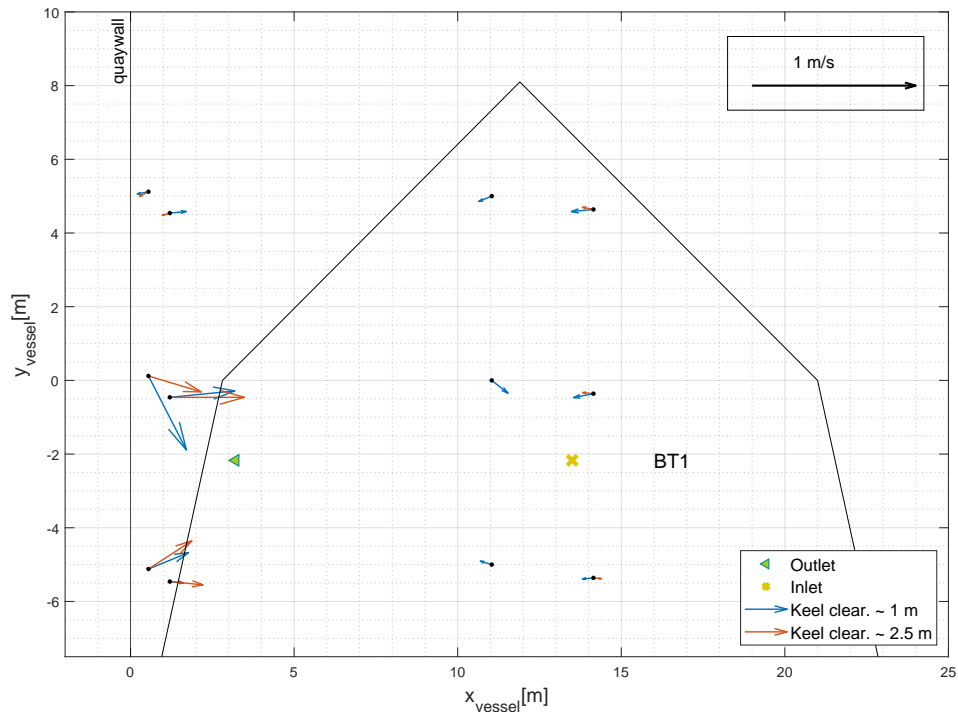


Figure 5.15: Mean horizontal velocity magnitude and dominant direction for tests 1, 5, 7, and 11, 14, 17 at 50% of applied power.

Flow pattern induced by bowthruster 1 at higher keel clearance doesn't seem to differ significantly from the one at the lower keel clearance. Velocities present roughly the same order of magnitude. Only exception is presented by ADCP1 when located the most towards the stern: with a mean velocity double than the one measured at low water, it might indicate a higher preference for the flow to go under the ship. Also concerning the dominant direction there are only two differences between a smaller and a larger keel clearance: ADCP1 when located next to the bow and ADCP2 in the position most towards the stern. In both cases the direction is opposite as the ones measured with a lower keel clearance. For ADCP2, this could either indicate a weak reflect flow, eased by the availability of space with a higher keel clearance. Since this behaviour is not replicated in any other position, though, it could also be due to factors external to the experiments.

Results for bowthruster 2, can be observed in figure 5.16.

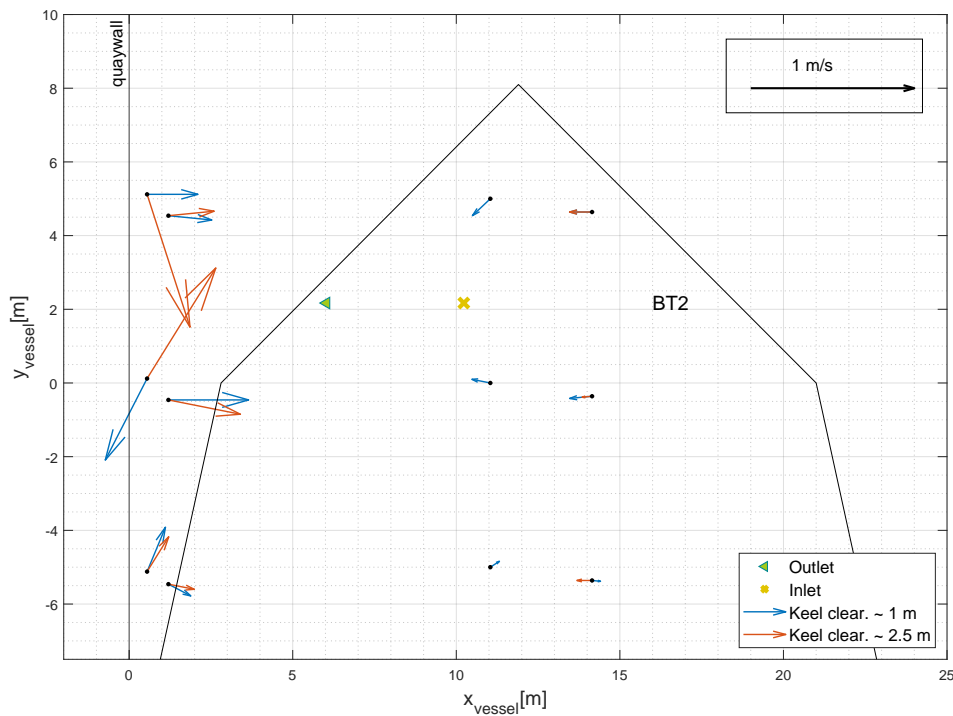


Figure 5.16: Mean horizontal velocity magnitude and dominant direction for tests 2, 4, 8, and 12, 15, 18 at 50% of applied power.

When comparing results from tests with different keel clearance for bowthruster 2, ADV1 records an increase in mean flow velocities and a change in dominant direction for the two location nearer to the outflow. This represents a difference with the impact of different keel clearances for bowthruster 1 observed in figure 5.15 and might suggest a different impact of the parameter on the two bowthrusters. Nonetheless, all the other instruments record similar mean velocities and dominant directions for both sets of tests.

5.5. Conclusions

After analysing results from the measurements, some general observations can be drawn. Firstly, recorded mean horizontal flow magnitudes are normally in the order of magnitude of 1 m/s, with the exception of Test 22, where one of the instruments records mean horizontal flow velocities in the order of magnitude of 2 m/s. The two instruments located nearer to the quay wall, ADV1 and ADCP1, show a clear increase of velocity with increase in applied power for tests conducted with the ship in position 1. ADV2, the instrument located in between the two suction points of the 4-channel bowthruster system, shows that at its location flow on the bottom is dominated by the inflow. ADCP2, located at the most external measuring point, doesn't seem to record flow velocities related with the use of bowthrusters. Use of bowthruster 1 or bowthruster 2, which have different wall clearances, seems to be indifferent for velocities at the bottom when tests conducted with a small keel clearance are compared. On the other hand, flow at the bottom induced by bowthruster 2, associated with a larger wall clearance, appears to be more affected by an increase in keel clearance: when comparing tests performed at high water, use of bowthruster 2 is associated with higher mean flow velocities than use of bowthruster 1. Differences in keel clearance might therefore have a different impact depending on the wall clearance. Use of both bowthruster simultaneously doesn't lead to differences in mean flow velocities larger than the ones between

the use of bowthruster 1 or bowthruster 2. When considering spatial variability of the flow at the bottom, a large variability in recorded direction has firstly to be noted. Then, the bowthruster-induced flow seems to be limited to the space between the outlet and the quay wall. Also in the direction parallel to the quay, the flow seems to be restricted to a couple of meters from the bowthruster outlet, although when bowthruster 2 is used its extent seems to be wider than the one associated with the use of bowthruster 1. Lastly, it can be observed a high variability in direction.

6

Comparison with theory and guidelines

In this chapter, a comparison of the tests results with the theoretical formulation of the flow velocities applied in the guidelines is presented. The maximum calculated velocities at the bottom are compared with measured data, focussing not only on magnitudes, but also in trends, use of multiple propellers and dependency on keel clearance. Then, focus is set on turbulence: relative turbulence intensity is calculated for measured data and compared with values found in literature. Lastly, results from the measurements are used in bottom protection design formulas, and compared to fully theoretical calculations. Goal of this comparison is to understand the impact of differences in calculated and measured velocities on the bottom protection design.

6.1. Maximum velocities at the bottom

As summarized in chapter 2, commonly used guidelines for bottom protection design, such as PIANC [15] and Rock Manual [6], propose two different methods to calculate the hydraulic load caused by transverse thrusters: German method and Dutch method. In figure 6.1 and 6.2, maximum velocities as calculated according the two proposed methods from the guidelines are compared with measured data from ADCP1 and ADV1. These, being the instrument closest to the quay wall, are considered to be the ones capturing the maximum velocities. Comparison is made both for bowthruster 1 and bowthruster 2, respectively using data from Test 1 and 2, considered representative for a low water example (figure 6.1), and Test 11 and 12, which were performed with a larger water depth (figure 6.2) . As measured maximum velocity, $\bar{V} + 3\sigma$ is used. Details about the calculations can be found in appendix D, and for the detailed formulas see chapter 2, equations 2.10, 2.13 and 2.14.

From figure 6.1, it appears how flow velocities measured with a small keel clearance seem to be significantly lower than the ones expected from calculations. By way of contrast, making the same comparison for tests conducted with a higher keel clearance, as in figure 6.2, data from ADV1 shows velocities which are higher than both guidelines formulas. Observing the trend presented by the data, there is a consistent increase in maximum velocity at the bottom with increase in applied power. However, not always the trend follows the proportionality to $P^{0.33}$ suggested by equation 2.4. ADCP1 at high water tends to have a flatter trend, as observable in figure 6.2; at low water, is the ADV that doesn't follow such as steep increase, as it can be seen in figure 6.1. Finally, comparing the two graphs it can be observed how the sensitivity of theoretical formulas to the change in wall clearance and keel clearance is not reflected by the data, that generally show lower variability than formulae. Especially when comparing graphs for bowthruster 1 and bowthruster 2, that differ only in wall clearance, the difference in variability of the theoretical values and the variability of data is evident. This leads to think that dependency of maximum bottom velocities on wall clearance and keel clearance might not be well represented by the Dutch and German method, especially for small wall clearances.

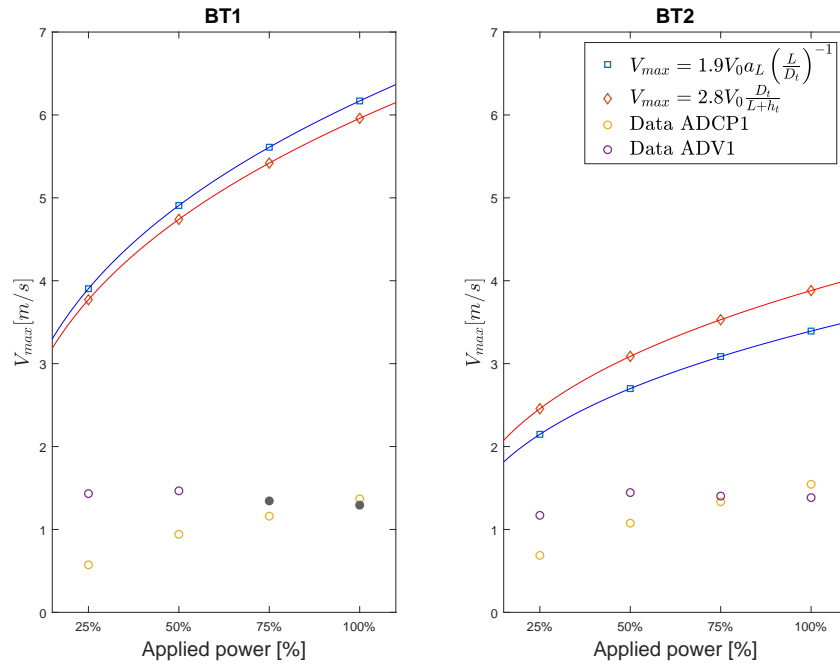


Figure 6.1: Comparison between maximum bottom velocities calculated by Dutch and German method, and measured maximum velocities from ADV1 and ADCP1 data in Test 1 and Test 2. Unreliable data is depicted in grey.

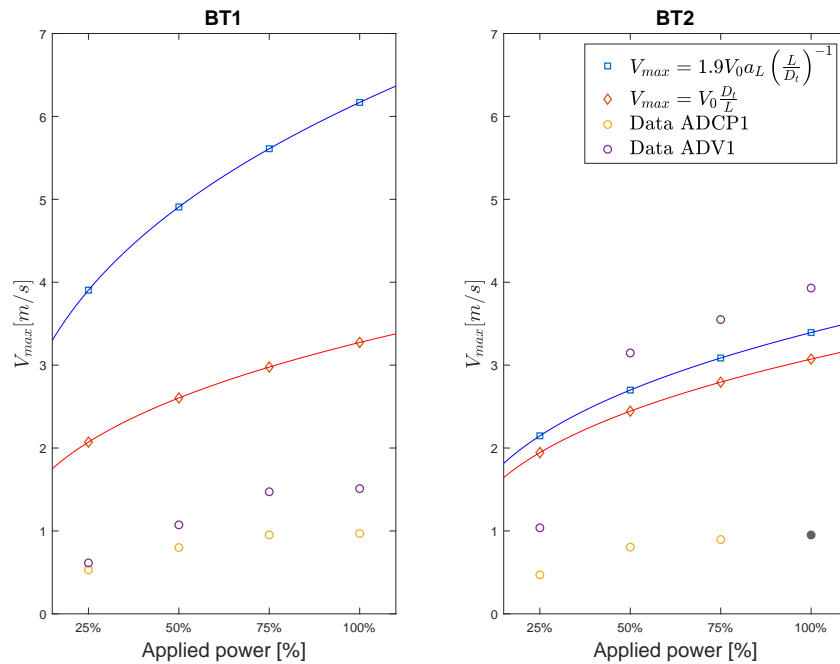


Figure 6.2: Comparison between maximum bottom velocities calculated by Dutch and German method, and measured maximum velocities from ADV1 and ADCP1 data in Test 11 and Test 12. Unreliable data is depicted in grey.

6.2. Use of multiple propellers

According to literature, two approaches are adopted to take into account the use of multiple propellers: either linear superposition [15], or proportionality to square root of number of propellers used [18]. Therefore, in this section, a comparison is made between maximum velocities at the bottom recorded during tests where both bowthrusters were used, and both theoretical relations are compared with data. Calculations made in section 6.1 have been used as a comparison with data from tests 13 (figure 6.3, and then tests 3 and 22 (figure 6.4). Maximum velocity at the bottom has been taken as $V_{max} = \bar{V} + 3\sigma$. Both theories reveal themselves to be conservative in most cases, with the exception of ADV1 data from test 22, which, as it can be seen in figure 6.4, give even higher velocities than expected one. Test 22, though, has already revealed itself to be an exception to the general behaviour of the dataset. It has to be highlighted how conditions in test 3 and test 22 are comparable, and, therefore, similar results would be expected.

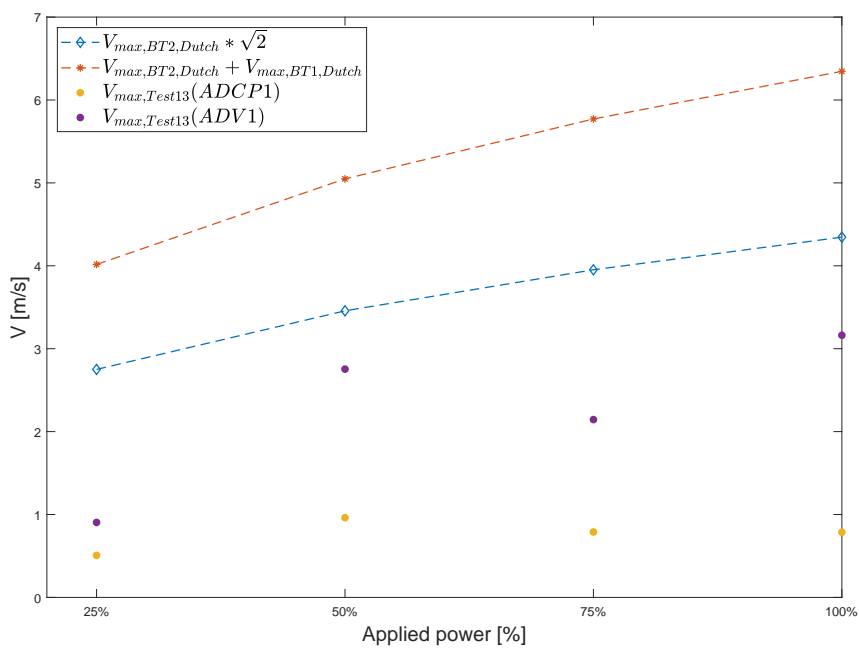


Figure 6.3: Comparison of theory of linear superposition and velocities being proportional to the square root of number of propellers used, with data from test 13. Dutch method used to calculate theoretical maximum velocities. Unreliable data are depicted in grey.

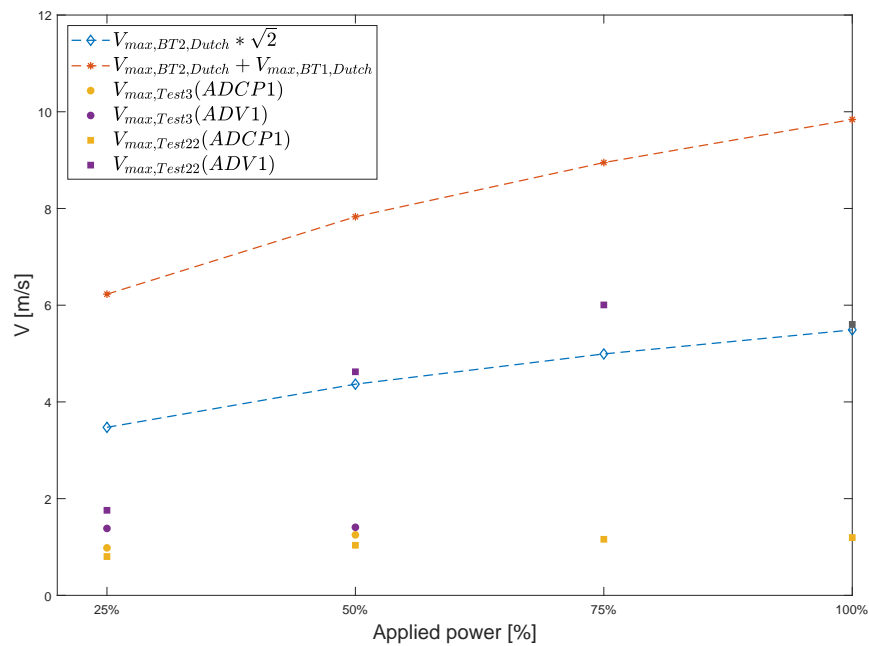


Figure 6.4: Comparison of theory of linear superposition and velocities being proportional to the square root of number of propellers used, with data from tests 3 and 22. Dutch method used to calculate theoretical maximum velocities. Unreliable data are depicted in grey.

Given that, as observed in section 6.1, variability due to the use of different bowthrusters according to both German and Dutch method is not well matched by the data, another check on the use of multiple propellers has been done applying the linear superposition theory and the multiplying by a factor $\sqrt{2}$ directly to data from tests where one propeller was used, and then comparing it to mean velocities recorded in tests where both propellers were used. In figure 6.5, both theories are compared with results from tests 11, 12 and 13. In tests 11, 12 and 13, respectively bowthruster 1, bowthruster 2 and both bowthruster simultaneously are used, in similar water depth conditions and with the vessel positioned symmetrically with respect to the outlets. Results from test 13 recorded by ADV1 appear to match data from test 11 multiplied by $\sqrt{2}$; however, it has to be considered that use of bowthruster 2 in test 12 induced significantly larger velocities. Therefore, theory appeared to be conservative in most of the cases. In test 22, though, a different behaviour appears: ADV1 shows velocities remarkably larger than both theories, as shown in figure 6.6.

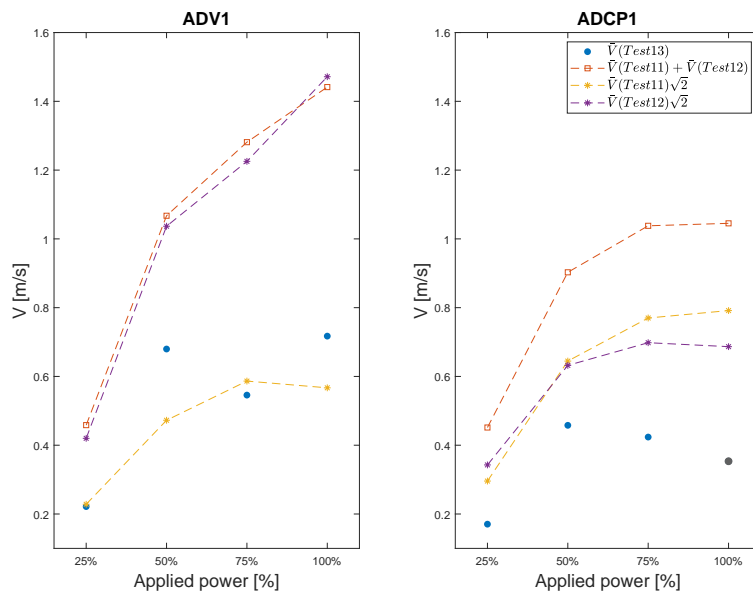


Figure 6.5: Comparison of theory of linear superposition and velocities being proportional to the square root of number of propellers used, with data from tests 11, 12 and 13 where respectively bowthruster 1, 2 and both bowthruster simultaneously are used. Unreliable data are depicted in grey.

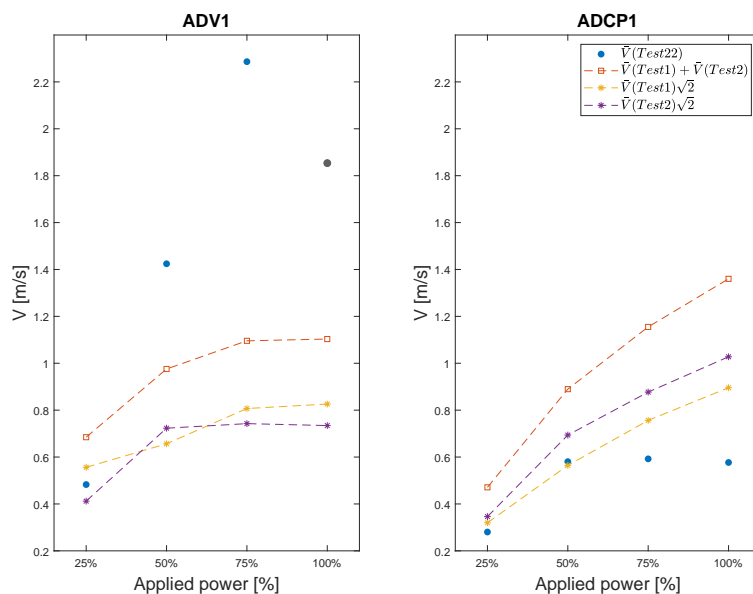


Figure 6.6: Comparison of theory of linear superposition and velocities being proportional to the square root of number of propellers used, with data from tests 1, 2 and 22 where respectively bowthruster 1, 2 and both bowthruster simultaneously are used. Unreliable data are depicted in grey.

6.3. Influence of keel clearance

While comparing the collected data with Dutch and German method, as in section 6.1 and 6.2, it can be noted how the formulae seem to have a higher sensitivity to keel clearance variation than the data. To further investigate this aspect, dependence on the height of thruster (h_t) in the water column is compared for data and guidelines, both for bowthruster 1 and bowthruster 2. Results can be observed in figures 6.7 and 6.8 respectively. Maximum velocities are compared. As previously observed, guidelines values obtained applying Dutch method are conservative when looking at use of bowthruster 1, while ADV1 records higher maximum velocities than expected, if tests where bowthruster 2 was used during high tide. Once again, there is a difference in what measured by ADV1 and ADCP1, despite their vicinity. ADCP1 records velocities lower than the guidelines, and which decrease with increase of height of the thruster in the water column, consistently with the trend identified by the Dutch method. ADV1, on the contrary, especially for higher values of applied power, seems to follow a different trend. Furthermore, if for the guidelines the change in wall clearance, which represents the main difference between bowthruster 1 and bowthruster 2, results in a clear difference in dependence on h_t , this difference is not reflected by the data. As previously noted in this report, commonly used guidelines recommended by PIANC do not seem to succeed in capturing the dependence on wall clearance and keel clearance for this dataset.

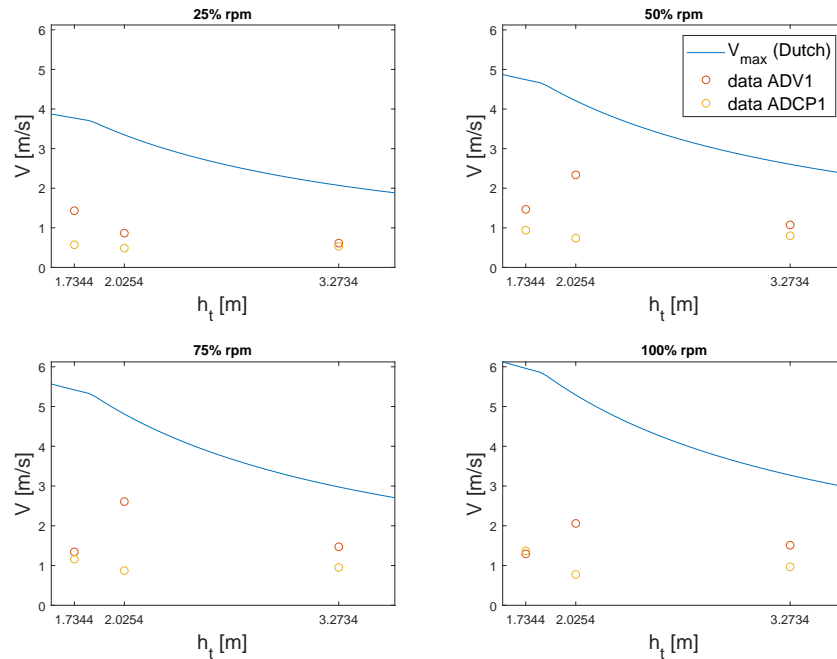


Figure 6.7: Dependence on thruster height in the water column for bowthruster 1, comparison between data and Dutch method.

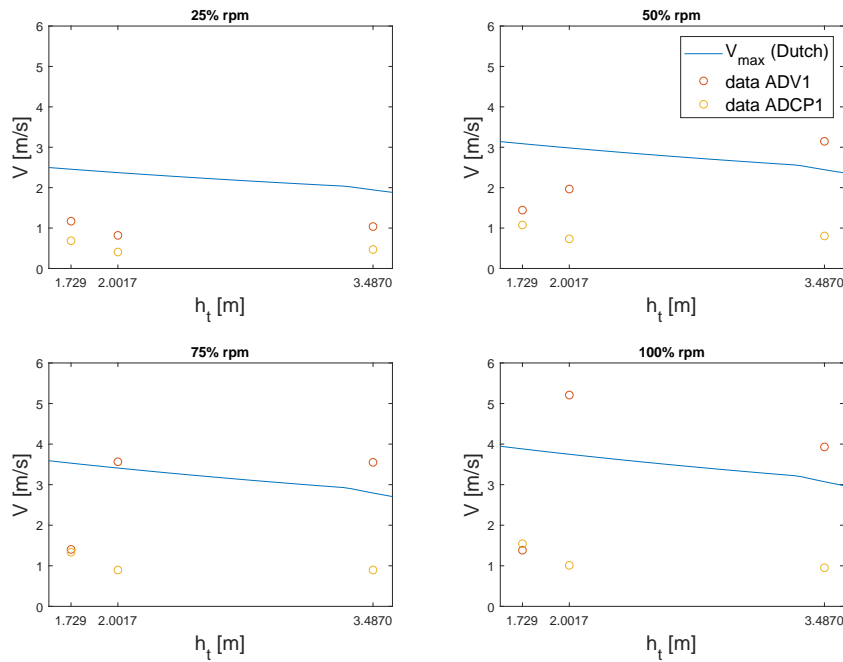


Figure 6.8: Dependence on thruster height in the water column for bowthruster 2, comparison between data and Dutch method.

6.4. Relative turbulence intensity

Turbulence can be quantified in several ways: one of the most common is the relative tur-

bulence intensity $r = \frac{\sqrt{u'^2}}{\bar{u}}$, where the root mean square value of the turbulent fluctuations (u') is compared with the average of the same flow velocity component (\bar{u}). It has to be noted that relative turbulence intensity loses its meaning when the mean flow velocities are low. In design formulas, the turbulence factor k it's often introduced to determine rock diameter. Turbulence factor can be derived from relative turbulence intensity as:

$$k = \frac{1 + 3r}{1.3} \quad (6.1)$$

Literature indicates 0.25 to 0.4 as typical range of values for propeller's jet induced relative turbulence intensity [15]. This large range of values derives from the different methods used to study it, and it is mainly derived without taking into account the influence of any restriction such as a vertical wall. According to equation 6.1, these values correspond to a turbulence factor between 1.35 and 1.69. In the Pilrczyk formula, k is squared. Correspondent values are therefore in the range of 1.82 - 2.86. Nonetheless, values of k^2 recommended by Rock Manual are between 5.2 and 6 [6]. In figure 6.9, measured relative turbulence intensity in function of the distance from the quay wall is shown, for both bowthrusters.

Turbulence intensity generally decreases with increasing distance from the quay wall, with the exception of data from the last instrument. It is important to note, though, that mean flow velocities measured by the last instrument are really low and this might affect the representativity of a parameter such as the relative turbulence intensity. Furthermore, relative turbulence intensity show a decreasing trend in relation with the increase in applied power for the instruments located near to the quay wall, while turbulence seems to increase with increase in applied power in the vicinity of the suction point of the bowthrusters. Concerning the difference within the two bowthrusters, bowthruster 2 presents generally higher values of turbulence intensity.

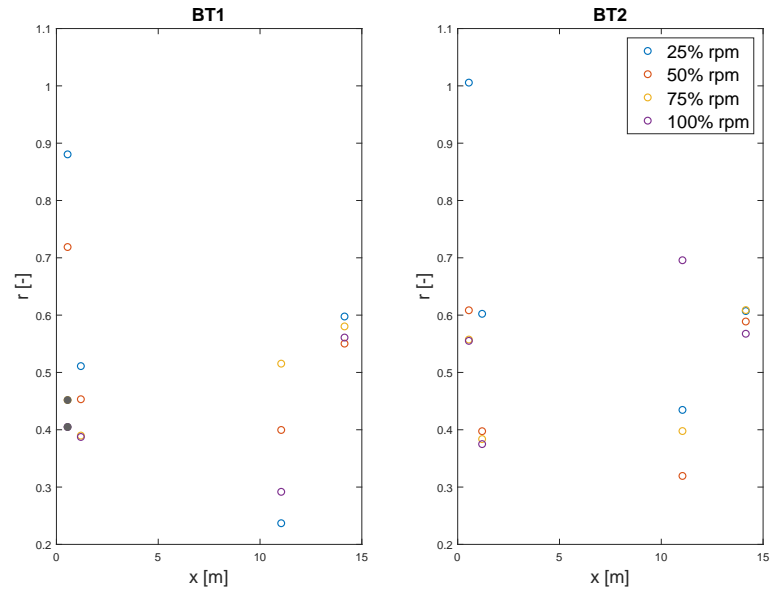


Figure 6.9: Relative turbulence intensity in function of the distance from the quay wall, associated with the use of bowthruster 1 (test 1) and bowthruster 2 (test 2). Unreliable data are depicted in grey.

Relative turbulence intensity values are then compared to the expected ones. Results are shown in figure 6.10.

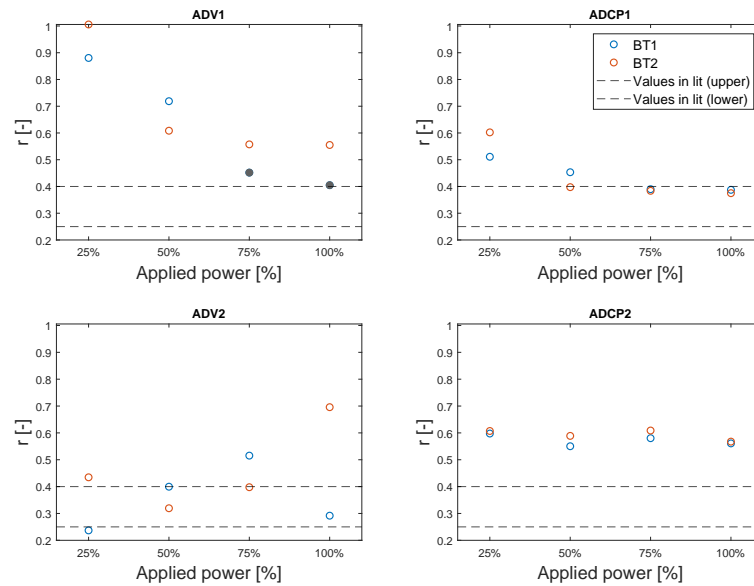


Figure 6.10: Relative turbulence intensity measured by each instrument for each step of applied power. Comparison between bowthruster 1 (Test 1) and bowthruster 2 (Test 2) is illustrated. Unreliable data are depicted in grey. Reference lines of turbulence intensity values expected from literature is illustrated.

Generally, the instruments near the quay wall record relative turbulence intensity levels higher than expected from literature, sometimes even in the order of magnitude of 1. A relative turbulence intensity of 1 would correspond to a squared turbulence factor of 9.47, higher even than the values between 5.2 and 6 recommended by guidelines for designing bottom protections. It has though to be noted that these levels of relative turbulence intensity are also related to velocity magnitudes which are lower than expected from theoretical calculations, and often in the same order of magnitude of the absolute turbulence intensity. The two instruments closer to the quay wall show a clear decreasing trend of turbulence intensity with the increase of applied power, but this has to be evaluated taking into account the increase in mean flow velocity. ADV2 shows different trends for bowthruster 1 and bowthruster 2, while ADCP2 records levels of turbulence intensity fairly constant, in accordance with the previously found results of ADCP2 not recording velocities related to the use of the bowthrusters.

6.5. Impact of measurements results on bottom protection design

In order to assess the impact of the measured velocities on the bottom material stability, calculations of rock sizes stable under the measured bowthruster-induced hydraulic load are conducted in this section. Both Izbash and Pilarczyk formulas have been applied. Three cases have been selected as representative of the load and, therefore, determining design parameters for an eventual redesign of the bottom protection: a summary of the cases is listed in table 6.1. Case 1 represents the worst case scenario for single use of Bowthruster 1: 100% of applied power with a low keel clearance (Test1, ADCP1 data). Case 2 represents the worst case scenario for single use of Bowthruster 2: 100% applied power with a high keel clearance (Test 12, ADV1 data). Finally, Case 3 represents the worst case scenario for use of both bowthrusters simultaneously, and the largest flow velocities recorded during the measurements: 75% applied power with a low keel clearance (Test 22, ADV1 data).

Table 6.1: Cases identified for calculation of rock size needed for the bottom protection. Both collected data and theoretical values according to Dutch method are presented.

Case	Description	Data						Dutch method		
		Test	\bar{V}	σ	V_{max}	r	k	V_{max}	B_{cr}	k
1	Bowthruster 1, low tide, 100%	1	0.63 m/s	0.25 m/s	1.38 m/s	0.40	1.69	2.13 m/s	0.8	2.45
2	Bowthruster 2, high tide, 100%	12	1.04 m/s	0.96 m/s	3.92 m/s	0.92	2.90	3.07 m/s	0.8	2.45
3	Both bowthrusters, low tide, 75%	22	2.29 m/s	1.25 m/s	6.04 m/s	0.55	2.03	3.01 m/s	0.8	2.45

General inputs necessary for Pilarczyk and Izbash formulas are listed in table 6.2.

Results of the calculations made using Izbash approach are shown in table 6.3, while results of calculations made using Pilarczyk formula are listed in table 6.4.

Table 6.2: General input used to calculate rock D_{50} stable under conditions described by case 1, 2 and 3 according to Pilarczyk and Izbash formulas.

Parameter	Description	Value	Unit of measures
Δ	Relative density of rock	1.65	[-]
g	Gravitational acceleration	9.81	$[m/s^2]$
Φ	Stability parameter for a continuous top layer	1	[-]
Ψ_{cr}	Critical Shields parameter for rock	0.035	[-]
kh	Velocity profile factor	1	[-]
ksl	Slope factor	1	[-]
B_{cr}	Coefficient for Izbash equation	0.8	[-]

Table 6.3: D_{50} and corresponding rock class calculated using Izbash approach. A comparison between values obtained from data, considering both mean velocity and maximum velocity $V_{max} = \bar{V} + 3\sigma$, and from theoretical values calculated following the Dutch method is presented.

Case	Data (\bar{V})		Data (V_{max})		Dutch method	
	D_{50}	Rock class	D_{50}	Rock class	D_{50}	Rock class
1	0.02 m	<30-60 mm	0.09 m	50-150 mm	0.22 m	5-40 kg
2	0.05 m	30-60 mm	0.74 m	0.3-1 t	0.45 m	60-300 kg
3	0.25 m	5-40 kg	1.76 m	6-10 t	0.44 m	40-200 kg

Table 6.4: D_{50} and corresponding rock class calculated using Pilarczyk formula. A comparison between values obtained from data, considering both mean velocity and maximum velocity $V_{max} = \bar{V} + 3\sigma$, and from theoretical values calculated following the Dutch method is presented.

Case	Data (\bar{V})		Data (V_{max})		Dutch method	
	D_{50}	Rock class	D_{50}	Rock class	D_{50}	Rock class
1	0.04 m	<30-60mm	0.20 m	5-40 kg	0.47 m	60-300 kg
2	0.33 m	10-60kg / 40-200 kg	4.75 m	>6-10 t	2.91 m	>6-10 t
3	0.79 m	0.3-1 t	5.52 m	>6-10 t	1.37 m	3-6 t

Firstly, it can be noted how theoretical calculation carried out following both Izbash and Pilarczyk formula are conservative for Case 1, which is the only case where the relative turbulence intensity is comparable with the values found in literature. In Case 2 and Case 3, where the large variability of velocity recorded by ADV1 yields to values of r and (in Case 2) even k larger than the ones recommended by PIANC [15] and Rock Manual [6], the rock sizes calculated with the Dutch method velocities are significantly lower than the ones obtained

using the data, especially when looking at Pilarczyk formula. Nevertheless, values thus obtained have to be considered also for themselves. The high values for D_{50} found out in the calculations suggest that only classes of rocks normally used for breakwater design would have withstood velocities measured in Case 3. Nonetheless, the existing bottom protection reported no damage, as highlighted by surveys effectuated after the measurements (see appendix E). Moreover, instruments didn't report any damage either. For Case 1, the calculation method for the hydraulic load is conservative if compared with the measured velocities, and it translates in an overdesign of the bottom protection. In addition, considering the large values of rock diameter obtained from Case 2 and Case 3 calculations, it comes natural to think that stability formulae might be overly conservative when applied to the situation covered in this research. For instance, it can be raised as a point of discussion if the formulas are able to well represent the balance between influence of the mean flow and turbulent fluctuations. As it can be observed by comparing values of stable rock sizes calculated using mean flow velocity and maximum flow velocity obtained as $V_{max} = \bar{V} + 3\sigma$, results are really sensitive to an increase in mean flow velocity. When a highly turbulent flow is present, incorporating the variability of velocity in $V_{max} = \bar{V} + 3\sigma$ yields to a sensible increase of rock diameter. Furthermore, as seen in section 6.4, in this research often low mean flow velocities magnitude, but with large fluctuations are found. This seems to be a case which might not be well represented by commonly used stability formulae.

6.6. Conclusions

Comparing data with values obtained following recommended methods ("Dutch" and "German") from PIANC guidelines, noticeable differences with the data collected in this research can be observed. Generally, the data presents lower values of mean flow velocities and higher values of relative turbulence intensity than expected. This leads to consider the guidelines generally conservative when concerning the situation considered in the measurements. Exceptions are usually represented by tests where the instruments record a highly turbulent flow, with large values of turbulent intensity. Dependency on parameters such as wall and keel clearance presented by Dutch method formulas are not reflected by the data. Wall and keel clearances as small as the one from this field measurement campaign, which are typical for inland vessels, fall outside the range considered by German method. Use of multiple bowthrusters doesn't appear to be well represented by theoretical calculations either. Concerning the impact on bottom protection design, stability formulae from Izbash and Pilarczyk appears to be conservative when the values of turbulence intensity fall within the range considered in the theory. Outside this range, they yield to stone sizes unusually big for a bed protection. These numbers are though inconsistent with the lack of damage on existing bottom protection and instruments. This fact could lead to think that balance between influence of mean flow velocity and turbulence on rock stability might not be well represented by the currently in use formulae when applied to use of 4-channel bowthrusters within the boundary conditions of this field measurement campaign.

7

Discussion

In this chapter, a discussion on the test results is presented. Measurement set-up and protocol are debated in light of the obtained results, the validity of assumptions taken during the fieldwork and data analysis is evaluated. Lastly, the impact of results on the bottom protection design is considered.

7.1. Assessment of the adopted measurement set-up and protocol **Spatial resolution of measurement points**

Fieldwork is always the result of several assumptions and compromises between what is ideal and what is feasible. This specific measurement set-up has been defined based on the necessity of minimizing movement of instruments and vessel due to time restrictions, and the will of testing both bowthrusters in as many different conditions as possible. Moreover, the decision to utilize accurate yet expensive equipment such as ADCPs and ADVs, affected the number of measurement points which could be planned. Therefore, it comes naturally to wonder if the adopted measurement set-up is indeed representative of the bowthruster induced flow pattern. Concerning ADCPs, in chapter 4 cell 2 has been assumed as most suitable to represent the flow characteristics. To test the boundaries of this assumption, a velocity profile along each beam has been made for ADCP1. Given the instrument position, if the bowthruster induced jet is reflecting perpendicularly from the quay wall, then one of the beams (depending on the bowthruster used) should intercept it at a distance from the instrument larger than the one occupied by cell 2.

In figure 7.1 and 7.2, in line velocities of ADCP1's beam 2 and beam 4, respectively for test 1 and test 2, are shown. An average for each step of applied power is taken.

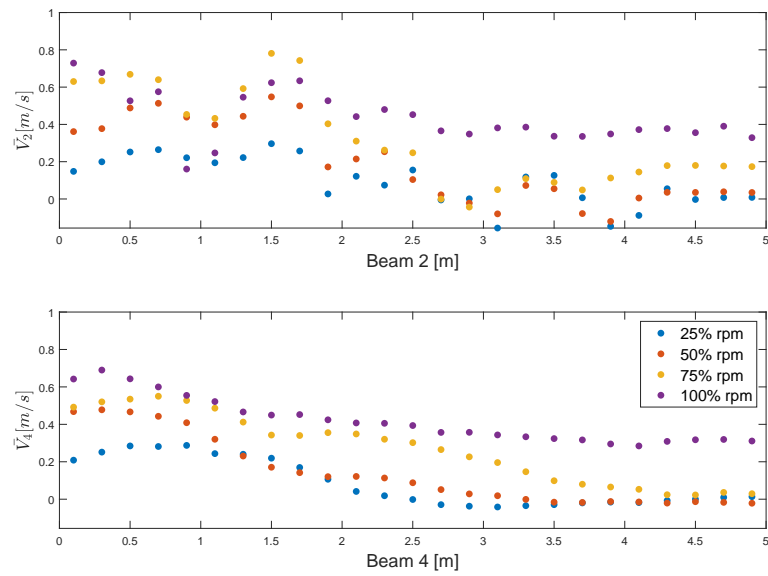


Figure 7.1: Beam velocity profile for ADCP1 test1. Average for each subtest is taken.

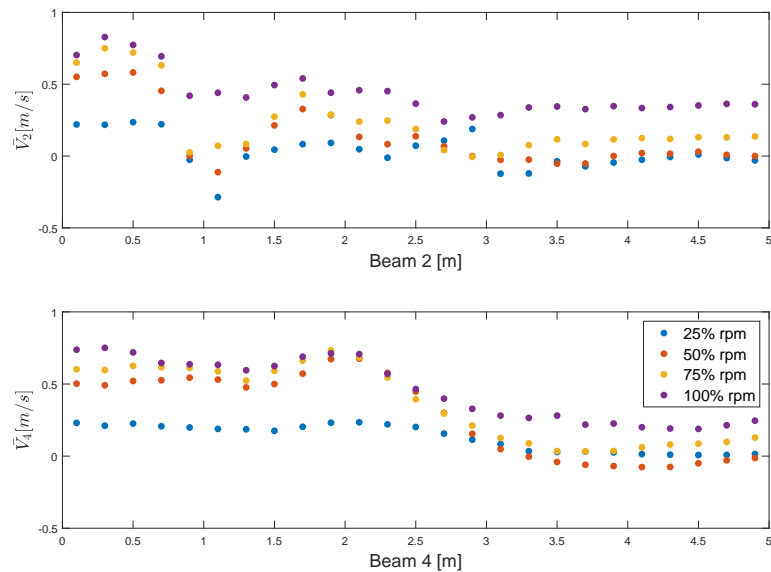


Figure 7.2: Beam velocity profile for ADCP1 test2. Average for each subtest is taken.

The profiles record a sudden peak in inline velocities at respectively 1.5 m along beam 2 (for test 1) and 2 m along beam 4 (for test 2). As it can be observed from figure 7.3, this is approximately the distance where the beams start measuring flow velocities underneath the ship. Therefore, the increase in in-line velocities at this location could be due to an acceleration of the returning flow caused by constriction between the ship's hull and the sea bed. After 1 m from the instrument, measurements are not considered representative anymore, due both to reliability problems such as loss of correlation, and to the increase in measuring volume. On the other side, recording an increase in inline velocities at 1.5 m

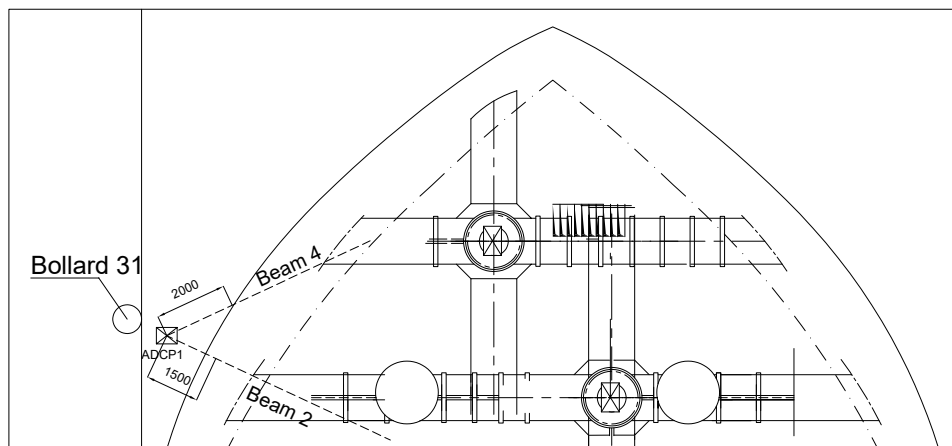


Figure 7.3: Illustration of ADCP1 with respect to the vessel. Beam 2 and 4 of the instruments are depicted by dashed lines, and distances where a sudden increase of in-line velocities along the beams is observed in test 1 and 2 are indicated. Source: author.

from the instrument with values similar to the ones recorded in the first cell, might suggest higher velocities happening at the corresponding point near the quay wall. Therefore, the limitations due to low spatial resolution of the measurement set-up are highlighted by this check.

Another discussion point is represented by the above mentioned discrepancies between measurements by ADV1 and ADCP1. Despite their vicinity, often ADV1 records higher mean velocities and larger standard deviation than ADCP1. Since both instruments are mostly reliable from a technical functioning point of view (there is no significant loss of correlation, or capping of the velocities, as shown in chapter 4), the possible explanation could lie in a variability of the flow so high to change in the space of few decimeters. When observing different cells of ADCP1, though, the flow characteristics do not seem to change so quickly, as seen in figure 4.16. An alternative explanation could be that ADCP is not able to capture perfectly such a turbulent flow: therefore, it records mean flow velocities lower than the adjacent ADV, but still within one standard deviation from ADV mean velocities, due to its larger variability. This is coherent also with the smaller variation in velocity direction presented by ADCPs with respect to ADVs, but would not explain fully tests where measurements from the two instruments are consistent.

Discrepancies in the measurements: analysis of pressure fluctuations

Furthermore, as seen in chapter 4, figure 4.13 and 4.14, there is a discrepancy present between pressure fluctuations and velocity magnitude recorded by ADCP1. To further investigate it, the fact that only horizontal velocity has been measured needs to be taken into account. Therefore, a fully 3D flow has been assumed:

$v_z^* = \max(v_x, v_y)$ has been taken as the instantaneous vertical component, and the subsequent

full 3D velocity $V^* = \sqrt{v_x^2 + v_y^2 + v_z^{*2}}$ has been calculated. As it can be observed from 7.4, even taking into account a fully 3D flow, the gap is still present.

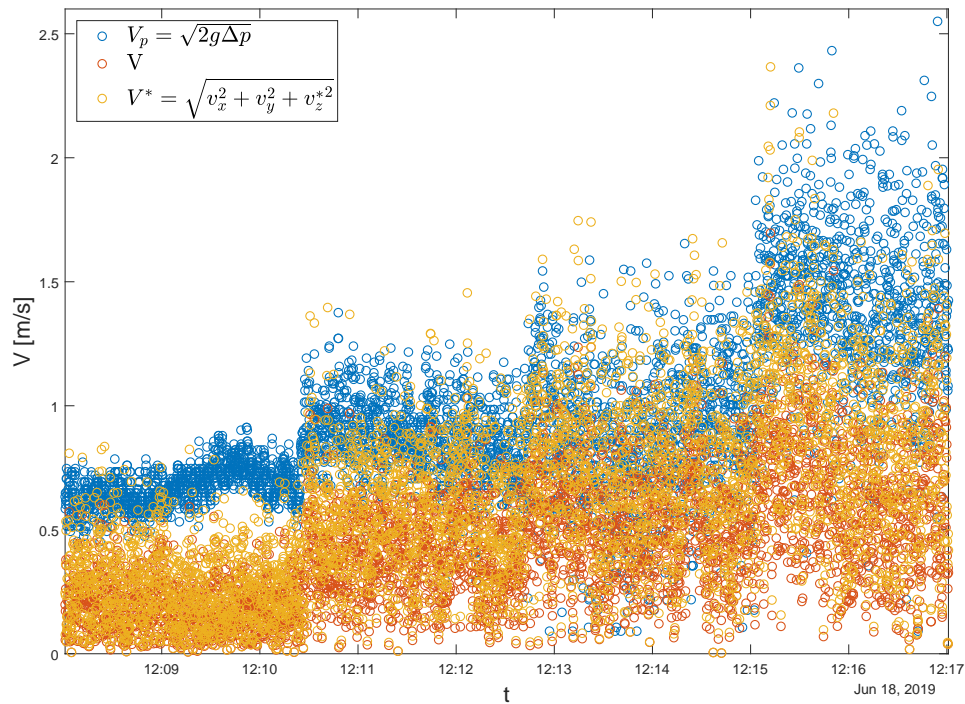


Figure 7.4: Comparison of velocity correspondent to pressure fluctuations according to Bernoulli's theorem, measured horizontal velocity magnitude and 3D velocity magnitude, calculated assuming vertical component equal to maximum between x and y measured components. Data presented for ADCP1.

Similar results can be found while repeating the same check for ADCP2. Unfortunately, due to the measurement set-up, the head of ADVs, where velocity measuring takes place, is not located in the same place as the pressure sensor, situated in a case positioned at several meters of distance from the head. Therefore, the very same check for the ADVs was not possible.

Interesting to note that discrepancies between measurement by ADV1 and ADCP1 are present especially when the flow has more space to develop: when bowthruster 2 is used and there is a larger distance between outlet of the bowthruster and quay wall, or during tests conducted with a higher keel clearance.

Pressure oscillations have then been investigated as an alternative to velocity magnitude. A comparison between the x-profile of measured velocities and velocities obtained through Bernoulli has been made and can be observed in figure 7.5. It has to be noted that the location of measurement of pressure and velocities for ADVs is different.

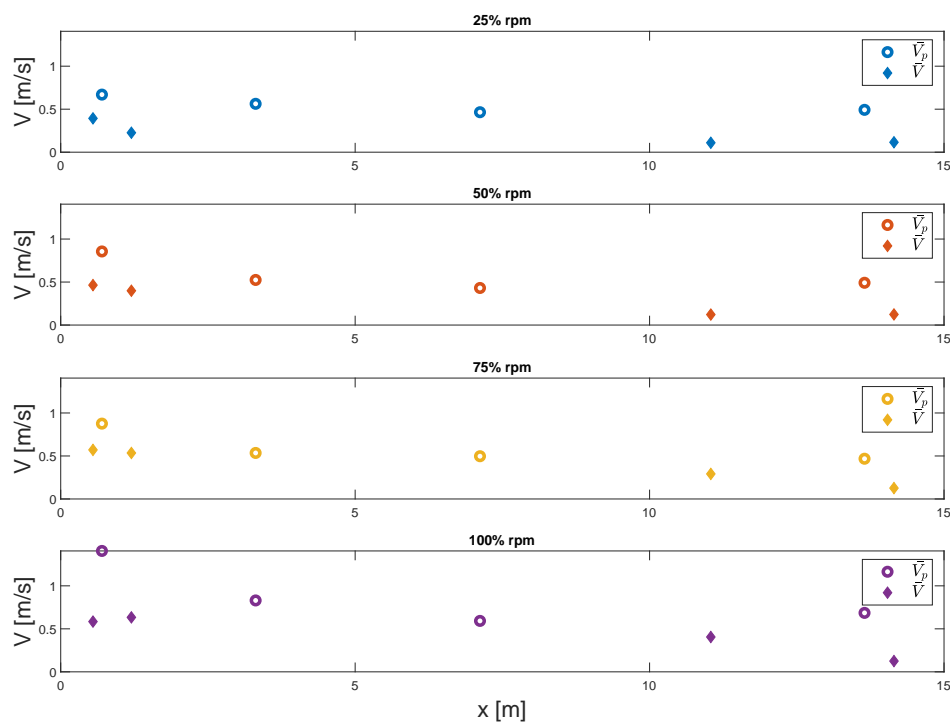


Figure 7.5: Velocity profile in the direction perpendicular to the quay wall, obtained combining measured velocities and velocities correspondent to pressure fluctuations for Test 1, for all steps of applied power.

It can be observed that the profile obtained for the pressure fluctuations has a less abrupt decay than the one obtained from measured velocities, where there is a clear difference between velocities measured at the quay wall and velocities recorded by the instruments farther away. Furthermore, pressure fluctuations give indication of higher velocity magnitudes than the measured ones. Difference is particularly significant for 100% of applied power. In figure 7.6, a different visualisation of comparison between pressure fluctuations and recorded velocities is sought, aiming at understanding differences between measured velocities and pressure fluctuations when it comes to relation with applied power.

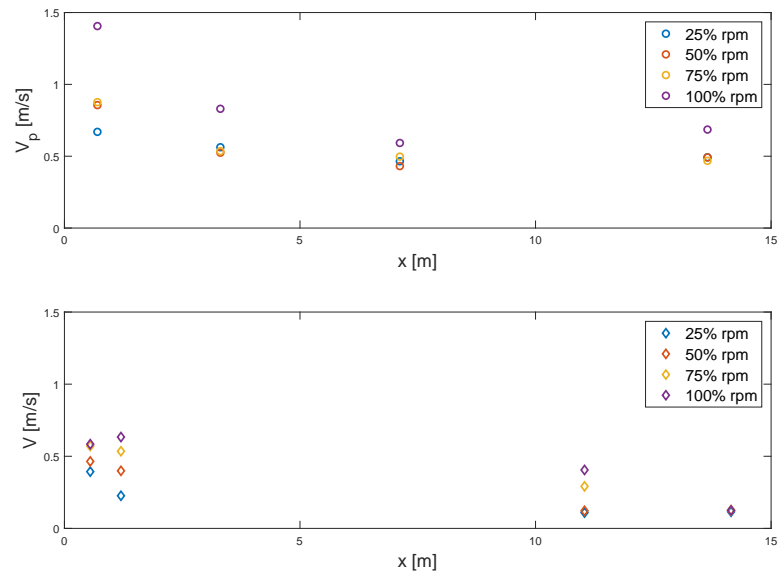


Figure 7.6: Velocity profile in the direction perpendicular to the quay wall for Test 1 as obtained from pressure fluctuations (upper graph) and measured velocities (lower graph). All steps of applied power are represented.

From the figure, it is clear how pressure fluctuations resent more of the variation in applied power, especially the ones at the quay. Decay along the x axis is not only smoother than for measured velocities, but profiles show differences in shape depending on the applied power. This might suggest that pressure fluctuations are indeed a more accurate measure for such a turbulent flow. On the other hand, seeing how pressure fluctuations of the three instruments farther away from the quay wall present little variation for percentage of applied power, supports the hypothesis of a limited extent of reflected flow from use of bowthrusters. Especially for the last measurement point, correspondent to ADCP2, there are almost no variations, with the except of 100% applied power. The latter, though, represents a trend change in the progressive decay of velocity along x axis, being higher than data from the previous instrument. Therefore, theory that ADCP2 measurements are not influenced by use of bowthrusters might hereby find confirmation.

Comparison with a realistic mooring operation

Another assumption underlying this research is that measurement conducted with a still ship, moored to the quay wall, are representative of a real life situation. During Test 23, a de-berthing manoeuvre is performed with both bow-thrusters activated at the maximum power, with a keel clearance of around 1.2 m. The velocities recorded during test 23 are compared with the ones measured in test 1, in order to assess the validity of the above mentioned assumption. In figure 7.7, a time series of velocities recorded during test 23 is presented.

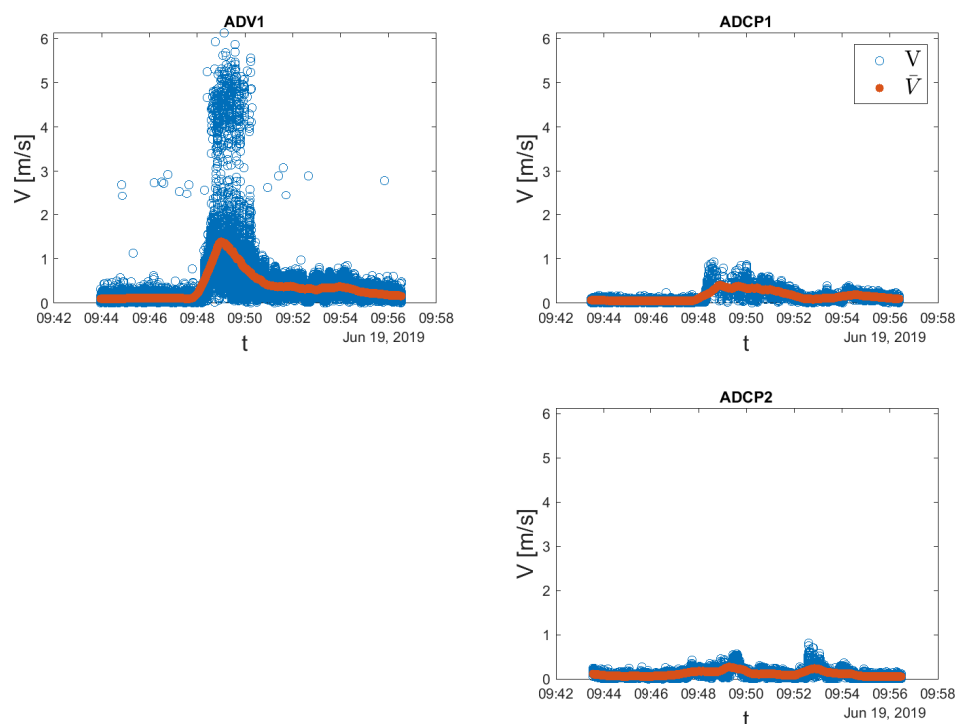


Figure 7.7: Test 23 results: mean horizontal velocity magnitude timeseries. All instruments are represented, except for ADV2.

Mean velocities recorded are of the same order of magnitude of the ones calculated for test 1. Consequently, the test results could be assumed to be quite representative of a real life situation. On the other hand, ADV1 is recording maximum velocities around 6 m/s; significantly higher than the ones recorded in stationary conditions. This might suggest that dynamic situations might be more governing than the stationary one.

7.2. Contextualisation in the theoretical framework

From comparison with Dutch and German calculation methods of flow velocities on the bottom recommended by PIANC guidelines presented in chapter 6, data collected in this study identified the guidelines as conservative in most cases. On the other side, data recorded by ADV1 in some tests, namely test 12 and 22, resulted in maximum velocities at the bottom larger than the expected ones. Both in test 12 and test 22, bowthruster 2 was used: in test 12 on its own, in test 22 simultaneously as bowthruster 1. Bowthruster 2 is characterised by a larger wall clearance, equal to $4.23 D_t$, while bowthruster 1 is located at $2.32 D_t$ from the quay wall. Most of the research upon which the guidelines have been based on considered situations where the flow was less restricted than in the case presented in this study: Blaauw and van de Kaa conducted on scale modelling for ducted and unducted propellers, measuring the velocities as the ship was moving in relatively unrestricted waters [21]. Schmidt studied

propeller's against a quay wall in a stationary situation, evaluating different wall and keel clearances. Wall clearance studied by Schmidt were between 7.3 and 4 times D_t , while height of the thruster in the water column was either 2.2 or 2.4 times D_t [19]. In this study, height of the bowthruster changed more gradually within the tests, covering values between 1.21 D_t and 2.45 D_t : in combination with the aforementioned wall clearances associated with the bowthruster system, it is immediate how the flow developed in a more restricted environment if compared with these studies. Already a research presented by Deltares found formulae in literature being generally conservative, with the exception of larger distances between quay wall and ship (9.5 D_t , see [8]). Blokland as well, in his field measurements, found higher flow velocities that expected from calculations; he as well performed field measurements with wall clearances between 3.2 D_t and 16 D_t . This might support the hypothesis that currently adopted guidelines do not reflect influence of wall and keel clearance accurately enough for situations outside a specific range. On the other side, the situation of small wall clearance considered in these field measurements could be representative for inland vessels, which are usually characterised by a hull shape that favours a small distance between the wall and the bowthruster's outlet.

Concerning stability formulas such as Izbash and Pilaczyk, then, it has to be remembered that they have not been specifically developed for propeller's jet. For propeller's jet induced damage, and stability in general, turbulence has been previously identified as a mechanism which might be even more important than mean flow velocity, for instance by Verhagen [24] and Hofland [10]. As observed in chapter 6, for low values of mean flow velocities and high relative turbulence intensities, the resulting D_{50} doesn't always appear to match observations (i.e. surveys conducted after the measurements, absence of damage for the instruments), leading to think that a more precise representation of the physical phenomena should be sought.

To summarize the flow field which has been observed during this research, Schmidt picture of the 5 zones of reflected flow, presented in chapter 2 (figure 2.4), can be resumed and thus modified according to the findings. An illustration of this modification can be observed in figure 7.8.

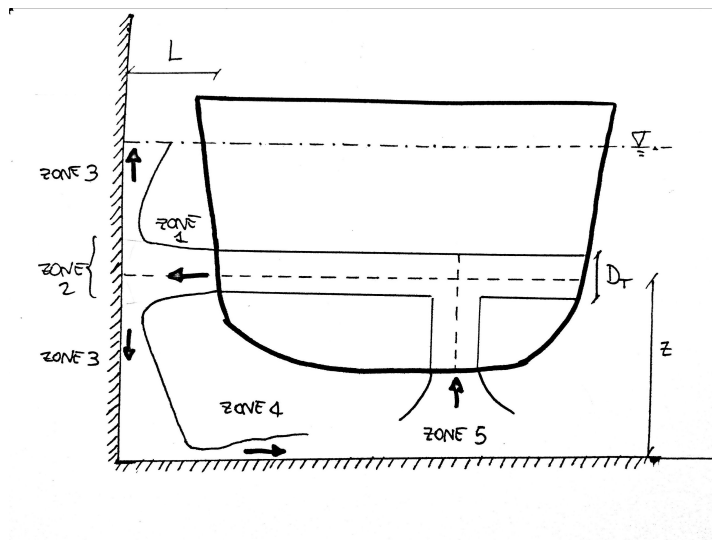


Figure 7.8: Re-elaboration of Schmidt identified zones for a reflected jet on a vertical quay wall. Created by the author based on [19].

The 5 zones are therefore redefined as:

- **Zone 1: Efflux zone.** During the field measurements of this research, the ship has been moored closely to the quay wall: the distance between bowthruster outflow and quay wall is thus around 3.3 m (2.32 times the outlet diameter) for bowthruster 1 and 6 m (4.23 times the outlet diameter) for bowthruster 1. Different flow establishment lengths have been proposed in literature, and they vary between 2 and 6 times the propeller's diameter [11]. Since the majority of authors proposes values around 2.6 - 2.77 times the diameter, both the situations should fall into the established flow situation. From the test results, though, use of bowthruster 2 presents higher flow velocities, which is not consistent with a more decayed flow. Therefore, the flow is assumed to be not yet established and only one zone is considered.
- **Zone 2: Impact zone.** Similarly to Schmidt zone 3, here the efflux velocity is transformed into pressure against the quay wall. Given the low velocities measured at the bottom, this might be where most of the kinetic energy from efflux jet gets transformed.
- **Zone 3: Reflection zone.** Here flow is reflected along the quay wall, comparably to Schmidt zone 4. It has to be noted that, although traditionally propeller's jet is assumed to be symmetric with respect to the axis, low velocities at the bottom, especially in the more confined spaces, might actually indicate a preference for the flow to go towards the surface.

- Zone 4: Return zone. In this zone, a return flow on the bottom is present. From observations, it seems that this zone doesn't extend far from the quay wall, but it is limited to the first few meters.
- Zone 5: Inflow zone. Differently than Schmidt, who conducted his experiments using traditional propellers, for 4-channel type of bowthrusters it is fundamental to take into account the inflow beneath the ship. Once the return flow is dissipated due to friction and turbulence, inflow under the suction point becomes a significant load that has to be taken into account.

7.3. Impact on bed protection design

Based on performed calculations and field measurements observation, a re-design of the existing bottom protection is proposed. Re-design has been done under the assumption that bowthrusters-induced velocities are the dominant load on the bottom, and that measured velocities are representative of a design scenario. A sketch of the proposed design is presented in figure 7.9, compared with dimensions of the existing bed protection.

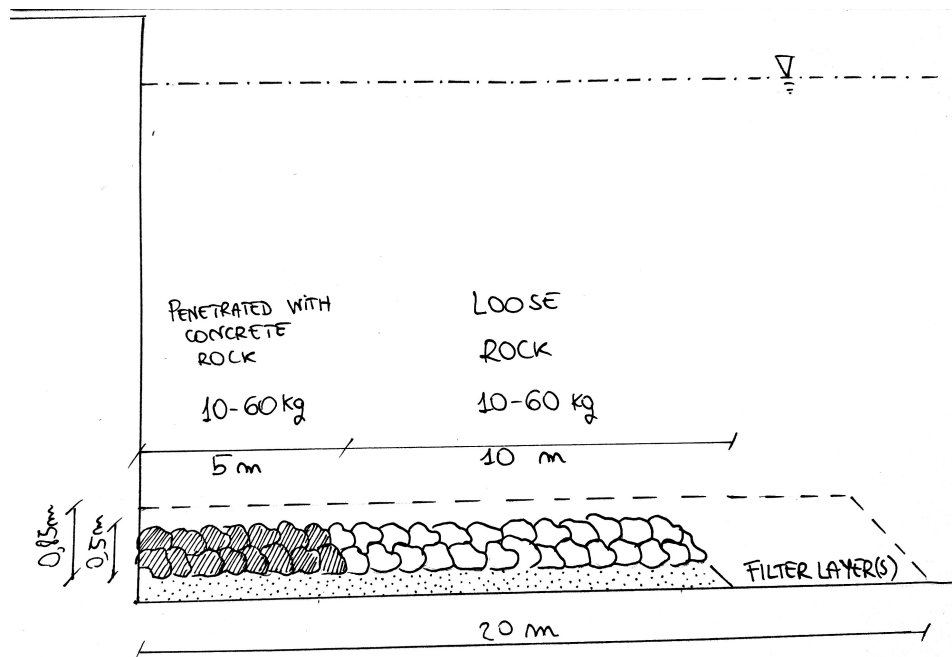
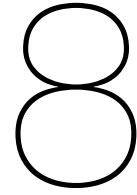


Figure 7.9: Cross-section of the proposed redesign of bottom protection at the Antarcticakade, based on the observed bowthruuster-induced flow. 10-60 kg rocks, penetrated with concrete for the first 5m from the quay wall, for a total width of 15 m.

10 to 60 kg rocks are used, as in the present bottom protection, but it is suggested to penetrate it with concrete only for the first 5 meters from the quay wall, that is where the flow on the bottom is affected by reflection of the jet at the quay wall. For the rest of the width, the bottom protection has to withstand velocities and turbulence caused by the inflow beneath the suction point, which are lower than velocities near the quay wall, but still significant. It is considered safe not to protect the bottom after 15 meters from the quay wall since, from the field measurements, flow on the bottom at this distance presents really low velocities that might derive from tidal currents, and doesn't show relation with use of the bowthrusters. It is proposed to apply the above cross-section uniformly along the quay, to allow berthing in any location.

7.4. Conclusions

In this section, some discussion points regarding the test results are highlighted. Adopted measuring set-up main limitation is identified in its low density of measurement points, and limited redundancy, which makes difficult to determine whether discrepancies observed between measurements of ADV1 and ADCP1, both located close to the quay wall, are due to a high spatial variability of the flow. Despite this drawbacks, measurements presented in this research are able to identify clear zones on the bottom where the flow is influenced by the bowthrustrer jet reflected at the quay wall, by the inflow generated underneath the suction points of the bowthrustrer system, or not influenced anymore by use of bowthrusters. Contextualisation of the presented results in the previously conducted research framework allowed to identify the discrepancies with the guidelines. Namely, different influence of relative wall and keel clearance is highlighted as determining when comparing data with calculated values. Furthermore, a knowledge gap concerning the flow pattern induced by the inflow in a 4-channel bowthrustrer system is found. Lastly, a propose for a re-design of the bottom protection based on the fieldwork measurements and observations is advanced.



Conclusions and recommendations

The results of this study contribute to enhance knowledge on the effect of bowthruster use near a vertical quay wall. The unique dataset hereby presented allowed to highlight differences between traditional transverse thruster systems, upon which commonly used guidelines and theories are based, and a 4-channel bowthruster system. The latter, drawing water from underneath the ship, determines a zone on the bottom where the flow is influenced by the inflow towards the suction points, and that is not present in other bowthruster systems. Furthermore, from this measurements appeared evident how the extent of the reflected flow on the bottom was limited to a narrow zone near the quay wall, and how at 14 m from the quay wall no influence of use of bowthrusters was measured. In addition, comparison with calculations made following the guidelines highlighted discrepancies both in expected velocity magnitude and in dependence from parameters such as keel and wall clearance. In this chapter, a summary of the main conclusions drawn from this study is presented. An answer to the main research question, and to the research subquestions is provided. Then, recommendation for further studies are suggested.

8.1. Conclusions

How does the flow generated by a 4-channel bowthruster develop and evolve on the bottom of a vertical quay wall?

Results from measurements presented in this research showed how the use of 4-channel type bowthrusters resulted in two different flow patterns on the bottom: near the quay wall, a highly turbulent reflected jet, was present; under the suction point of the 4-channel bowthruster system, the flow was not affected by the outflow of the bowthrusters or the presence of the vertical quay wall anymore, but it was only determined by the inflow of the 4-channel bowthruster system. Instruments located between the bowthruster outlet and the quay wall recorded the highest flow velocities and showed a clear relation between use of bowthrusters and increase in flow velocity at the bottom. Mean flow velocities recorded were generally in the order of magnitude of 1 m/s, but the flow was characterized by large turbulent fluctuations. This combination of low mean flow velocities and large variation led to values of relative turbulence intensity often outside the range of values found in literature, and even close to 1. Flow was largely variable also in direction: therefore, the return flow present underneath was less clearly defined than what found in previous research. According to measured data, in the direction parallel to the quay, extent of the influence of the bowthruster-induced flow appeared to depend on wall clearance. For bowthruster 1 (wall clearance = $2.32 D_t$), it was more limited than for bowthruster 2 (wall clearance = $4.23 D_t$). Influence of keel clearance on velocities on the bottom was, as well, dependent on wall clearance and more pronounced for bowthruster 2. Furthermore, influence of keel clearance affected turbulence intensity more than mean flow velocity. Importance of the relative in-

fluence of wall and keel clearance parameter have already been identified by the previous research (see for instance [21], [19]), which resulted in development of the commonly used guidelines recommended by PIANC. Nonetheless, both Dutch method and German method resulted to be generally conservative when compared with data from this research. Furthermore, it appeared that both formulae's sensitivity to wall and keel clearance was not reflected by the data. Similarly, methods recommended by PIANC to take into account use of multiple propellers didn't find confirmation in this dataset and resulted to be generally conservative of the expected flow velocities. However, test 12 and 22 represented an exception, since data recorded by ADV1 appeared to be higher than theoretical maximum velocities. Flow beneath the suction point presented lower mean flow velocities, in the order of magnitude of 0.5 m/s, and a limited spatial extent. Results from this measurement showed no influence of bowthruster-induced flow at 14 m from the quay wall.

How did the proposed measurement set-up perform?

The adopted set-up was successful in identifying a zone where the flow on the bottom was influenced by the bowthruster jet reflected by the quay wall, a zone where flow pattern was determined by the inflow beneath the suction points of the 4-channel bowthruster system, and a zone where the flow is not influenced anymore by the use of bowthrusters. Furthermore, duration of two minutes for each step of applied power was sufficient to eliminate any transitional effect. On the other hand, the low spatial resolution of the instruments represented the most significant limitation of the set-up. Using three different ship positions allowed to gain a spatial idea of the flow pattern on the bottom, but the flow resulted to be so highly variable that a measurement grid with a resolution in the order of 0.5 m would have been needed to have the absolute certainty of capturing the maximum velocities at the bottom, and to have a precise spatial view of the flow. Limited redundancy within the instruments made difficult to reduce uncertainty due to discrepancies in the measurements. Especially when comparing ADV1 and ADCP1, which often present different measurements despite being close to each other, the reason of this discrepancies is not clear. A larger number of measurement point could have been used to clarify if the differences were caused by a flow so variable to present such large variations even in the space of few decimeters, or to the different nature of the instruments. ADCPs, in fact, are commonly used to measure currents: suitability of their use for a flow as turbulent as the bowthruster-induced one should be validated further.

How is the flow field on the bottom influenced by parameters such as: relative distance between outlet and quay wall, height of the outlet in the water column?

From the results of the measurements, influence of keel and wall clearance resulted to be strictly related. Flow near the quay wall induced by bowthruster 2, characterized by a larger wall clearance ($4.23 D_t$), resulted to be more sensitive to variation of the height of the thruster in the water column. However, turbulence intensity seemed to be more affected than mean flow velocity. A larger wall clearance appeared to lead to slightly higher mean flow velocities and larger turbulence intensities, as seen in results from tests where bowthruster 2 was used. It is worth to note how, when comparing test results to Dutch method and German method recommended in PIANC guidelines and commonly used to calculate hydraulic load at the bottom of a vertical quay wall, sensitivity to wall and keel clearance differed remarkably between formulae and data. Influence of wall and keel clearance found in data, in fact, appeared not to be well reflected by both Dutch and German method.

In a 4-channel bowthruster system, what is the difference in the flow field if one or two bowthrusters are used? Does the different configuration of the two bowthruster result in a difference in the flow velocities?

The flow field generated by use of both bowthrusters simultaneously led to slightly higher mean flow velocities, and larger turbulence intensities. This difference was not comparable, though, with the relations suggested in design guidelines. Differences within the two

bowthrusters, differentiated mainly by their wall clearance, appeared to be related mainly to the extent of the flow along the quay wall, turbulence intensity and sensitivity to an increase in keel clearance. Both use of bowthruster 1 and use of bowthruster 2, though, led to velocities within the same order of magnitude.

How can the results of the measurements impact the stability of the bottom material and, consequently, the design of the bottom protection, according to the commonly used guidelines?

Results from this study show that the extent of 4-channel bowthruster induced flow is limited to a narrow zone near to the quay wall. Beneath the bowthrusters' suction point, flow is determined by the inflow, which is characterized by lower flow velocities than flow at the joint between quay wall and bottom. At 14 m from the quay wall, the flow didn't appear to be influenced by the use of bowthrusters. Therefore, if only bowthrusters are used during mooring operations, the 20 m extent of the current bed protection appeared to be wider than necessary. Furthermore, methods commonly recommended in bottom protection design to calculate maximum velocities at the bottom resulted to be generally conservative if compared with data from this research. However, one instrument in test 12 and test 22 recorded maximum velocities at the bottom higher than theoretical values. Lastly, commonly used stability formulae to determine rock size didn't appear to frame precisely the balance between low mean flow velocities and high turbulent fluctuations found in this study.

8.2. Recommendations

With the objective of pursuing an increase in knowledge on bowthruster-induced flow when interacting with a vertical quay wall, the following recommendations are suggested. Recommendations are divided in 4 parts: firstly, more insight through analysis of remaining data from the current dataset is advised. Then, a phase of sensitivity analysis on bowthruster-induced flow is recommended through use of data collected in this study to validate a numerical model, and/or reproduction of the field measurements in a on-scale physical model. Once a further understanding on the flow induced by a 4-channel bowthruster system is reached, new full scale measurements are suggested, with the final objective of developing new guidelines for bed protection design.

Furhter analysis on the current dataset

In this research, results from a full scale field measurement of channel type bowthruster induced bottom velocities are presented. The collected data set is quite unique; therefore, it is suggested to gain an understanding on data as complete as possible. The following first steps are suggested:

- **Analysis of Tests 24 to 30.** Analysis of the tests conducted in free flow conditions was beyond the scope of this research, but important information that could give new insight also on the first set of tests. For instance, a measure of the outflow velocity, which is the element upon all the commonly used formulae are based on, would allow further insights on the differences found between theoretical values and data.
- **Comparison of results with an analytical or numerical model.** Using an analytical model to gain a better understanding on the dataset and its discrepancies is recommended in order to increase the confidence level in data. In addition, CFD computational methods could be used to generate a flow field based on the measurements existing conditions, with creation of synthetic turbulence. Sampling the beam components from ADCPs could help in assessing the validity of the post-processing method, and determine the reason of discrepancies in measurements by the two instruments near the quay wall.

Use of the current dataset to develop a better understanding on the bowthruster-induced flow through other research methods

As mentioned above, the most significant limitation of this study is the low spatial resolution of the measurement points. Furthermore, repeatedly testing of different situations with changing parameters is not easily done for full scale field measurements. Therefore, in order to gain a better understanding on the spatial variation of the flow and the relative dependency on wall and keel clearance, it is advised to:

- **Use the current dataset to validate a numerical model.** Developing a numerical model based on the case analysed in this study would allow to assess the actual influence of low spatial resolution and absence of redundancy of the present study. Furthermore, numerical models are particularly suitable tools for sensitivity analysis of the changing boundary conditions, allowing to better understand the influence of wall clearance and keel clearance on the flow.
- **Development of a scale model reproducing the conditions of measurements presented in this study.** For a flow as turbulent as the one induced by bowthrusters, physical modelling is relevant to better understand turbulent structures. Furthermore, most of the scale modelling research conducted on bowthrusters implemented rough models of bowthrusters, mainly consisting in a propeller screwed to a wood block. On-scale reproduction of the 4-channel bowthruster system utilized in this research, which is commonly used for inland vessels, would help in gaining a better understanding on the relative influence of reflected flow and inflow beneath the suction points. Furthermore, laboratory conducted on-scale modelling allows to use more precise measurements methods, such as PIV (Particle Image Velocimetry).

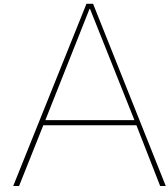
New full scale measurements

If new full scale measurements have to be performed again, deriving from limitations of this study it is strongly advised:

- **To use a denser measurement grid.** The monitoring method developed by Abramowicz et al. [1], consisting in pressure sensors mounted on a grid of stainless steel segmented pipes, could be modified and implemented also for use on the sea bed. The measurement grid should cover the space between the quay wall and the zone where the influence of use of bowthrusters can't be noticed anymore; results from this measurements show this distance to be around 14-15 m. In the direction parallel to the quay wall, this research showed how a span of 10 m already presents significant variation of the bowthruster induced flow. Pressure sensors should be positioned at regular intervals and within 0.5 m of distance. Sufficient redundancy of measurement points should be ensured.
- **Have measurement points also on the quay wall and at the outflow.** Implementing measurements points on the quay wall would allow to gain a complete measurement of the bowthruster flow. Measurement of the efflux velocity would allow for a better understanding of its relation with maximum velocities at the bottom.

Development of new bottom protection guidelines

The results from this study showed that commonly used guidelines method to calculate the hydraulic load are generally conservative for the situation taken into exam. Furthermore, they don't seem to capture dependency on parameter such as wall and keel clearances shown by the data. It has to be noted how the guidelines taken into account were developed for traditional types of propellers, without suction point beneath the ship, and taking into account larger values of wall clearance. Therefore, once a better understanding of the complex flow caused by use of bowthrusters near a vertical quay wall is obtained, new formulas, representing more accurately the physical phenomenon should be developed.



Measurement of the free flow

In this appendix, details about the measurement programme and set-up for the measurements of the free flow are presented.

A.1. Measurement set-up

To measure free flow velocities, ship is turned and moored to the quay wall on the starboard side. This way, the same outlets of bowthruster 1 and 2 used for reflected flow measurements are used. Frame with instruments is then positioned on the outer side of the ship. A top view of the instruments location is illustrated in figure A.1.

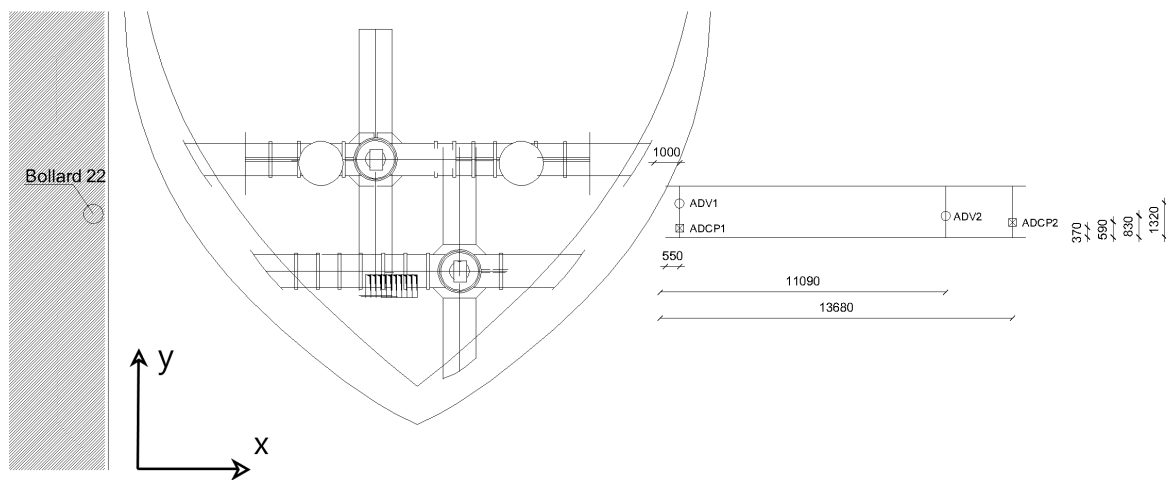


Figure A.1: Top view of measurement set-up for the free flow. Dimensions are indicated in millimeters.

A.2. Considered ship positions

In figures A.2 and A.3, the two ship positions used to measure the free flow are presented. The reference line in correspondence of bollard 22 indicates the position of the instruments. The length of the line does not correspond to the effective length of the instrument frame.

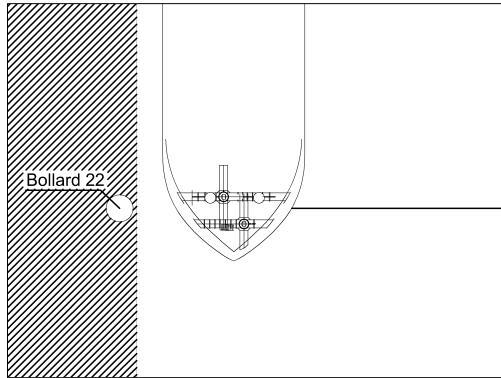


Figure A.2: Ship position 4.

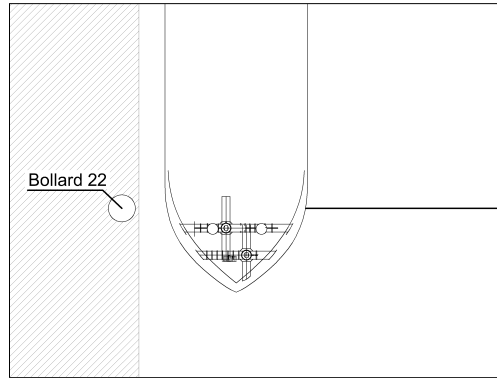


Figure A.3: Ship position 5.

A.3. Measurement programme

For the free flow, each bow-thruster is activated for 2 minutes for 4 applied power steps (25%, 50%, 75% and 100%), then both bow-thrusters are activated. The three tests are repeated for two different ship positions: at first, the ship is positioned such that the instruments are in the middle between the two bow-thrusters axis (position 4), then the ship is moved a few meters ahead (position 5). In table A.1, a summary of the tests characteristics can be found.

Table A.1: Table illustrating the measurement protocol for tests 24-30 (Free Flow). For each test are stated the power steps applied, the duration of each subtest, the number of subtests, total duration of the test, which bow thruster is used, the position of the ship, the set-up of the instruments and the average water depth at the quay.

Test	Subtest			Bow thruster	Ship Position	Set-up	Average water depth at the quay [m]
	Steps of applied power	Duration of each subtest [min]	Total duration of the test [min]				
24	25%, 50%, 75%, 100%	2	8	1	4	2	6.67
25	25%, 50%, 75%, 100%	1	4	2			6.69
26	25%, 50%, 75%, 100%	1	4	Both			6.71
27	25%, 50%, 75%, 100%	1	4	1	5	(Free Flow)	6.75
28	25%, 50%, 75%, 100%	1	4	2			6.78
29	25%, 50%, 75%, 100%	1	4	Both			6.8
30	50%, 100%	1	2	Both			6.83

B

Test Results

In this appendix, results for every test are presented. Each picture presents mean horizontal velocity magnitude and errorbars long 2 times the standard deviation, calculated for each subtest (correspondent to an increase of 25% in applied power and 2 minutes long). All the instruments are represented for all tests, with the exception of ADV2, which stopped working after test 9.

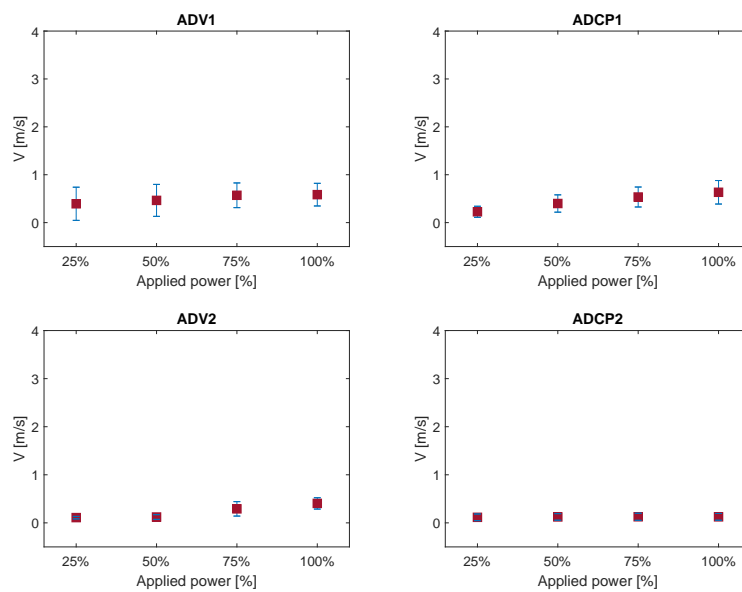


Figure B.1: Results of test 1. Mean of horizontal velocity magnitude and standard deviation represented for each instrument, for each subtest.

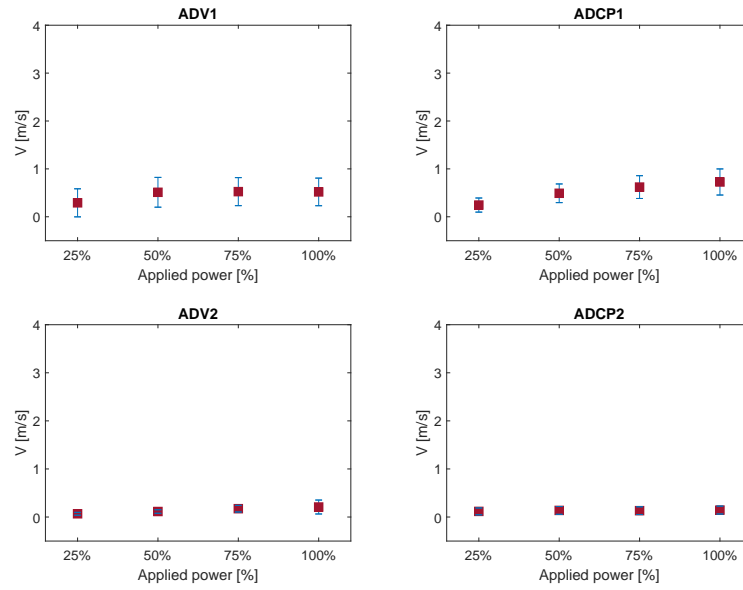


Figure B.2: Results of test 2. Mean of horizontal velocity magnitude and standard deviation represented for each instrument, for each subtest.

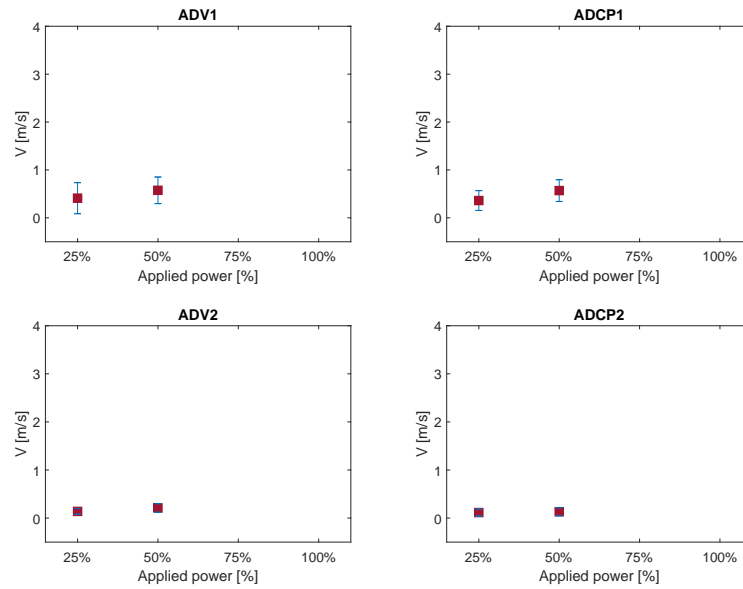


Figure B.3: Results of test 3. Mean of horizontal velocity magnitude and standard deviation represented for each instrument, for each subtest.

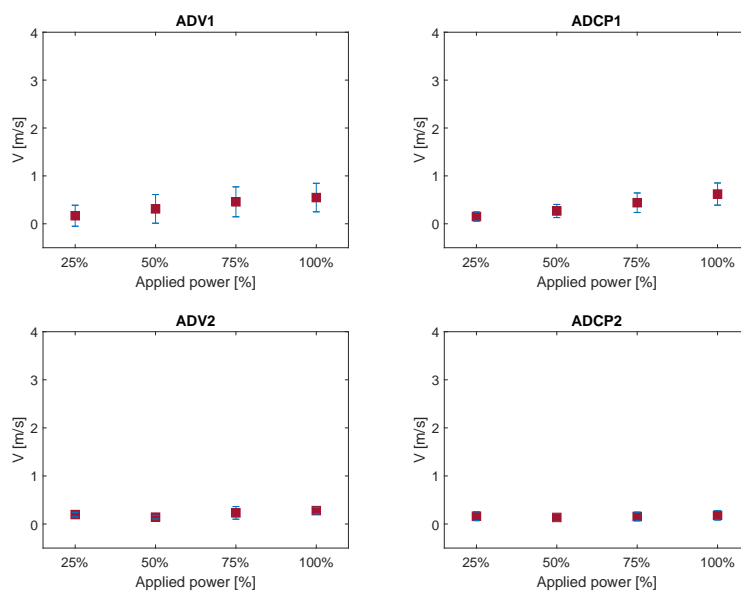


Figure B.4: Results of test 4. Mean of horizontal velocity magnitude and standard deviation represented for each instrument, for each subtest.

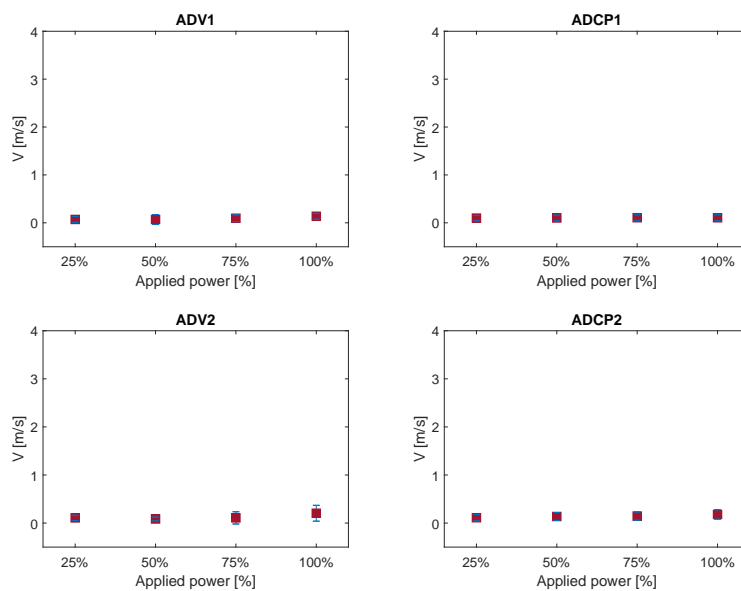


Figure B.5: Results of test 5. Mean of horizontal velocity magnitude and standard deviation represented for each instrument, for each subtest.

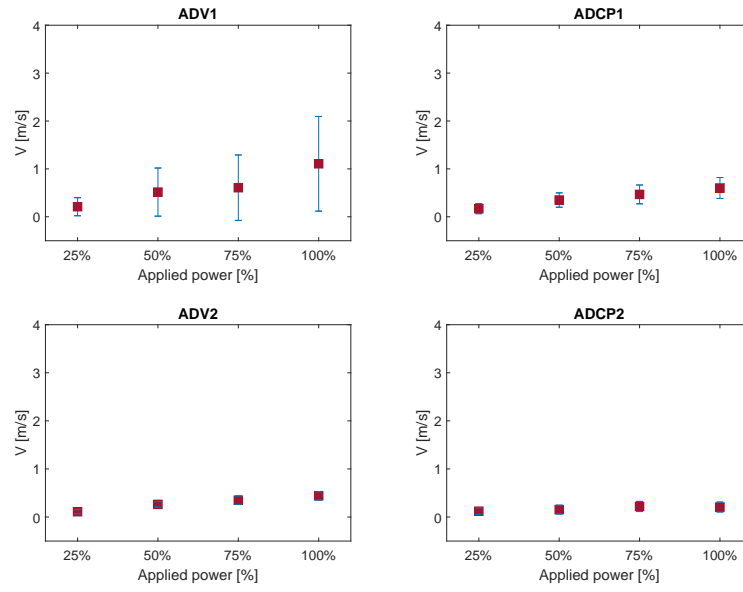


Figure B.6: Results of test 6. Mean of horizontal velocity magnitude and standard deviation represented for each instrument, for each subtest.

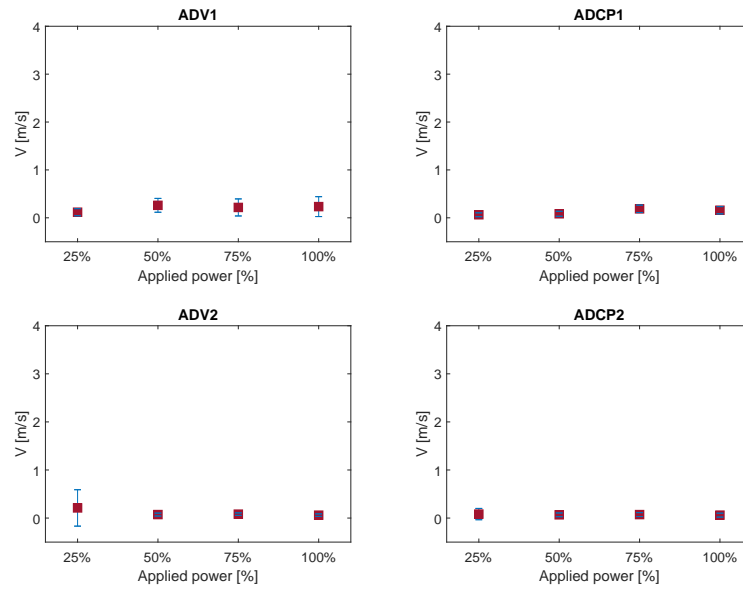


Figure B.7: Results of test 7. Mean of horizontal velocity magnitude and standard deviation represented for each instrument, for each subtest.

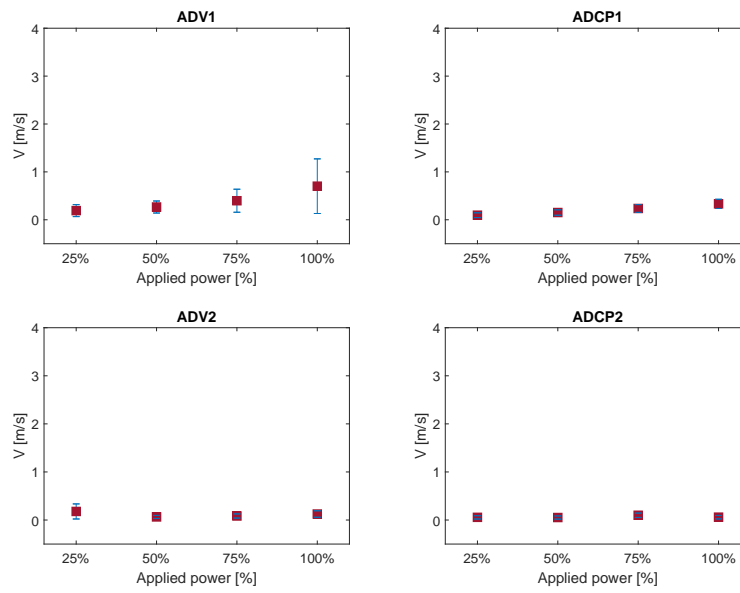


Figure B.8: Results of test 8. Mean of horizontal velocity magnitude and standard deviation represented for each instrument, for each subtest.

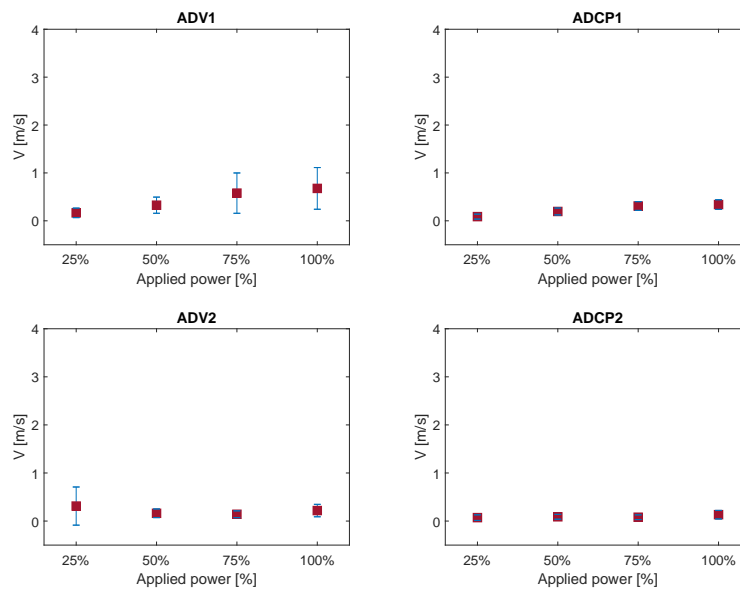


Figure B.9: Results of test 9. Mean of horizontal velocity magnitude and standard deviation represented for each instrument, for each subtest.

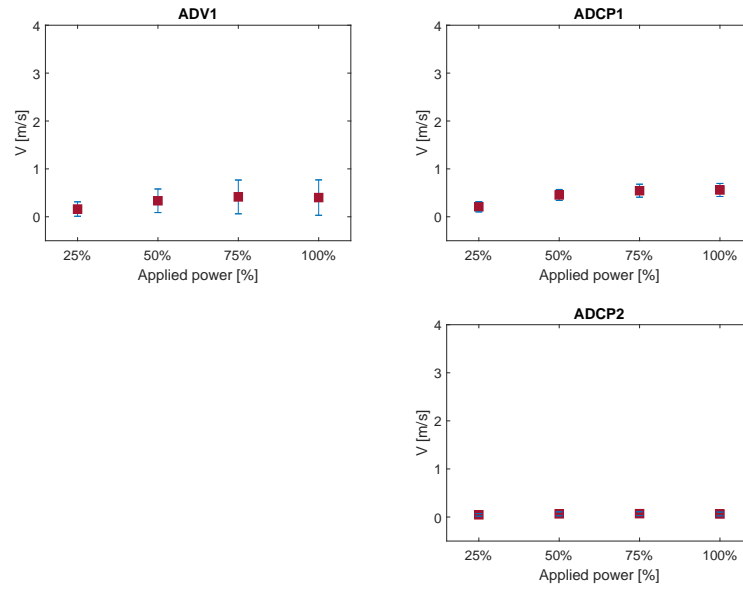


Figure B.10: Results of test 11. Mean of horizontal velocity magnitude and standard deviation represented for each instrument, for each subtest.

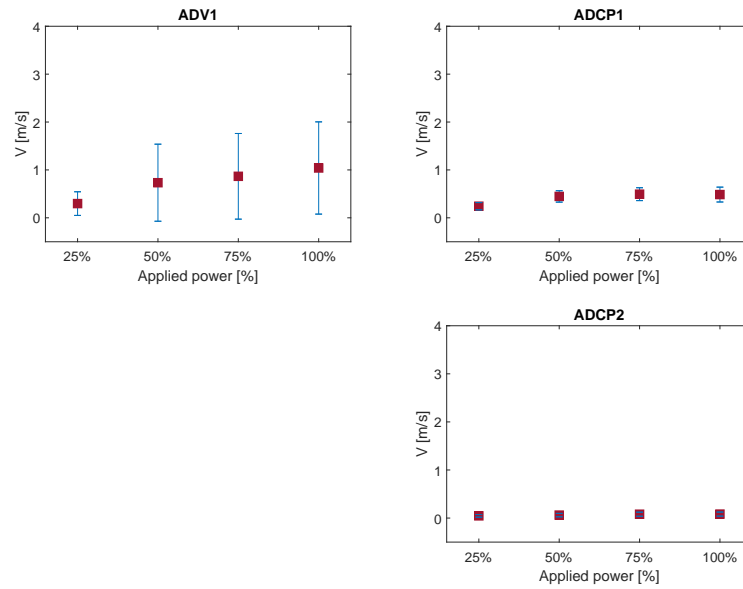


Figure B.11: Results of test 12. Mean of horizontal velocity magnitude and standard deviation represented for each instrument, for each subtest.

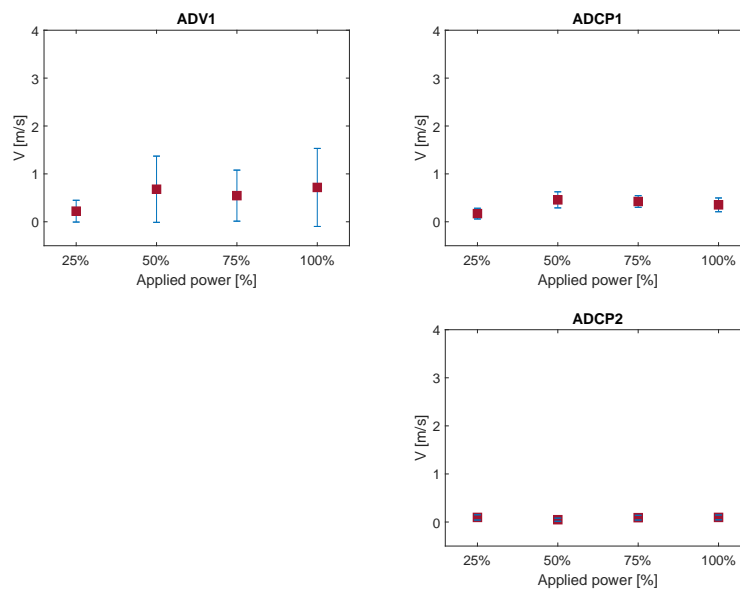


Figure B.12: Results of test 13. Mean of horizontal velocity magnitude and standard deviation represented for each instrument, for each subtest.

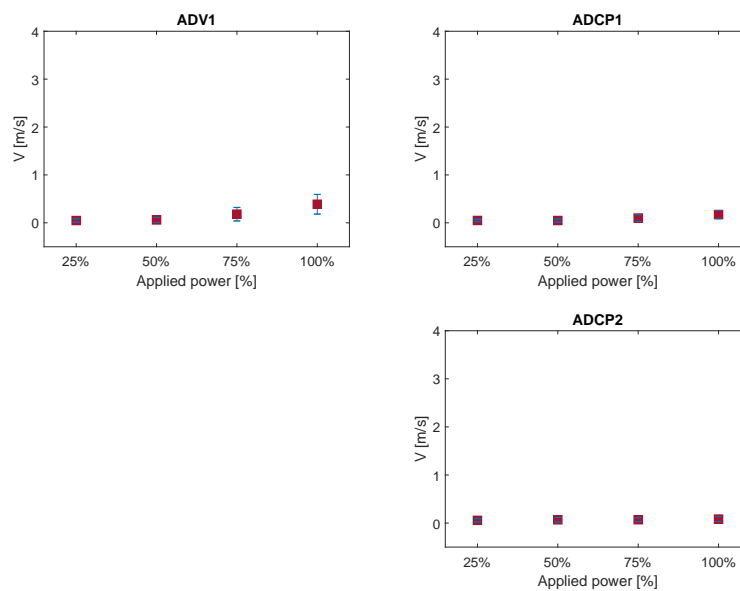


Figure B.13: Results of test 14. Mean of horizontal velocity magnitude and standard deviation represented for each instrument, for each subtest.

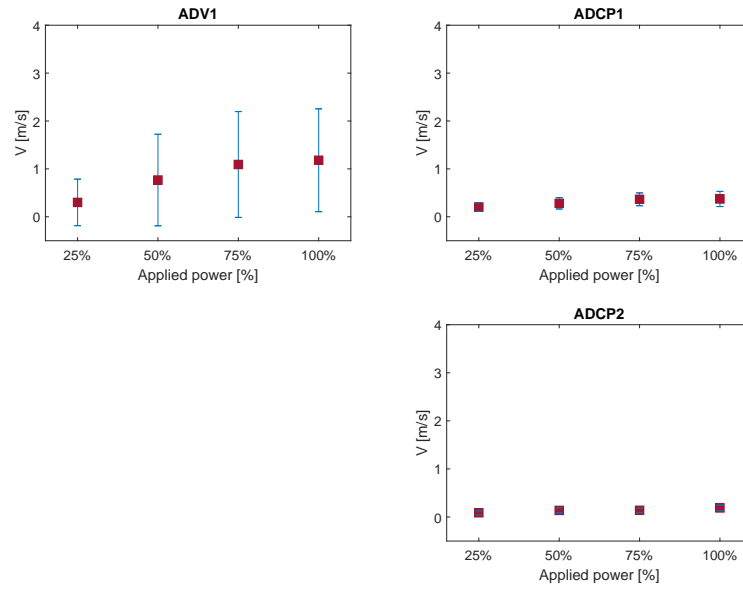


Figure B.14: Results of test 15. Mean of horizontal velocity magnitude and standard deviation represented for each instrument, for each subtest.

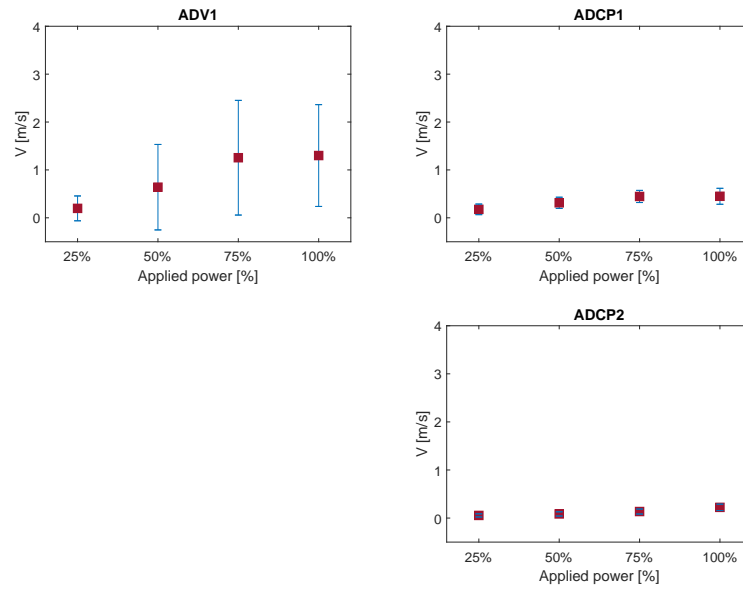


Figure B.15: Results of test 16. Mean of horizontal velocity magnitude and standard deviation represented for each instrument, for each subtest.

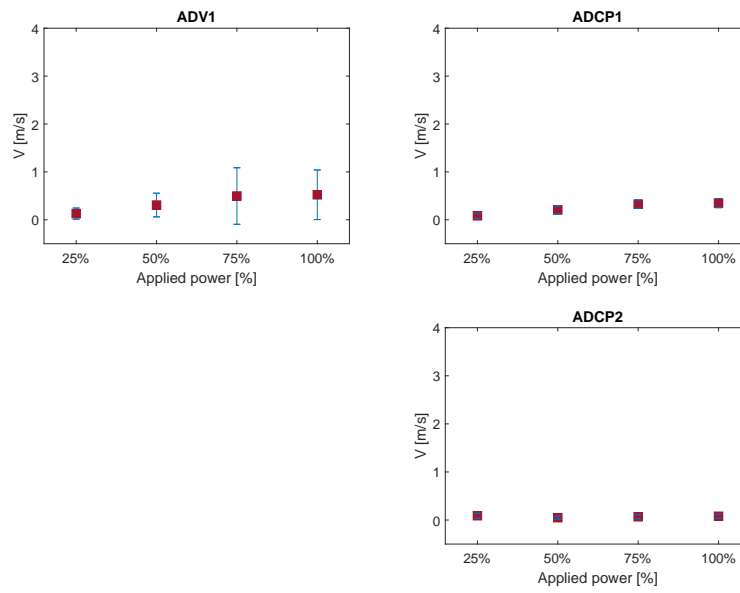


Figure B.16: Results of test 17. Mean of horizontal velocity magnitude and standard deviation represented for each instrument, for each subtest.

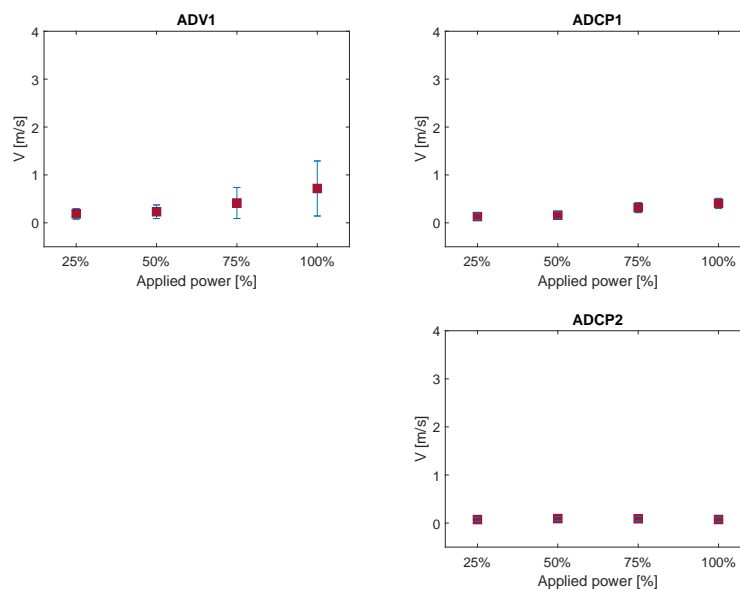


Figure B.17: Results of test 18. Mean of horizontal velocity magnitude and standard deviation represented for each instrument, for each subtest.

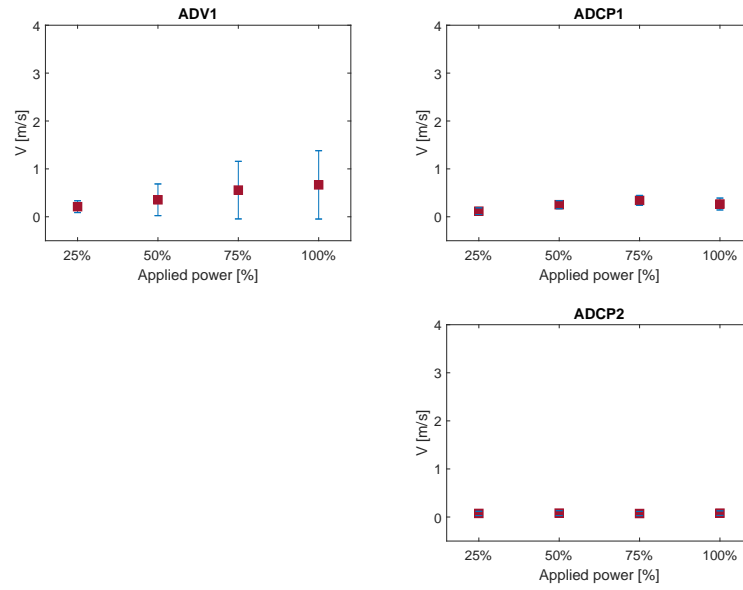


Figure B.18: Results of test 19. Mean of horizontal velocity magnitude and standard deviation represented for each instrument, for each subtest.

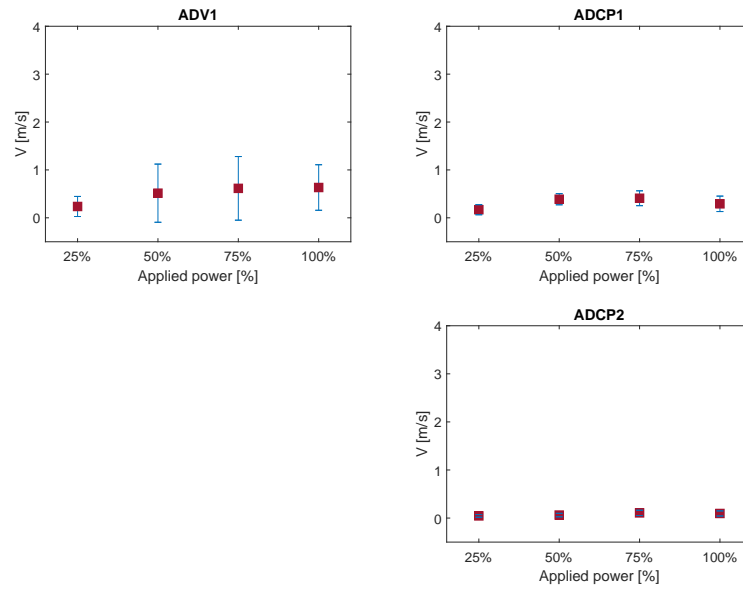


Figure B.19: Results of test 20. Mean of horizontal velocity magnitude and standard deviation represented for each instrument, for each subtest.

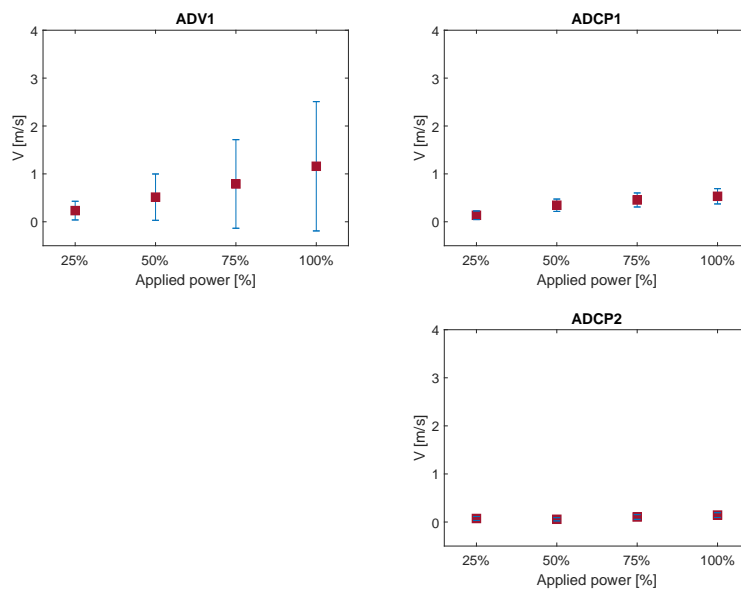


Figure B.20: Results of test 21. Mean of horizontal velocity magnitude and standard deviation represented for each instrument, for each subtest.

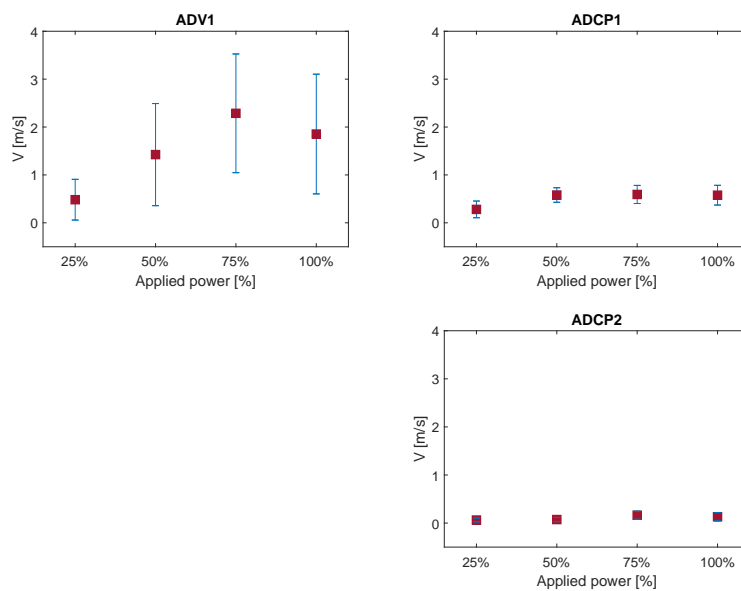
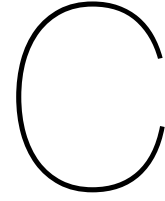


Figure B.21: Results of test 22. Mean of horizontal velocity magnitude and standard deviation represented for each instrument, for each subtest.



Tables of test results

Numerical results from each instruments are presented in this appendix, for tests 1-9 and 11-22. For ADV2, only results from tests 1-9 are presented, since contact with the instrument was lost for the consequent tests. Mean flow velocity \bar{V} , standard deviation σ , relative turbulence intensity $r = \frac{\sigma}{\bar{V}}$, maximum velocity $V_{max} = \bar{V} + 3\sigma$, dominant direction θ_{dom} and standard deviation of direction σ_{theta} are reported for each step of applied power.

Table C.1: ADV2 results form test 1-9. Mean flow velocity \bar{V} , standard deviation σ , relative turbulence intensity $r = \frac{\sigma}{\bar{V}}$, maximum velocity $V_{max} = \bar{V} + 3\sigma$, dominant direction θ_{dom} and standard deviation of direction σ_{theta} are reported for each step of applied power.

Test	Applied power	\bar{V} [m/s]	σ [m/s]	r [-]	$V_{max} = \bar{V} + 3\sigma$ [m/s]	θ_{dom} [degrees]	σ_{θ} [degrees]
Test 1	25%	0.109358794	0.025909059	0.23691793	0.187085972	70	16.39925284
	50%	0.121852792	0.048695474	0.399625427	0.267939213	-35	45.95475252
	75%	0.291363936	0.150155362	0.515353285	0.74183002	-60	39.44233019
	100%	0.405057461	0.118158641	0.291708344	0.759533384	-40	35.19208954
Test 2	25%	0.067414492	0.029300064	0.434625593	0.155314683	-155	81.2348271
	50%	0.114727623	0.036646385	0.319420768	0.22466678	170	124.6642008
	75%	0.17350597	0.069008743	0.397731231	0.380532199	90	34.91447029
	100%	0.20823827	0.144884685	0.695763969	0.642892326	170	87.22233578
Test 3	25%	0.13857187	0.059230711	0.427436757	0.316264003	-155	76.37597285
	50%	0.210522107	0.089220534	0.423806009	0.478183709	40	29.67967782
Test 4	25%	0.196708314	0.046810301	0.237968085	0.337139217	-140	26.10778105
	50%	0.143028318	0.038268701	0.26756031	0.257834421	-140	47.3469132
	75%	0.231954317	0.131335275	0.566211816	0.625960141	-135	41.80583919
	100%	0.279153889	0.067381898	0.241379039	0.481299581	-145	24.99380837
Test 5	25%	0.107559092	0.053895458	0.501077657	0.269245465	-50	33.94418464
	50%	0.08449215	0.03993741	0.472675985	0.204304381	-160	115.9250404
	75%	0.107778951	0.127063306	1.178925058	0.48896887	-150	119.0718778
	100%	0.20405862	0.164958974	0.808390131	0.698935543	-155	105.305118
Test 6	25%	0.110496648	0.042318527	0.382984714	0.237452229	-90	18.32682496
	50%	0.263325961	0.055707652	0.211553969	0.430448918	-120	13.32829491
	75%	0.348979716	0.08880566	0.254472269	0.615396696	-115	25.60747889
	100%	0.440873082	0.086123232	0.195346996	0.699242778	-115	11.00245825
Test 7	25%	0.210903575	0.378875143	1.796437748	1.347529003	-60	64.85601958
	50%	0.07253062	0.030499084	0.420499421	0.164027871	165	120.1339484
	75%	0.081475066	0.026147387	0.320925014	0.159917226	-175	148.8017126
	100%	0.060176551	0.0262692	0.436535484	0.138984151	155	129.4294903
Test 8	25%	0.178361327	0.156745236	0.878807299	0.648597035	-70	20.79521615
	50%	0.064493077	0.031313579	0.485533953	0.158433813	30	56.66522161
	75%	0.083804515	0.043002498	0.513128658	0.21281201	-180	154.3996221
	100%	0.124778863	0.067487487	0.540856724	0.327241323	-140	74.17931853
Test 9	25%	0.31182276	0.39681505	1.272566025	1.502267909	-40	54.27027675
	50%	0.161481513	0.089990664	0.557281529	0.431453506	45	32.38450014
	75%	0.141392362	0.070566488	0.499082742	0.353091824	0	53.90288209
	100%	0.218454591	0.129468762	0.592657545	0.606860876	-25	56.75768888

Table C.2: ADV1 results form test 1-9 and 11-22. Mean flow velocity \bar{V} , standard deviation σ , relative turbulence intensity $r = \frac{\sigma}{\bar{V}}$, maximum velocity $V_{max} = \bar{V} + 3\sigma$, dominant direction θ_{dom} and standard deviation of direction σ_{θ} are reported for each step of applied power.

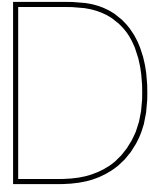
Test	Applied power	\bar{V} [m/s]	σ [m/s]	r [-]	$V_{max} = \bar{V} + 3\sigma$ [m/s]	θ_{dom} [degrees]	σ_{θ} [degrees]
Test 1	25%	0.393315892	0.346314305	0.880499142	1.432258808	-60	87.37479373
	50%	0.464315071	0.333749763	0.718800194	1.465564361	-60	96.00971053
	75%	0.570671482	0.257842558	0.4518231	1.344199156	-60	101.6190806
	100%	0.584051624	0.236436647	0.404821486	1.293361564	-55	104.5339308
Test 2	25%	0.291347542	0.292994528	1.005652996	1.170331127	60	86.42359513
	50%	0.511301344	0.311095361	0.608438378	1.444587426	-120	92.28151241
	75%	0.525043242	0.292649686	0.557382065	1.4029923	60	98.20424982
	100%	0.519243838	0.288240184	0.555115271	1.38396439	65	97.01180634
Test 3	25%	0.410205084	0.324376909	0.790767647	1.383335811	85	86.85154415
	50%	0.574264627	0.277706774	0.483586766	1.407384948	-180	100.7041542
Test 4	25%	0.168029929	0.219245934	1.304802867	0.82576773	-40	75.88981796
	50%	0.311387643	0.29948751	0.961783542	1.209850172	0	73.72419324
	75%	0.458498311	0.312644905	0.681888891	1.396433026	10	86.14203109
	100%	0.54746032	0.297704641	0.54379218	1.440574243	120	100.4159072
Test 5	25%	0.070224308	0.061838458	0.88058479	0.255739681	70	100.7811911
	50%	0.069941285	0.103812185	1.484276212	0.38137784	-170	108.5787157
	75%	0.094963315	0.069730966	0.734293726	0.304156213	85	66.18330075
	100%	0.136718515	0.061532148	0.450064485	0.321314958	80	39.65221321
Test 6	25%	0.209925787	0.188424696	0.897577658	0.775199875	-65	69.33489307
	50%	0.515589456	0.502493419	0.974599875	2.023069713	-60	45.72550407
	75%	0.607385437	0.683411525	1.125169429	2.657620014	-30	56.75994166
	100%	1.106579584	0.988327521	0.893137317	4.071562146	-60	78.82463285
Test 7	25%	0.117196973	0.073993753	0.631362317	0.339178231	55	56.56920193
	50%	0.260721704	0.144660828	0.554847665	0.694704189	20	44.93217431
	75%	0.216777558	0.178118979	0.821667063	0.751134495	5	63.25121811
	100%	0.233874921	0.207738143	0.888244633	0.85708935	0	77.0430751
Test 8	25%	0.191500935	0.125193935	0.653751041	0.567082741	65	29.64008066
	50%	0.26641118	0.125568849	0.471334756	0.643117726	65	27.63785229
	75%	0.397773758	0.240317601	0.604156499	1.118726562	65	30.70469427
	100%	0.701475646	0.570331046	0.813044685	2.412468783	60	54.7354894
Test 9	25%	0.166158919	0.099870113	0.601051774	0.465769259	70	39.41171385
	50%	0.326241167	0.168840804	0.517533717	0.832763577	70	31.88152458
	75%	0.578269511	0.420931752	0.727916213	1.841064768	85	38.44612568
	100%	0.676734839	0.435300746	0.643236791	1.982637078	80	42.61821703
Test 11	25%	0.161421485	0.150883845	0.934719723	0.614073021	-45	72.22043522
	50%	0.334146918	0.24631612	0.73714916	1.073095279	-15	57.41123123
	75%	0.414712233	0.352565658	0.850145306	1.472409208	10	63.02931306
	100%	0.40086159	0.369781474	0.922466714	1.510206013	90	71.36128871
Test 12	25%	0.297013926	0.246919743	0.831340626	1.037773154	60	56.68622717
	50%	0.733114989	0.804573243	1.097472095	3.146834717	55	57.12515855
	75%	0.866524349	0.894386984	1.032154475	3.549685301	50	65.03246282
	100%	1.040546216	0.963126388	0.925596934	3.929925379	60	72.96487767
Test 13	25%	0.221587167	0.227544147	1.026883233	0.904219609	-35	74.85079152
	50%	0.679735342	0.691294562	1.017005471	2.753619027	-35	58.61499193
	75%	0.545735925	0.533092095	0.976831597	2.14501221	-75	76.53589225
	100%	0.717230901	0.81487898	1.136145945	3.161867841	-125	105.5503688
Test 14	25%	0.047675662	0.033793069	0.708811738	0.149054868	75	42.33266134
	50%	0.060495596	0.052472287	0.867373674	0.217912457	-155	121.0202627
	75%	0.180127222	0.141404712	0.785026886	0.604341359	-85	86.70601128
	100%	0.387777186	0.205761167	0.530617	1.005060689	-90	44.0958108
Test 15	25%	0.300093969	0.485738676	1.61862192	1.757309995	-50	77.27101047
	50%	0.767472107	0.955887382	1.245501137	3.635134251	-70	76.08022698
	75%	1.091893775	1.104743176	1.011767996	4.406123304	-50	87.88852221
	100%	1.180342037	1.073734956	0.909681196	4.401546905	120	96.43453331
Test 16	25%	0.197158211	0.2593615	1.31549936	0.975242712	85	67.07375929
	50%	0.639625428	0.892446965	1.395264987	3.316966323	-40	65.29460659
	75%	1.254919488	1.197199158	0.954004754	4.846516961	-175	97.82049844
	100%	1.30046992	1.06301152	0.817405696	4.48950448	120	95.44468654
Test 17	25%	0.128568178	0.116537976	0.906429396	0.478182106	55	80.50806984
	50%	0.307374813	0.247200493	0.804231453	1.048976292	30	43.22967594
	75%	0.496018273	0.590215831	1.189907436	2.266665767	30	57.96451692
	100%	0.522275651	0.517838606	0.9915044	2.075791468	30	59.93602106
Test 18	25%	0.188341088	0.110626438	0.58737283	0.520220401	55	31.16077833
	50%	0.231144624	0.142194012	0.615173347	0.657726659	55	53.56875581
	75%	0.413567555	0.324020523	0.783476652	1.385629124	60	38.94469357
	100%	0.716781428	0.574314384	0.801240604	2.439724581	65	46.28460707
Test 19	25%	0.210806656	0.123898093	0.587733305	0.582500933	20	46.9208241
	50%	0.354381511	0.331135973	0.934405329	1.34778943	35	43.31235724
	75%	0.556888	0.6014131	1.079953419	2.361127298	15	59.93093569
	100%	0.666354322	0.713267454	1.070402684	2.806156685	65	74.21772883
Test 20	25%	0.236744991	0.209497952	0.884909755	0.865238845	105	98.35249937
	50%	0.514317141	0.607434833	1.181051115	2.336621641	115	93.36684056
	75%	0.615069348	0.664628492	1.080574889	2.608954824	135	89.33737744
	100%	0.632908085	0.475714337	0.75163258	2.060051096	130	84.03210883
Test 21	25%	0.233287898	0.195220008	0.836820124	0.818947923	65	62.6682024
	50%	0.514391957	0.483698294	0.940330204	1.965486838	30	60.11713513
	75%	0.789724173	0.924876818	1.171139051	3.564354629	55	67.96143069
	100%	1.158913506	1.349973825	1.164861587	5.20883498	55	86.53927049
Test 22	25%	0.482714895	0.425311721	0.881082654	1.758650059	30	47.56744365
	50%	1.424347804	1.06626766	0.748600628	4.623150785	30	60.17570956
	75%	2.28633712	1.239591142	0.542173388	6.005110546	30	86.54581667
	100%	1.853580405	1.249879927	0.674305751	5.603220185	35	79.44789794

Table C.3: ADCP1 results form test 1-9 and 11-22. Mean flow velocity \bar{V} , standard deviation σ , relative turbulence intensity $r = \frac{\sigma}{\bar{V}}$, maximum velocity $V_{max} = \bar{V} + 3\sigma$, dominant direction θ_{dom} and standard deviation of direction σ_{θ} are reported for each step of applied power.

Test	Applied power	\bar{V} [m/s]	σ [m/s]	r [-]	$V_{max} = \bar{V} + 3\sigma$ [m/s]	θ_{dom} [degrees]	σ_{θ} [degrees]
Test 1	25%	0.226159647	0.115576461	0.51103927	0.57288903	-5	41.16512299
	50%	0.399014056	0.180849493	0.453240907	0.941562533	5	20.09530449
	75%	0.534821093	0.208491504	0.389834109	1.160295606	-5	19.37201881
	100%	0.63338536	0.245381415	0.387412514	1.369529605	0	16.4954052
Test 2	25%	0.244720712	0.147389457	0.602276183	0.686889082	0	68.2444458
	50%	0.490588307	0.194994405	0.397470551	1.075571522	0	14.89019585
	75%	0.620179117	0.23798579	0.383737187	1.334136486	-5	13.6949358
	100%	0.726725101	0.272503644	0.374974861	1.544236034	-5	15.79346085
Test 3	25%	0.360741377	0.207129881	0.574178328	0.982131019	5	57.65932465
	50%	0.568877578	0.227208942	0.39939866	1.250504404	5	12.53579426
Test 4	25%	0.151392892	0.095135793	0.628403301	0.436800271	-5	66.27215576
	50%	0.267025203	0.137251332	0.514001417	0.6787792	-5	37.75971603
	75%	0.440182328	0.203669474	0.462693435	1.051190749	0	27.04704285
	100%	0.620894074	0.231365308	0.372632495	1.314989999	5	17.31212616
Test 5	25%	0.097895227	0.056095257	0.573013199	0.266181	-5	76.82843781
	50%	0.101157039	0.061152015	0.60452555	0.284613084	5	85.89446259
	75%	0.106630795	0.063362122	0.594219726	0.296717159	-10	82.40973663
	100%	0.105460666	0.063944176	0.606331993	0.297293194	-10	75.3361969
Test 6	25%	0.169782102	0.105597571	0.621959378	0.486574814	15	75.96815491
	50%	0.34969908	0.149987102	0.428903335	0.799660385	5	27.82494354
	75%	0.467038393	0.196316063	0.420342452	1.055986583	0	19.4154129
	100%	0.600881517	0.219214052	0.36482076	1.258523673	5	15.66753769
Test 7	25%	0.063621186	0.040369786	0.634533699	0.184730545	-5	74.50375366
	50%	0.084250174	0.051696103	0.613602327	0.239338484	-5	66.16822815
	75%	0.187321946	0.077663608	0.414599621	0.42031277	-5	19.88763046
	100%	0.158426151	0.07559447	0.47715904	0.38520956	-5	47.13318253
Test 8	25%	0.095829546	0.049658425	0.518195348	0.244804822	-20	52.33024597
	50%	0.151513815	0.057028778	0.376393254	0.322600149	-25	27.70258904
	75%	0.235888392	0.081436031	0.345231192	0.480196483	-20	13.5535593
	100%	0.332297564	0.096143059	0.289328211	0.620726742	-25	22.28695679
Test 9	25%	0.087515764	0.05163113	0.589963773	0.242409155	-10	52.45409393
	50%	0.195092708	0.072080925	0.369470114	0.411335483	-15	17.11823463
	75%	0.309179783	0.091251142	0.295139422	0.58293321	-20	13.38386726
	100%	0.339293569	0.100506507	0.296222846	0.64081309	-15	18.1146946
Test 11	25%	0.209154382	0.107522428	0.514081641	0.531721666	0	44.32815552
	50%	0.455819428	0.114749804	0.251743996	0.80006884	0	8.376157761
	75%	0.544411004	0.135932058	0.249686463	0.952207178	0	27.64190102
	100%	0.559706688	0.136478677	0.24383964	0.96914272	5	58.88598633
Test 12	25%	0.242344081	0.075793013	0.312749594	0.46972312	-10	14.2518301
	50%	0.447001219	0.119349487	0.267000362	0.80504968	-10	15.85298824
	75%	0.49362731	0.134375721	0.272221003	0.896754473	-5	30.28597832
	100%	0.485524744	0.15518409	0.319621383	0.951077014	-5	47.83910751
Test 13	25%	0.170433193	0.112190709	0.658267948	0.507005319	0	52.30027771
	50%	0.457865328	0.167873904	0.366644718	0.96148704	-5	34.2182579
	75%	0.423728019	0.121854715	0.287577667	0.789292164	-10	25.19425583
	100%	0.353392243	0.14402236	0.407542506	0.785459325	-5	28.16123009
Test 14	25%	0.048849661	0.026361359	0.539642626	0.127933739	-30	70.36549377
	50%	0.048008967	0.030657681	0.638582384	0.139982009	-165	109.0571213
	75%	0.099892981	0.069757484	0.698322174	0.309165433	10	67.36367035
	100%	0.172257617	0.086063378	0.499620156	0.43044775	5	34.48339081
Test 15	25%	0.204057008	0.090964645	0.445780549	0.476950943	-5	37.6533699
	50%	0.28127718	0.118639663	0.421789151	0.637196168	5	20.03826714
	75%	0.36487031	0.134200513	0.367803326	0.76747185	5	18.42376137
	100%	0.371619821	0.158313558	0.426009456	0.846560493	5	27.05433083
Test 16	25%	0.176554143	0.110828795	0.627732617	0.509040527	0	55.24558258
	50%	0.313251734	0.116869763	0.373085764	0.663861021	0	8.77634716
	75%	0.445848942	0.126815557	0.284436152	0.826295614	0	18.76003647
	100%	0.449536622	0.166503608	0.370389419	0.949047446	0	23.5125618
Test 17	25%	0.083630674	0.053605177	0.640975066	0.244446203	0	104.8518372
	50%	0.204525664	0.082000665	0.400930932	0.450527661	-5	16.04199028
	75%	0.327188969	0.087306149	0.266837081	0.589107417	0	7.335865498
	100%	0.348802149	0.096390411	0.276346953	0.637973383	0	10.68663692
Test 18	25%	0.129733518	0.068338744	0.52676244	0.334749751	-5	54.189785
	50%	0.161019236	0.074041285	0.459828816	0.38314309	-10	21.92796898
	75%	0.317836881	0.104944065	0.330182152	0.632669076	-10	10.08541965
	100%	0.405597895	0.104174927	0.256842868	0.718122676	-10	19.10915947
Test 19	25%	0.116845779	0.06985154	0.597809699	0.326400399	-5	43.97243881
	50%	0.252654582	0.084295057	0.333637554	0.505539753	-10	10.36932182
	75%	0.342287958	0.104563765	0.305484791	0.655979253	-5	11.58979797
	100%	0.266460836	0.124188222	0.466065572	0.639025502	0	21.53268242
Test 20	25%	0.169319928	0.105758235	0.624605953	0.486594632	-15	46.65592957
	50%	0.38847658	0.116645709	0.300264455	0.738413706	-15	13.1229887
	75%	0.40880543	0.155161828	0.379549332	0.874290913	-10	58.77511597
	100%	0.292072386	0.161153719	0.551759519	0.775533542	-10	70.06134796
Test 21	25%	0.135577679	0.090299271	0.666033465	0.406475492	-10	45.85413742
	50%	0.345505029	0.129027411	0.373445827	0.732587263	-10	13.90721893
	75%	0.455448836	0.14672634	0.322157679	0.895627856	-5	38.74532318
	100%	0.532037377	0.159414038	0.299629396	1.010279492	0	47.52682114
Test 22	25%	0.28031072	0.174228385	0.621554484	0.802995875	0	38.57429886
	50%	0.580350578	0.151689872	0.261376275	1.035420194	0	43.87474823
	75%	0.592235625	0.189007759	0.31914284	1.159258902	0	87.95785522
	100%	0.576875687	0.206026956	0.357142728	1.194956556	0	100.2849808

Table C.4: ADCP2 results form test 1-9 and 11-22. Mean flow velocity \bar{V} , standard deviation σ , relative turbulence intensity $r = \frac{\sigma}{\bar{V}}$, maximum velocity $V_{max} = \bar{V} + 3\sigma$, dominant direction θ_{dom} and standard deviation of direction σ_{θ} are reported for each step of applied power.

Test	Applied power	\bar{V} [m/s]	σ [m/s]	r [-]	$V_{max} = \bar{V} + 3\sigma$ [m/s]	θ_{dom} [degrees]	σ_{θ} [degrees]
Test 1	25%	0.115306184	0.068906173	0.597593042	0.322024703	-170	120.7788391
	50%	0.123553149	0.067992613	0.55031064	0.327530988	-170	103.4010544
	75%	0.126584306	0.073455304	0.580287605	0.346950218	-165	117.6784897
	100%	0.1252065	0.070225969	0.560881175	0.335884407	-150	103.1808548
Test 2	25%	0.117194362	0.071150675	0.60711688	0.330646388	175	128.3591766
	50%	0.137716681	0.081096098	0.588861838	0.381004974	-175	144.8413544
	75%	0.132215902	0.080496937	0.608829465	0.373706713	-180	124.1704636
	100%	0.144589797	0.082057148	0.567516866	0.390761241	-180	144.7222748
Test 3	25%	0.114766143	0.071421362	0.622320838	0.329030231	-175	112.4223175
	50%	0.131501928	0.083867311	0.637764881	0.383103862	-170	107.950325
Test 4	25%	0.162347302	0.092486769	0.569684669	0.439807609	-175	148.4091187
	50%	0.13672854	0.082706086	0.604892631	0.384846799	-180	140.9104309
	75%	0.156814635	0.089981422	0.573807553	0.4267589	175	147.9142151
	100%	0.179885849	0.096108899	0.534277148	0.468212545	-180	155.0811462
Test 5	25%	0.111257493	0.065612711	0.589737455	0.308095627	-180	106.2739563
	50%	0.136658773	0.08240997	0.603034615	0.383888684	-175	140.6398773
	75%	0.144975334	0.086124487	0.594063035	0.403348796	-180	144.7398224
	100%	0.179550514	0.097682126	0.544037017	0.472596891	-180	153.6847229
Test 6	25%	0.121877581	0.071858428	0.589595132	0.337452866	-180	129.2071228
	50%	0.154714465	0.090947762	0.587842656	0.427557752	-175	137.1252441
	75%	0.219655305	0.105486773	0.480237766	0.536115624	-175	148.4685059
	100%	0.207576901	0.102830857	0.495386802	0.516069472	-165	126.8608627
Test 7	25%	0.082815796	0.117576025	1.419729459	0.435543872	-180	116.0674896
	50%	0.067322642	0.038870867	0.57738179	0.183935244	-175	153.7864227
	75%	0.072010867	0.040674504	0.564838411	0.194034379	-175	151.8928986
	100%	0.060900349	0.040680062	0.667977484	0.182940535	-180	138.6860199
Test 8	25%	0.055964798	0.033823807	0.604376468	0.157436218	-10	87.4240036
	50%	0.052017409	0.032542009	0.625598416	0.149643436	-5	81.02539063
	75%	0.099300332	0.045021888	0.45339111	0.234365996	-180	163.560318
	100%	0.059653033	0.036014758	0.603373254	0.167697307	-180	132.7652435
Test 9	25%	0.071541704	0.05814771	0.812780607	0.245984834	-5	100.6322861
	50%	0.088942863	0.050010756	0.56227958	0.23897513	10	49.85464096
	75%	0.079871118	0.048696958	0.609694201	0.225961991	5	59.32832336
	100%	0.133081719	0.088819757	0.667407647	0.399540991	5	72.61044312
Test 11	25%	0.046080623	0.027413437	0.594901619	0.128320934	-10	97.93508911
	50%	0.066450559	0.040669248	0.612022658	0.188458301	175	145.7335968
	75%	0.069854289	0.040067811	0.573591271	0.190057721	-180	146.9046783
	100%	0.063278727	0.039078541	0.617562059	0.180514351	-170	143.1509399
Test 12	25%	0.045952909	0.027386494	0.595968672	0.128112391	-170	114.6983337
	50%	0.06169543	0.035735395	0.579222716	0.168901615	-175	135.119812
	75%	0.080104172	0.042271335	0.527704532	0.206918176	-175	144.343689
	100%	0.082558699	0.041971587	0.508384788	0.208473459	-180	148.0835876
Test 13	25%	0.095984347	0.054556474	0.568389281	0.259653769	175	152.0872498
	50%	0.048202585	0.032507055	0.674384044	0.145723749	-10	102.1810608
	75%	0.090651952	0.049245629	0.543238491	0.23838884	165	136.2745209
	100%	0.096117772	0.05005879	0.520806802	0.246294141	160	85.444664
Test 14	25%	0.05665857	0.033931009	0.598868091	0.158451598	-175	139.7631683
	50%	0.068030961	0.047809992	0.702768142	0.211460937	170	140.8609924
	75%	0.069867514	0.040462732	0.579135137	0.191255711	175	153.1916504
	100%	0.082583956	0.051590499	0.624703644	0.237355452	-175	152.6676483
Test 15	25%	0.08846733	0.04189907	0.473610657	0.21416454	175	148.7556915
	50%	0.137740359	0.052365839	0.380177894	0.294837877	-180	162.064643
	75%	0.139704004	0.043582998	0.311966708	0.270452999	175	155.6423492
	100%	0.189388841	0.058383841	0.308274979	0.364540365	175	160.7471619
Test 16	25%	0.054898109	0.032364126	0.5895308	0.151990488	-180	137.5180206
	50%	0.086000502	0.044062588	0.512352687	0.218188267	175	161.7849884
	75%	0.135844514	0.051940408	0.382351897	0.291665737	-170	138.8531494
	100%	0.222528383	0.066049635	0.296814431	0.420677289	-175	142.6332397
Test 17	25%	0.089430094	0.051516362	0.576051745	0.243979178	-5	44.35347748
	50%	0.048793413	0.030736724	0.629935932	0.141003584	-5	91.0305481
	75%	0.068014912	0.039903101	0.586681644	0.187724214	175	145.9229431
	100%	0.078071482	0.040226467	0.515251737	0.198750883	175	148.822403
Test 18	25%	0.072442293	0.040445298	0.55831057	0.193778187	-170	139.4902954
	50%	0.092878997	0.044042505	0.4741923	0.225006513	-180	159.3744659
	75%	0.089633152	0.04818102	0.537535708	0.234176211	175	152.0465393
	100%	0.074177921	0.045739267	0.616615652	0.211395722	175	133.2328796
Test 19	25%	0.074838281	0.044228166	0.590983197	0.20752278	-175	149.6004791
	50%	0.081172526	0.050641697	0.623877308	0.233097617	-180	148.0843506
	75%	0.072734132	0.04374779	0.601475383	0.203977503	170	129.5135803
	100%	0.080724724	0.047248382	0.585302495	0.22246987	170	120.6473083
Test 20	25%	0.044955544	0.027833907	0.619142921	0.128457265	175	119.7024612
	50%	0.062467415	0.035977449	0.575939461	0.170399763	165	90.57080841
	75%	0.107628286	0.054743666	0.508636422	0.271859284	25	45.35085297
	100%	0.095438465	0.052965973	0.554975107	0.254336383	160	95.34896088
Test 21	25%	0.073487289	0.040648229	0.553132791	0.195431978	170	146.4486084
	50%	0.057151522	0.033604205	0.587984417	0.157964136	175	134.1735229
	75%	0.10480924	0.04901487	0.467657912	0.25185385	-180	164.4147339
	100%	0.144389808	0.049385637	0.342029937	0.292546719	-180	170.7442169
Test 22	25%	0.062909916	0.039745145	0.631778693	0.18214535	-180	128.37146
	50%	0.072837599	0.042700868	0.58624761	0.200940203	20	84.82663727
	75%	0.163110405	0.083445616	0.511589778	0.413447253	0	38.55003357
	100%	0.130742937	0.085461922	0.653663775	0.387128703	-5	61.1191597



Calculation parameter for comparison with theory

In this appendix, calculation details on the comparison with the guidelines are presented. To compare the PIANC guidelines with the data, maximum velocities at the bottom that could be expected have been calculated according both to German and Dutch method. In both cases, the first step consists in evaluating the efflux velocity, according to equation 2.4:

$$V_{0,thruster} = 1.15 \left(\frac{P_{thruster}}{\rho_w D_{thruster}^2} \right)^{0.33} \quad (D.1)$$

Being the efflux velocity dependent only on the thruster characteristics ($D_{thruster} = 0.4m$) and on the applied power ($P_{thruster} = 618kW$), the efflux velocity is the same for all tests taken into account. V_0 calculated for each step of applied power is listed in table D.1.

Table D.1: Efflux velocity calculated for each step of applied power.

Applied power	V_0
25%	4.78 m/s
50%	6.00 m/s
75%	6.86 m/s
100%	7.55 m/s

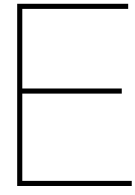
Parameters used to calculate expected maximum velocities at the bottom according to Dutch and German method are presented in table D.2, while data of recorded velocities are presented in table D.3.

Table D.2: Parameters used to calculate maximum expected velocities at the bottom according to German and Dutch method, for each test taken into account.

Test	L [m]	h_t [m]	a_L [-]
1	3.3	1.73	1
2	6	1.73	1
11	3.3	3.27	1
12	6	3.27	1

Table D.3: Data recorded by ADCP1 and ADV1 during the tests 1, 2, 11, 12. Mean flow velocity magnitude, standard deviation, and maximum velocity calculated as $V_{max} = \bar{V} + 3\sigma$ are presented.

Test	Applied power [%]	ADCP1			ADV1		
		\bar{V} [m/s]	σ [m/s]	V_{max} [m/s]	\bar{V} [m/s]	σ [m/s]	V_{max} [m/s]
1	25	0.23	0.12	0.57	0.39	0.35	1.43
	50	0.40	0.18	0.94	0.46	0.33	1.47
	75	0.53	0.21	1.16	0.57	0.26	1.34
	100	0.63	0.25	1.37	0.58	0.24	1.29
2	25	0.24	0.15	0.69	0.29	0.29	1.17
	50	0.49	0.20	1.08	0.51	0.31	1.45
	75	0.62	0.24	1.33	0.53	0.29	1.40
	100	0.73	0.27	1.54	0.52	0.29	1.38
11	25	0.21	0.11	0.53	0.16	0.15	0.61
	50	0.46	0.11	0.80	0.33	0.25	1.07
	75	0.54	0.14	0.95	0.41	0.35	1.47
	100	0.56	0.14	0.97	0.40	0.37	1.51
12	25	0.24	0.08	0.47	0.30	0.25	1.04
	50	0.45	0.12	0.81	0.73	0.80	3.15
	75	0.49	0.13	0.90	0.87	0.89	3.55
	100	0.49	0.16	0.95	1.04	0.96	3.93



Surveys

In this appendix, surveys from the day of the measurements are presented.

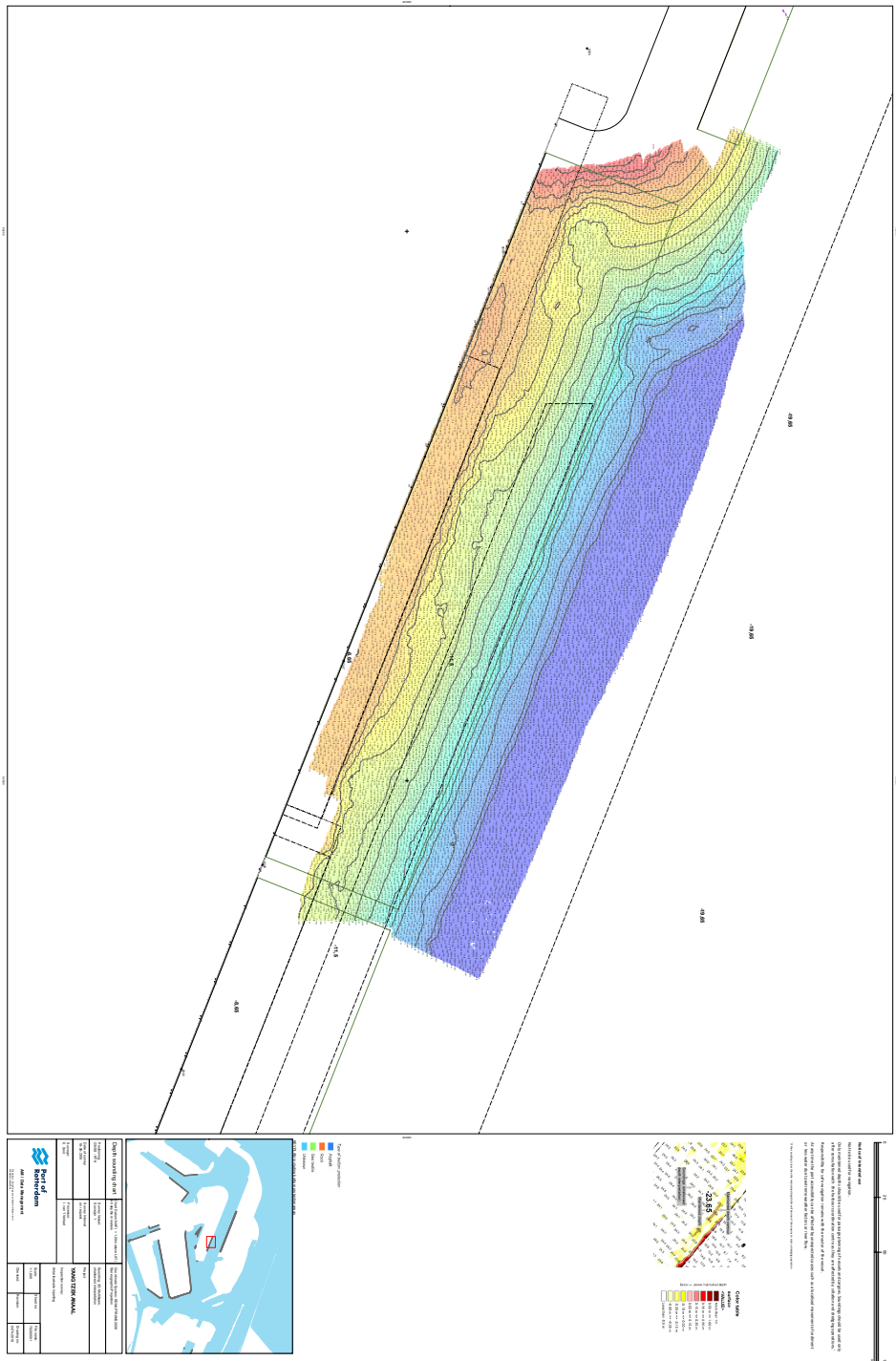


Figure E. 1: Survey of the Yangtzekanaal near to the Antarcicakade, Ports of Rotterdam, taken in the morning of 18 June 2019, before the measurements.

Bibliography

- [1] Teresa et al. Abramowicz-Gerigk. Full scale measurements of pressure field induced on the quay wall by bow thrusters – indirect method for seabed velocities monitoring. *Ocean Engineering*, 162(April):150–160, 2018. ISSN 00298018. doi: 10.1016/j.oceaneng.2018.05.036. URL <https://doi.org/10.1016/j.oceaneng.2018.05.036>.
- [2] Dai Y. B. Jensen R. A. Albertson, M. L. and H. Rouse. Diffusion of a submerged jets. *Transcript of the ASCE (Paper No. 2409)*, 115:639–697, 1950.
- [3] BAW. Principles for the design of bank and bottom protection for inland waterways (gbb), 2010.
- [4] T. Blokland. Schroefstraal tegen kademuur - Stroomsnelheid en erosie meting, 1996.
- [5] J.R. Calizo Manaois. Pumpjets in de binnenvaart, 2011.
- [6] CETMEF CIRIA, CUR. *The Rock Manual. The use of rock in hydraulic engineering (2nd edition)*. C683, CIRIA, London, ISBN 978-0-86017-683-1.
- [7] M. Fuehrer and K. Römisch. Propeller jet erosion and stability criteria for bottom protection of various constructions. *PIANC, Bulletin No. 58.*, 1987.
- [8] M. de Jong G. van Velzen. Propeller jets , Knowledge gap 7, 2015.
- [9] G. A. Hamill and C. Kee. Predicting axial velocity profiles within a diffusing marine propeller jet. *Ocean Engineering*, 124:104–112, 2016. ISSN 00298018. doi: 10.1016/j.oceaneng.2016.07.061. URL <http://dx.doi.org/10.1016/j.oceaneng.2016.07.061>.
- [10] B. Hofland. *Rock and Roll - Turbulence-induced damage to granular bed protections*. PhD thesis, TU Delft, 6 2005.
- [11] W. Lam, G. A. Hamil, Y. C. Song, D. J. Robinson, and S. Raghunathan. A review of the equations used to predict the velocity distribution within a ship's propeller jet. *Ocean Engineering*, 38(1):1–10, 2011. ISSN 00298018. doi: 10.1016/j.oceaneng.2010.10.016. URL <http://dx.doi.org/10.1016/j.oceaneng.2010.10.016>.
- [12] Nortek. The Comprehensive Manual. *Nortek Manuals*, page 152, 2017. ISSN 1096-6080. doi: 10.1093/toxsci/kft290. URL <https://www.nortekgroup.com/assets/documents/ComprehensiveManual{ }Oct2017{ }compressed.pdf>.
- [13] Nortek AS. Principles of Operation - Signature Manual. 2017.
- [14] Nortek AS. The Comprehensive Manual for Velocimeters. 2018. ISSN 0196-6553. doi: 10.1002/ejoc.201200111.
- [15] PIANC. *Report No180. Guidelines for Protecting Berthing Structures from Scour Caused by Ships*. 2015. ISBN 9782872232239.
- [16] Veth Propulsion. Veth jet. URL <https://www.vethpropulsion.com/products/bow-thrusters/veth-jet/>.
- [17] Donal Ryan, Gerard A. Hamill, and Harold T. Johnston. Determining propeller induced erosion alongside quay walls in harbours using Artificial Neural Networks. *Ocean Engineering*, 59:142–151, 2013. ISSN 00298018. doi: 10.1016/j.oceaneng.2012.10.018. URL <http://dx.doi.org/10.1016/j.oceaneng.2012.10.018>.

- [18] Gerrit J. Schiereck. *Introduction to Bed, bank and shore protection*. Delft Academic Press / VSSD, 2016.
- [19] E. Schmidt. Belastungen Geschwindigkeit. In *Dresdner Wasserbauliche Mitteilungen*, number 18, pages 145–157. Technische Universität Dresden, Institut für Wasserbau und technische Hydromechanik (Hrsg.), 2000.
- [20] E. A. van Blaaderen. Modelling bowthruster induced flow near a quay-wall, 2006.
- [21] E.J. van de Kaa and H.G. Blaaw. Erosion of bottom and sloping banks caused by the screw race of manoeuvring ships . Publ . no . 202 , Delft Hydraulics Labora. *7th International Harbour Congress*, (May), 1978.
- [22] A. van der Hout. Veldmetingen schroefstraalbelastingen, 2018.
- [23] T. van der Laan. Het ontwikkelen van een model voor boegschroefstralen bij verticale kademuren, 2005.
- [24] Henk Jan Verhagen. Bowthrusters and the stability of a riprap revetment. (January 2001), 2014.
- [25] Henk Verheij. Comparison of water jets and conventional propeller jets. *Waterloopkundig Laboratorium*, (Figure 1), 1983.
- [26] Henk Verheij and Gijs Hoffmans. Jet scour. *Maritime Engineering*, 164(1):1–12, 2011.
- [27] Maoxing Wei and Yee Meng Chiew. Impingement of propeller jet on a vertical quay wall. *Ocean Engineering*, 183(April):73–86, 2019. ISSN 00298018. doi: 10.1016/j.oceaneng.2019.04.071. URL <https://doi.org/10.1016/j.oceaneng.2019.04.071>.